

NONINVASIVE LASER VASECTOMY

by

Christopher Michael Cilip

A dissertation submitted to the faculty of
The University of North Carolina at Charlotte
in partial fulfillment of the requirements
for the degree of Doctor of Philosophy in
Optical Science and Engineering.

Charlotte, NC

2012

Approved by:

Dr. Nathaniel Fried

Dr. Patrick Moyer

Dr. Susan Trammell

Dr. Yasin Raja

Dr. Mehdi Miri

© 2012
Christopher Michael Cilip
ALL RIGHTS RESERVED

ABSTRACT

CHRISTOPHER MICHAEL CILIP. Noninvasive laser vasectomy. (Under the direction of DR. NATHANIEL FRIED)

Development of a noninvasive vasectomy technique may eliminate male fear of complications (incision, bleeding, infection, and scrotal pain) and result in a more popular procedure. These studies build off previous studies that report the ability to thermally target tissue substructures with near infrared laser radiation while maintaining a healthy superficial layer of tissue through active surface cooling. Initial studies showed the ability to increase the working depth compared to that of common dermatological procedures and the translation into an *ex vivo* canine model targeting the vas deferens in a noninvasive laser vasectomy. Laser and cooling parameter optimization was required to determine the best possible wavelength for a safe transition to an *in vivo* canine model. Optical clearing agents were investigated as a mechanism to decrease tissue scattering during *in vivo* procedures to increase optical penetration depth and reduce the overall power required. Optical and thermal computer models were developed to determine the efficacy for a successful transition into a human model. Common clinical imaging modalities (ultrasound, high frequency ultrasound, and optical coherence tomography) were tested as possible candidates for real-time imaging feedback to determine surgical success. Finally, a noninvasive laser vasectomy prototype clamp incorporating laser, cooling, and control in a single package was designed and tested *in vivo*. Occlusion of the canine vas deferens able to withstand physiological burst pressures measured post-operative was shown during acute and chronic studies. This procedure is ready for azoospermia and recanalization studies in a clinical setting.

ACKNOWLEDGEMENTS

The author sincerely thanks and especially acknowledges Gino R. Schweinsberger for his contributions to Chapter 7. Given my preliminary Monte Carlo work, Gino was able to simulate the necessary parameters that may allow this surgery to have a successful transition from a canine to a human model. Gino modeled and simulated the optical and thermal properties, then calculated the change in each parameter necessary to achieve success. These simulations could not have been completed without the help and guidance of my committee advisor Dr. Susan R. Trammell who assisted Gino and advised him throughout his undergraduate research project.

This research was supported by a grant from the NIH National Institute of Child Health and Human Development (NICHD) and United States Agency for International Development (USAID) through a subcontract from Family Health International (Durham, NC).

Serhat Tozburun, Ph.D. and Thomas Hutchens, M.S. for extensive travel and their help in many animal studies. Additionally, the preparation of my thesis presentation and numerous conference talks. Christina Crothers, for collection of animal tissues for the *ex vivo* tissue studies. Laurie Pipitone and Dawn Ruben D.V.M. for assisting with the *in vivo* animal studies. Dr. Jonathan Jarow, M.D., Dr. Ashley Ross, M.D., Dr. Mohamad Allaf, M.D., and Dr. Philip Pierorazio, M.D., of the Department of Urology, Johns Hopkins Hospital, for their surgical assistance, academic research and consultation regarding this procedure. James Hsia of the Candela Corporation (Wayland, MA), for providing the cryogen spray cooling system used in these studies. Nancy Tresser of the Imalux Corporation (Cleveland, OH), for providing the optical coherence tomography

system used in these studies. John Walsh and Lyn Pugh of Aloka (Wallingford, CT) for providing the high-frequency (13 MHz) ultrasound system using in these studies. Paul Wilson of Longport, inc (Great Britain) for providing the high-frequency (20 MHz) ultrasound system using in these studies.

The Department of Physics and Optical Science and The Graduate School of the University of North Carolina at Charlotte. For GPSG support, travel funding, and the use of the many facilities that aided in the advancement of the systems used in this project. The Department of Computer and Electrical Engineering, University of North Carolina, Charlotte. For their encouragement in attending graduate school at UNCC and to follow the research path that best interested me.

Finally, I give special thanks to my mentor, Dr. Nathaniel Fried. Dr. Fried has provided me the opportunity to collaborate with other highly acclaimed institutions and to present my work at international conferences. Most importantly, Dr. Fried has taught me that high productivity, perseverance, and a good work ethic will lead to success.

TABLE OF CONTENTS

LIST OF TABLES	xi
LIST OF FIGURES	xii
LIST OF ABBREVIATIONS	xv
CHAPTER 1: INTRODUCTION	1
1.1 Minimally Invasive Sterilization Techniques	3
1.2 Theory of Laser Tissue and Cooling Interactions	4
1.2.1 Laser Parameters	4
1.2.2 Cooling Parameters	9
CHAPTER 2: NONINVASIVE LASER COAGULATION OF DEEP SUBSURFACE TISSUE STRUCTURES	10
2.1 Introduction	10
2.2 Materials and Methods	10
2.2.1 Tissue Preparation	10
2.2.2 Laser Parameters	11
2.2.3 Cooling System	11
2.2.4 Statistical Analysis	13
2.3 Results	13
2.4 Discussion	15
2.5 Conclusions	17
CHAPTER 3: NONINVASIVE LASER COAGULATION OF THE CANINE VAS DEFERENS, <i>EX VIVO</i>	18
3.1 Introduction	18
3.2 Materials and Methods	19

3.2.1	Tissue Studies	19
3.2.2	Laser and Cooling Parameters	20
3.2.3	Tissue Temperature Measurements	21
3.2.4	Burst Pressure Measurements	22
3.2.5	Statistical Analysis	22
3.3	Results	22
3.3.1	Thermal Coagulation of the Vas	22
3.3.2	Tissue Temperature Measurements	23
3.3.3	Burst Pressure Measurements	24
3.4	Discussion	24
3.5	Conclusions	25
CHAPTER 4: NEAR-INFRARED WAVELENGTHS FOR NONINVASIVE LASER VASECTOMY		26
4.1	Introduction	26
4.2	Methods	26
4.2.1	Laser Parameters	26
4.2.2	Cryogen Cooling System	27
4.2.3	Burst Press Measurements	28
4.2.4	Statistical Analysis	28
4.3	Results	28
4.4	Discussion	31
4.5	Conclusions	33
CHAPTER 5: NONINVASIVE LASER COAGULATION OF THE CANINE VAS DEFERENS, <i>IN VIVO</i>		34

5.1	Introduction	34
5.2	Materials and Methods	34
5.2.1	Animal Studies	34
5.2.2	Laser Parameters	35
5.2.3	Cooling Parameters	35
5.2.4	Indicators of Vas Occlusion	35
5.3	Results	36
5.4	Discussion	38
5.5	Conclusions	40
CHAPTER 6: USE OF AN OPTICAL CLEARING AGENT DURING NONINVASIVE LASER VASECTOMY		42
6.1	Introduction	42
6.2	Methods	43
6.2.1	Optical Clearing Agent (OCA)	43
6.2.2	<i>Ex Vivo</i> Tissue Studies	44
6.2.3	<i>In Vivo</i> Animal Studies	44
6.2.4	Laser Parameters	45
6.2.5	Cooling Parameters	46
6.2.6	Indicators of Vas Occlusion	46
6.3	Results	47
6.3.1	Transmission Studies	47
6.3.2	Noninvasive Laser Vasectomy Studies	47
6.4	Discussion	50
6.5	Conclusions	51

CHAPTER 7: OPTICAL AND THERMAL SIMULATIONS OF HUMAN VAS DURING LASER VASECTOMY	52
7.1 Introduction	52
7.2 Methods	52
7.2.1 Monte Carlo Model of Light Transport in Tissue	52
7.2.2 Heat Transfer Model	56
7.3 Results	57
7.4 Discussion	62
7.5 Conclusions	64
CHAPTER 8: ULTRASOUND IMAGING OF THE CANINE VAS DEFERENS	65
8.1 Introduction	65
8.2 Methods	66
8.2.1 Animal Studies	66
8.2.2 Laser Parameters	66
8.2.3 Cooling Parameters	67
8.2.4 Ultrasound Imaging	67
8.3 Results	68
8.3.1 Noninvasive Laser Vasectomy	68
8.4 Discussion	71
8.5 Conclusions	73
CHAPTER 9: OCT AND HIGH FREQUENCY US IMAGING OF THE CANINE VAS DEFERENS	74
9.1 Introduction	74
9.2 Methods	75

	x
9.2.1 Animal Studies	75
9.2.2 Laser Parameters	75
9.2.3 Cooling Parameters	75
9.2.4 OCT Parameters	77
9.2.5 High Frequency Ultrasound Parameters	78
9.3 Results	79
9.3.1 OCT Results	79
9.3.2 High Frequency Ultrasound Results	81
9.3.3 Histology Results	83
9.4 Discussion	85
9.5 Conclusions	87
CHAPTER 10: CONCLUSION	88
REFERENCES	89
APPENDIX A: TECHNOLOGICAL DEVELOPMENT OF A NOVEL VASECTOMY CLAMP	96
APPENDIX B: SCHEMATICS OF NONINVASIVE LASER VASECTOMY PROTOTYPE CLAMP	105
APPENDIX C-1: MAIN SIGNAL GENERATION PROGRAM	109
APPENDIX C-2: CLOCK INITIALIZATION	121
APPENDIX C-3: LCD INITIALIZATION	123
APPENDIX D: RECOGNIZED WORKS	131

LIST OF TABLES

TABLE 1: Optimal laser and cooling parameters.	13
TABLE 2: Lesion dimensions.	15
TABLE 3: Canine tissue dimensions.	19
TABLE 4: Summary of laser and cooling parameters.	20
TABLE 5: Dimensions of thermal lesions in the canine vas.	23
TABLE 6: Summary of treatment parameters.	27
TABLE 7: Summary of burst pressure and skin burn results for the three near-IR lasers.	29
TABLE 8: Acute and chronic burst pressure measurements of coagulated canine vas.	37
TABLE 9: Comparison of burst pressure results for <i>ex vivo</i> and <i>in vivo</i> noninvasive laser vasectomy studies performed with and without an optical clearing agent (OCA).	48
TABLE 10: Optical properties of human tissues at 1064 nm.	55
TABLE 11: Optical properties of human skin at 1064 nm after application of an optical clearing agent.	55
TABLE 12: Thermal properties of human tissues.	56
TABLE 13: Laser and cooling parameters used in this study.	57

LIST OF FIGURES

FIGURE 1: Skin incision made to expose the vas.	2
FIGURE 2: Vas is delivered and occluded.	2
FIGURE 3: Absorption curves for protein, collagen, hemoglobin, melanin, and water.	6
FIGURE 4: Distribution of light in tissue for flat collimated laser beams.	8
FIGURE 5: Laser probe.	12
FIGURE 6: Experimental setup (Noninvasive substructure coagulation).	12
FIGURE 7: Temperature profile during pre-ablation tissue cooling (Liver).	14
FIGURE 8: Gross and histology images of liver lesion.	15
FIGURE 9: Experimental setup (Noninvasive laser vasectomy showing burst pressure setup).	21
FIGURE 10: Gross and histology images of coagulated vas deferens.	23
FIGURE 11: Temperature vs. time graph of scrotal skin during pre-ablation cooling phase.	24
FIGURE 12: Images of three tabletop, near-infrared lasers.	27
FIGURE 13: Photograph of experimental setup for measuring vas burst pressures.	28
FIGURE 14: Gross images of canine vas immediately after noninvasive thermal coagulation.	30
FIGURE 15: Gross images of canine scrotal skin immediately after coagulation of the vas.	31
FIGURE 16: Optical penetration depth in human skin and water absorption coefficients in the near-infrared.	33
FIGURE 17: Experimental Setup using a standard NSV clamp.	36
FIGURE 18: Gross images of vas at day 0 and day 21 of chronic study.	38
FIGURE 19: Gross images of scrotal skin at day 0 and day 21 of chronic study.	38

FIGURE 20: Experimental setup image showing noninvasive laser vasectomy.	45
FIGURE 21: Optical transmission increase from use of an optical clearing agent.	47
FIGURE 22: Gross images of vas and scrotal skin post procedure, under the effects of an OCA.	50
FIGURE 23: Geometry and boundaries of tissue used for thermal and Monte Carlo modeling.	54
FIGURE 24: Monte Carlo modeling of photon absorption and energy flux.	59
FIGURE 25: Thermal model of tissue during laser radiation.	60
FIGURE 26: Thermal simulation of dermis, epidermis, and vas during cooling.	61
FIGURE 27: First iteration of noninvasive vasectomy prototype clamp, using standard NSV clamp.	66
FIGURE 28: Ultrasound image; pre-operative, day 0, day 28.	69
FIGURE 29: Gross images of canine vas deferens at day 0, day 28.	69
FIGURE 30: Gross images of canine scrotal skin; pre-operative, day, day 28.	71
FIGURE 31: NSV clamp with detachable customized clamp extension.	77
FIGURE 32: Photographs of the NIRIS O.C.T. and EPISCAN H.F.U.S.	78
FIGURE 33: OCT results.	80
FIGURE 34: HFUS results.	82
FIGURE 35: A thermally coagulated vas segment showing significant blanching and shrinkage of the vas wall.	83
FIGURE 36: H&E-stained histologic sections of the vas.	84
FIGURE A-1: Experimental setup concept drawing.	97
FIGURE A-2: Concept drawing with the necessary components for noninvasive laser vasectomy.	98
FIGURE A-3: Concept drawing of a clamp attachment with four degrees of freedom using a cylindrical coordinate system with integrated roll feature.	99

FIGURE A-4: Extra lab equipment required for experimental setup (oscilloscope, function generators).	100
FIGURE A-5: Concept drawing of the second iteration of the noninvasive vasectomy clamp, using a NSV clamp.	101
FIGURE A-6: Project box housing Renesas microcontroller board with BNC connectors	102
FIGURE A-7: Programmed Renesas microcontroller board.	102
FIGURE A-8: Final iteration of the noninvasive vasectomy prototype clamp.	104
FIGURE B-1: Schematic of laser/cryogen holder for CNC machining.	105
FIGURE B-2: Schematic of base post insert for machining.	106
FIGURE B-3: Schematic of base post holder for machining.	107
FIGURE B-4: Schematic of connection rod for press fitting.	108

LIST OF ABBREVIATIONS

CW: Continuous Wave
DCD: Dynamic Cooling Device
DMSO: Dimethyl Sulfoxide
Ex Vivo: Excised tissue
FEP: Fluorinated Ethylene Propylene
H&E Stain: Hematoxylin and Eosin Stain
HFUS: High Frequency Ultrasound
ID: Inner Diameter
In Vivo: Living Tissue
IR: Infrared
IVP: Intravasal Pressure
MC: Monte Carlo
Nd:YAG: Neodymium: Yttrium Aluminum Garnet
OCA: Optical Clearing Agent
OD: Outer Diameter
PEG: Polyethylene Glycol
TTL: Transistor-to-Transistor Logic
US: Ultrasound
Vas : Vas Deferens
WHO: World Health Organization

CHAPTER 1: INTRODUCTION

Active cooling methods are currently used in dermatology to preserve the skin surface during cosmetic laser procedures, including skin resurfacing, hair removal, and treatment of vascular birthmarks. These technologies include both contact cooling (e.g. cold water, sapphire window) and non-contact cooling (e.g. cold air, cryogen spray) [1, 2]. In dermatology, the tissue structures of interest for laser therapy are usually superficial, requiring preservation of only a thin layer of tissue (e.g. epidermis and papillary dermis), measuring approximately 200-400 μm .

The ability to spare the tissue surface to a depth on the order of a few millimeters during laser therapy could result in the development of noninvasive laser procedures beyond cosmetic surgery. Our laboratory has previously demonstrated the creation of deep subsurface thermal lesions in a variety of tissues using both non-contact and contact cooling techniques [3-5], with the long-range goal of developing a noninvasive form of male sterilization.

Surgical sterilization is currently the most common method of contraception among married couples in the United States [6]. Male sterilization (vasectomy) has a higher success rate, lower morbidity and mortality rate, is less expensive, and easier to perform than female sterilization (tubal ligation) [6-8]. Despite these advantages, however, female sterilization is more commonly performed. Fear of complications related to surgery is cited as the primary reason for a couple choosing tubal ligation

instead of vasectomy [6, 7, 9]. In the U.S., for example, there are approximately 500,000 vasectomies and 1 million tubal ligations performed each year [10]. Worldwide, approximately 40 million men have had a vasectomy [11]. While there have been no reported cases of vasectomy-related deaths in the U.S., there are 10-20 deaths each year due to tubal ligation [12, 13]. Worldwide, these numbers are even greater [13]. Complication rates of vasectomy range from 1-6% and include sterilization failure, hematoma, infection, sperm granuloma, and epididymitis [14-16]. However, several studies have reported much higher rates of infection (12-38%) which may be due primarily to the experience of the physician performing the procedure [10].

During vasectomy, the vas deferens is separated from the spermatic cord vessels and manipulated to a superficial position under the scrotal skin. A needle is used to inject local anesthesia around the vas, producing a vasal nerve block. Then 1-cm-long incisions are made through the vas sheath until the vas is exposed (Figure 1). The vas is delivered and the deferential artery, veins, and nerves are dissected free of the vas and spared (Figure 2). A 1-cm-long vas segment is then removed and the ends of the vas are occluded using thermal cautery, followed by the placement of hemoclips [10].

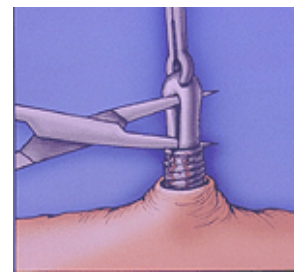
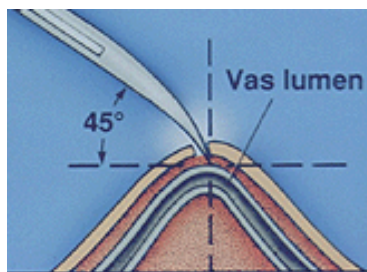


Figure 1. Skin incision made to expose the vas. Figure 2. Vas is delivered and occluded.

Images reproduced from: Center for Male Reproductive Medicine and Microsurgery, Weill Medical College of Cornell University.

1.1 Minimally Invasive Sterilization Techniques

Complications with conventional surgical vasectomy and efforts to enhance the popularity of vasectomy have motivated the search for a less invasive vasectomy technique. In recent years, the “no-scalpel” vasectomy technique has been developed to minimize complications associated with incision during the procedure [17]. This method eliminates the use of the scalpel, results in fewer hematomas and infections, and leaves a smaller wound than conventional methods [10]. The success of this method is proven by a complete reversal in the ratio of male to female sterilizations, now 3 to 1, in the Szechuan province of China [9]. However, despite the name “no-scalpel-vasectomy”, this procedure still requires a puncture through the skin and does not completely eliminate the possibility of bleeding, infection, and scrotal pain.

A percutaneous approach to vasectomy has also been performed in over 500,000 men using chemical ablation with cyanoacrylate and phenol [18-20]. A needle is placed into the lumen of the vas using a series of tests involving dye injections for confirmation. Although pharmacologic tests of the cyanoacrylate-phenol mixture have demonstrated no toxicity, these chemicals are not approved for use in the U.S. Another concern with this method is the great skill involved with gaining percutaneous access to the 300- μ m-diameter lumen of the vas deferens.

Thermal methods of vas occlusion have also been studied for producing more reliable permanent vas occlusion. Some of these studies have suggested that thermal destruction of the vas luminal integrity provides more successful prevention of vas recanalization than does suture ligation during wound healing, with failure rates decreasing from 1-6% to 0.24% [14, 21]. As a result, it is now common for physicians to

cauterize the cut ends of the vas as an alternative to ligation. There is also evidence that more uniform thermal necrosis of the vas lumen with hot wire rather than superficial lumen destruction using electrocautery provides more successful results [22]. These studies used thermal techniques in either a minimally invasive surgical or percutaneous approach to vasectomy [14, 22, 23].

Although conventional vasectomy is a simple, inexpensive procedure with minimal morbidity, there are several reasons for exploring a noninvasive approach to male sterilization. An incision-less method of male sterilization would eliminate surgery and the associated risks of infection, bleeding, and scrotal pain. This may lead to greater acceptance of vasectomy by men, reducing the morbidity, mortality, and cost associated with tubal ligation.

1.2 Theory of Laser Tissue and Cooling Interactions

There is a large matrix of laser and cooling parameters which needs to be optimized to maximize the layer of surface tissue preserved during noninvasive laser coagulation of subsurface tissue structures.

1.2.1 Laser Parameters

1.2.1.1 Wavelength

Previous studies have used wavelengths in which the laser radiation is selectively absorbed by the target, termed “selective photothermolysis” [4]. For example, in the treatment of port-wine stains, a pulsed dye laser is used because the orange laser light ($\lambda = 585 \text{ nm}$) is preferentially absorbed by the targeted blood vessel, reducing the probability of skin damage. This laser wavelength is adequate if the targeted blood vessels are located relatively close to the skin surface in the papillary dermis. However, if it is

desired to target tissue structures 1-2 mm below the tissue surface or deeper (e.g. below the dermis), as proposed here, then a laser wavelength should be chosen which provides optimal penetration of the light in tissue. In the near-infrared spectrum, there is an “optical window” from approximately 800-1300 nm, which provides the deepest penetration of light in tissue (Figure 3). Absorption by major tissue chromophores (e.g. melanin, hemoglobin, collagen, water) is low in the near-IR spectrum. There are at least three high-power laser sources in this spectrum range which could potentially be used for our application: the Nd:YAG laser ($\lambda = 1064$ nm), used in our preliminary studies, and diode lasers ($\lambda = 808$ nm and 980 nm). These lasers provide deep penetration of light in tissue and are commercially available at high laser powers necessary for tissue coagulation. A comparison of these three laser sources will be conducted in chapter 4 to determine if there is a significant difference in thermal lesion depth and size produced with these three laser sources.

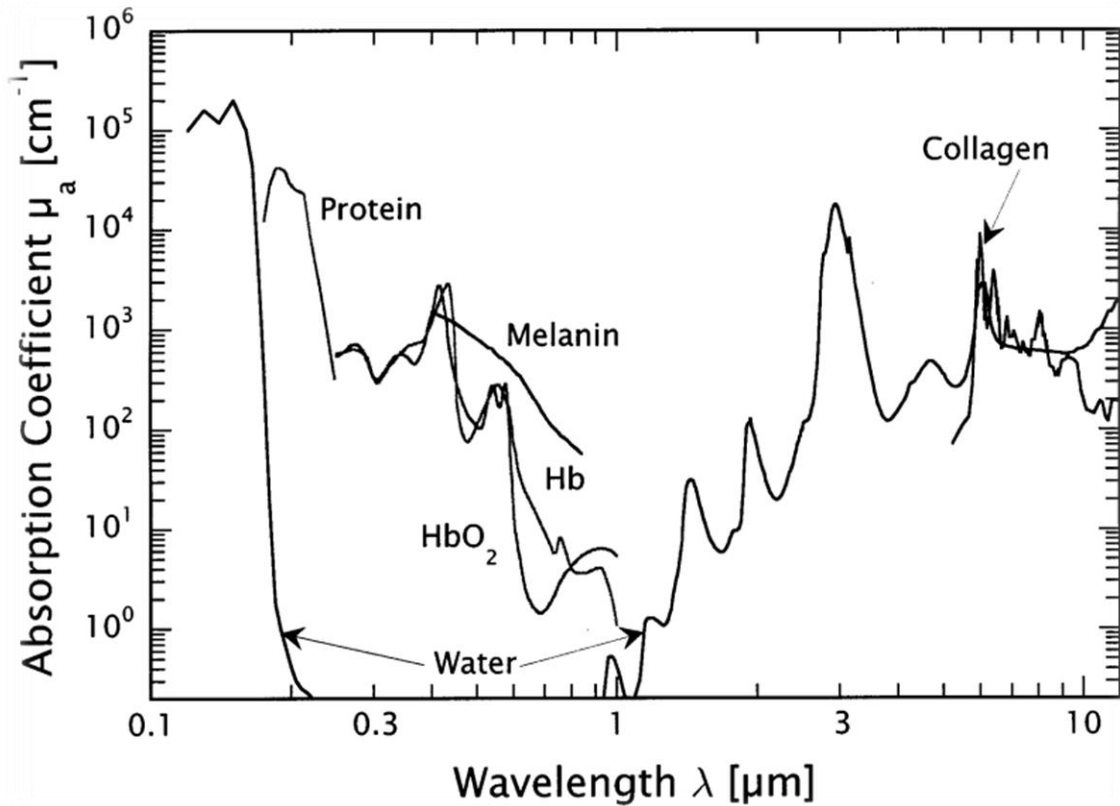


Figure 3. Absorption curves for protein, collagen, hemoglobin, melanin, and water.

1.2.1.2 Spot Size

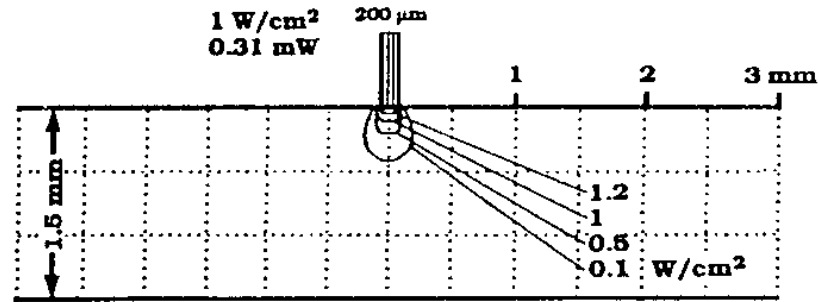
In the near-infrared wavelength range, scattering of radiation dominates absorption. Scattering of photons within the tissue can result in a significant decrease in penetration depth of the radiation and cause a temperature gradient with tissue depth. By using a large diameter laser beam a larger ratio of area to circumference is created. This reduction in peripheral scattering compared to beam area allows the radiation to penetrate deeper into the tissue; thus, the temperature distribution is more uniform, and laser coagulation of deeper tissue structures can be achieved, as has been demonstrated in previous studies (Figure 4) [24-27]. A large laser spot also provides treatment of a larger tissue volume in a single application.

1.2.1.3 Pulse Duration

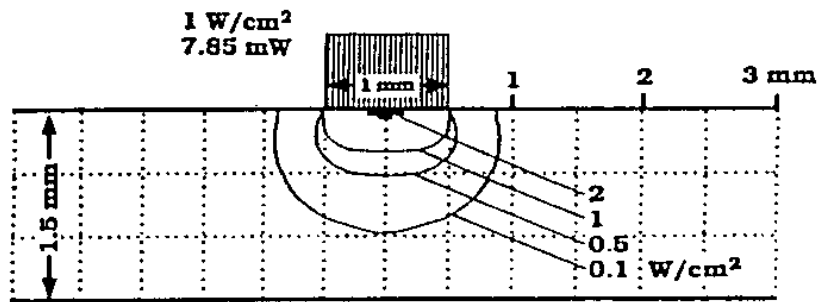
Delivering laser radiation in a pulsed mode limits heat diffusion during the laser pulse, thus preventing undesirable heating of adjacent tissue structures. For our application, pulsed delivery will prevent significant heat from diffusing to the surface of the tissue which would otherwise counteract the benefits of surface cooling, and reduces the probability of thermal buildup at the surface itself from direct absorption of the laser radiation [28, 29].

1.2.1.4 Irradiation Time

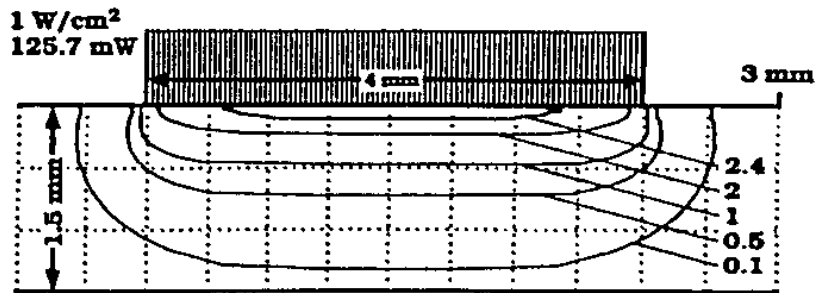
The laser power and total irradiation time will be studied to determine the optimal combination of laser parameters necessary to produce a subsurface thermal lesion. Multiple pulses of laser radiation will be applied to the tissue, allowing subsurface tissue temperatures to rise above the threshold for thermal coagulation, resulting in cumulative thermal damage at the subsurface target site [30].



(a)



(b)



(c)

Figure 4. Distribution of light in tissue for flat collimated laser beams with diameters of (a) 200 μm , (b) 1 mm, and (c) 4 mm. The same laser irradiance (1 W/cm^2) is used for all three laser spot diameters. Note, however, that as the laser spot size is increased the penetration depth of the laser radiation also increases. For example, the 0.1 W/cm^2 irradiance line in the tissue is located at depths of 0.4 mm, 1.0 mm, and 1.3 mm for the spot sizes used in diagrams a, b, and c, respectively. The distribution of the laser radiation is also more uniform for larger laser spot diameters [25].

1.2.2 Cooling Parameters

1.2.2.1 Pulse Duration

For non-contact cryogen cooling of the tissue surface, the pulse duration is critical to providing effective cooling of the tissue surface. Short pulse lengths will not effectively counteract the absorption of laser radiation and consequent heating of the tissue surface, thus resulting in thermal damage at the tissue surface. Long pulse lengths will cause excessive cooling of the tissue surface, resulting in ice formation that may absorb incoming laser radiation and possibly cause frost damage to the tissue surface.

1.2.2.2 Pulse Repetition Rate / Duty Cycle

The pulse repetition rate will have a similar effect as the cryogen pulse duration, with low repetition rates resulting in thermal damage at the tissue surface, and higher repetition rates resulting in ice formation and buildup on the surface. The goal of applied cooling is to cool the tissue surface as rapidly as possible to prevent thermal damage and limit the operation time, without causing such adverse effects.

1.2.2.3 Spot Size / Working Distance

The cooling area or spot size may play an important role in determining the optimal matrix of cooling parameters. During preliminary studies, we used a relatively large cryogen spot diameter of 2 cm, with the 3-mm-diameter laser beam concentric within the cryogen spot. However, there may be concerns with the cryogen spray diverging and becoming less dense in the air during application, thus possibly becoming less effective in cooling the tissue surface.

CHAPTER 2: NONINVASIVE LASER COAGULATION OF DEEP SUBSURFACE TISSUE STRUCTURES

2.1 Introduction

The objective of this *ex vivo* tissue study was to optimize a laser probe design and laser and cooling parameters to provide rapid creation of a subsurface thermal lesion while maximizing the thickness of preserved tissue at the surface of the tissue sample. The ability to create subsurface lesions will lead to further studies on clinically viable applications using this technique, primarily, noninvasive laser vasectomy.

2.2 Materials and Methods

2.2.1 Tissue Preparation

Porcine liver tissue was used as a model because the thermal lesions can be easily quantified by analysis of the gross tissue immediately after completion of the study. The livers were sectioned into 50 x 50 x 15 mm (L x W x D) samples and then used either fresh or frozen for future studies. The porcine liver samples were immersed in a saline bath, placed on a controlled heating plate, and maintained at a physiological temperature of 37 °C with monitoring by embedded micro-thermocouples.

2.2.2 Laser Parameters

A 50-Watt Ytterbium fiber laser with a wavelength of 1075 nm was used for the experiments. This near-infrared laser wavelength was chosen to provide the deepest optical penetration depth (approximately 2-3 mm) of the laser radiation in soft tissues. The laser radiation was coupled into a custom-made laser probe using a 100-mm-FL lens and a 400- μm -core fiber optic patch-cord. The laser probe was assembled using lens tubes with a 12.7-mm-ID, housing the optics, including a lens for collimating the laser radiation and a mirror for 90° delivery. The average laser power and spot diameter at the tissue surface measured 12.5 W and 6.4 mm ($1/e^2$), respectively. Laser power output was calibrated using a power meter. The Gaussian laser beam was measured by using an infrared beam analyzer and by performing a razor blade scan. The transmission rate for laser power through the probe measured approximately 73%.

2.2.3 Cooling System

The cooling element of the laser probe consisted of a compact 210 W thermoelectric recirculating chiller. A solution consisting of 25% ethylene alcohol and 75% water by volume was used as a coolant and allowed the chiller to operate at a temperature of - 5 °C. The coolant flowed at a rate of 8.5 ml/sec through the flow cell with a cooling power of approximately 38 W at - 5 °C. The custom-built flow cell consisted of aluminum housing with a sapphire plate mounted at the surface (Figure 5).

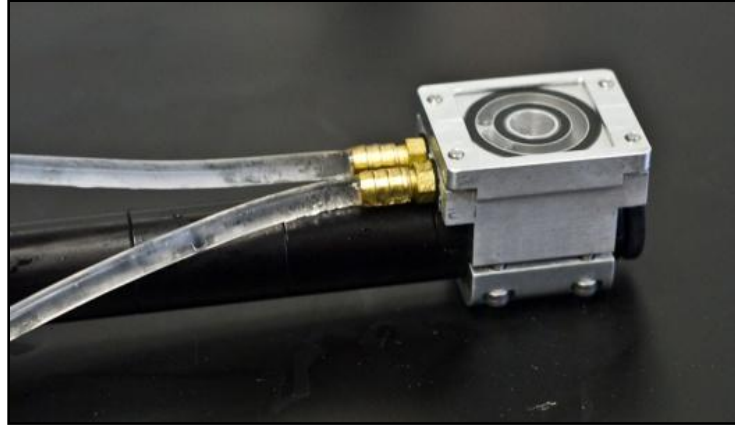


Figure 5. Laser probe. The black stem consists of a series of lens tubes housing the optics. The aluminum housing is a custom made flow-cell with a sapphire window.

The coolant flowed through a circular channel around the circumference of the flow cell, while an 8-mm-diameter aperture in the center of the flow cell provided an optical window for transmission of the laser radiation through the sapphire plate. The sapphire plate served as a transparent window for transmission of the laser radiation, while also acting as a thermally conductive material for cooling the tissue surface. The experimental setup is shown in Figure 6 and the laser/cooling parameters are summarized in Table 1.

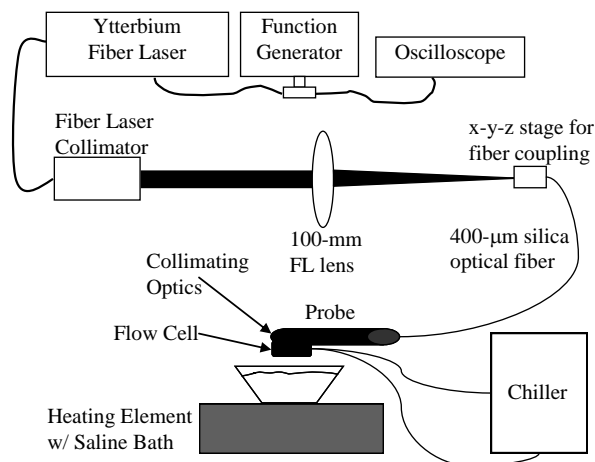


Figure 6. Experimental setup (Noninvasive substructure coagulation).

Table 1. Optimal Laser and Cooling Parameters

Laser Parameters		Cooling Parameters	
Average Power at Surface (W)	12.5	Cooling Power at 20 °C (W)	210
Spot Diameter (mm)	6.4	Cooling Power at - 5 °C (W)	8
Irradiance (W/cm ²):	39	Chiller Temperature (°C)	-5
Pulse Duration (ms)	50	Sapphire Window Temperature (°C)	-1
Pulse Repetition Rate (Hz)	10	Tissue Surface Temperature (°C)	13
Duty Cycle	1:1	Temperature 1.5mm Below Surface (°C)	28
Total Number of Laser Pulses	300	Pre-ablation Cooling Time (s)	15
Laser Irradiation Time (s)	30		
Total Treatment Time (s)	45		

2.2.4 Statistical Analysis

After creating the thermal lesion in the liver tissue, both gross and histologic examination was used to measure the lesion characteristics in the liver. Lesion dimensions and the thickness of the preserved surface tissue layer were measured in the samples, with the mean \pm standard deviation (S.D.) recorded (Table 2).

2.3 Results

Temperature measurements were conducted using insulated micro-thermocouples interfaced to a personal computer with automated acquisition of temperature vs. time data. The thermocouples were inserted at 0 and 1.5 mm below the tissue surface using 16-G syringe needles, which were removed from the tissue prior to the experiments. Temperature measurements were recorded during the pre-ablation cooling phase at a sampling rate of 1 s (Figure 7).

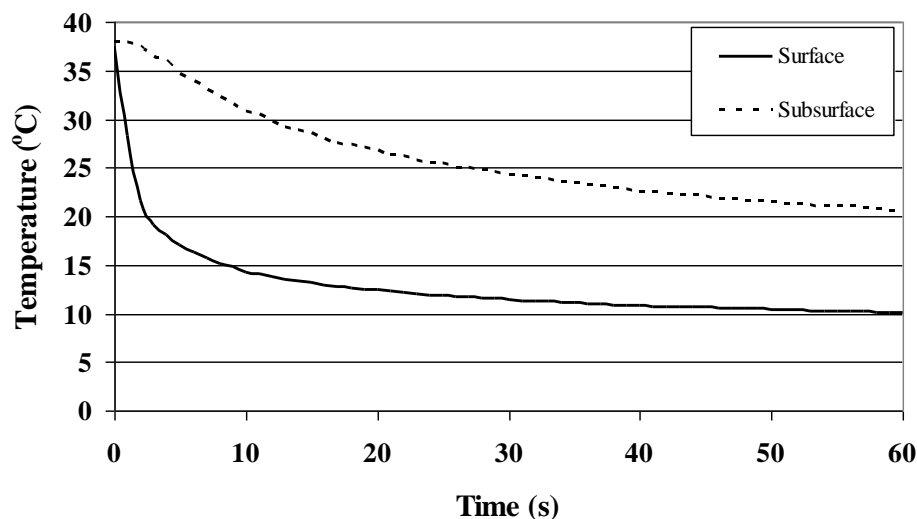


Figure 7. Temperature profile during pre-ablation tissue cooling. The temperature at the surface decreases at a much lower rate after about 15 s, while temperature 1.5 mm below surface continues to decrease, lowering the overall temperature differential.

The temperature at the tissue surface initially decreased rapidly upon sapphire contact cooling, and then bottomed out after about 15 s, with only a smaller decrease in temperature afterwards, at the expense of increased treatment time. Also, longer cooling times continued to decrease the subsurface tissue temperature near the targeted lesion site, an undesirable effect. Hence, an optimal pre-ablation cooling time of 15 s was chosen for the laser studies.

A wide range of laser and cooling parameters were tested. The optimal treatment parameters are listed in Table 1, based on a set of 10 tissue samples. Gross and histologic examination was used to quantify thermal lesion dimensions (Figure 8). Liver lesions measured 5.8 mm in diameter, while preserving the tissue surface to a depth of 1.5 mm (Table 2). The layer of preserved tissue observed was a function of the cooling parameters used. The lesion depth was determined in part by the $1/e$ optical penetration depth at the laser wavelength of 1075 nm for liver tissue, which is approximately 2-3 mm, and the thermal diffusion in the tissue during the quasi-CW application of the laser

radiation. The lesion width is directly proportional to the laser spot diameter chosen, 6.4 mm ($1/e^2$), but also in part a function of thermal diffusion in the tissue.

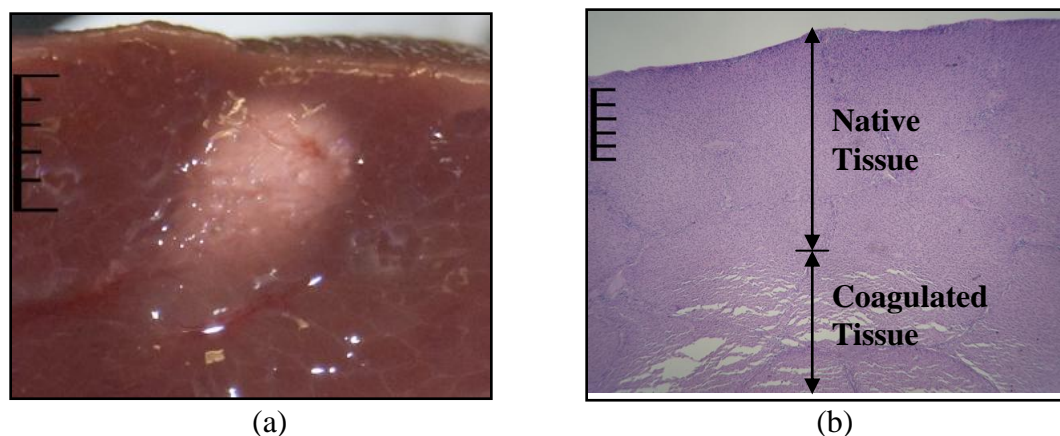


Figure 8. Gross and histology images of liver lesion: (a) Gross image showing thermal coagulation (in white) of subsurface liver tissue, while tissue surface is preserved to a depth of 1.5 mm (Scale bar = 1 mm increments); (b) H&E-stained histologic cross-section showing native liver tissue that has a dense granular appearance to a depth of 1.5 mm, in comparison with thermally coagulated subsurface liver tissue that has a less dense appearance (Scale bar = 100 μm increments).

Table 2. Lesion Dimensions

Preserved Surface Tissue Layer (mm)	1.5 ± 0.2
Lesion Width (mm)	5.8 ± 0.6
Lesion Depth (mm)	5.8 ± 1.0
Lesion Area (mm ²)	28.3 ± 5.4

2.4 Discussion

Active cooling methods in dermatology have focused on the preservation of a superficial layer of skin during cosmetic laser procedures to reduce erythema and pain during the procedure. Typically, only 200-400 μm of skin is preserved during cosmetic laser procedures since the targeted subsurface tissue structures are usually superficial. This study has demonstrated that more aggressive cooling of the tissue surface in combination with deeper laser heating of the subsurface tissues may preserve the tissue surface to a greater depth, while also targeting deeper subsurface tissue structures for

thermal therapy applications. A 1.5-mm-thick tissue layer at the surface of the liver was preserved, while thermal lesions of approximately 5.8-mm-diameter were created. This result is significantly greater than the 400- μ m layer of tissue preserved in liver samples previously reported by other research groups [31]. It should be emphasized that while the results of these preliminary *ex vivo* tissue studies appear promising, *in vivo* animal studies will be necessary to more accurately determine the effects of tissue hydration and blood perfusion on the size and depth of the thermal lesions.

The ability to target deep subsurface anatomical structures using combined laser/cooling techniques may potentially result in new applications of lasers for completely noninvasive procedures in urology and other surgical fields. Previous reports have shown that thermal ablation techniques can potentially be used for applications in noninvasive male sterilization, treatment of female stress urinary incontinence, and testicular ablation. For example, experimental procedures using therapeutic focused ultrasound have been used to noninvasively thermally coagulate the vas deferens in the male reproductive tract, while preserving the overlying scrotal skin layer which measures only about 1 mm thick [32, 33]. In female urology, radiofrequency ablation is being used to thermally remodel the bladder muscles in a minimally invasive method for treatment of female urinary stress incontinence without thermal damage to the vaginal mucosa [34, 35]. Therapeutic ultrasound has also been used to noninvasively target and destroy small testicular tumors [36].

In all of these applications, a noninvasive method which preserves the tissue surface from thermal damage while targeting tissue structures a few millimeters below the surface may be beneficial. However, noninvasive application of radiofrequency

energy is limited due to its shallow penetration depth in tissue. Therapeutic focused ultrasound may also be limited by the relatively slow creation of thermal lesions. This study describes an alternative laser-based method for rapid noninvasive creation of deep thermal lesions in tissue.

2.5 Conclusions

Deep subsurface thermal lesions were created in tissue using a laser and contact cooling probe. These preliminary results suggest that noninvasive procedures targeting anatomic structures within a few millimeters of the tissue surface are feasible.

CHAPTER 3: NONINVASIVE LASER COAGULATION OF THE CANINE VAS DEFERENS, *EX VIVO*

3.1 Introduction

By successfully creating deep subsurface thermal lesions while sparing the skin surface our laboratory is able to pursue clinical applications using this energy based technique as a way to replace or compliment other techniques. Our laboratory previously reported the use of therapeutic focused ultrasound for noninvasive vasectomy in a canine model [32, 33]. An ultrasound clip was used to noninvasively grasp the vas deferens through the scrotal skin and deliver ultrasound energy to thermally occlude the vas. The ultrasound transducer was mounted on a plastic clip with an ultrasound focus that coincided with the vas once it was grasped within the clip's jaws. Cold water was flowed through a balloon on the front side of the clip to cool the scrotal skin during sonication. Ultrasound heating of the vas deferens produced thermal coagulation, necrosis, and scarring of the vas, with the resulting occlusion leading to sterilization. Unfortunately, complications included inconsistent vas occlusion and scrotal skin burns.

Recent studies showing successful creation of deep subsurface thermal lesions while sparing the surface of the skin using near infrared laser radiation [3-5] present a viable alternative to ultrasound vas occlusion. A laser-based approach offers several advantages over ultrasound. First, unlike ultrasound, the laser energy can be delivered to the tissue in a non-contact mode without the need for a coupling medium. This allows a conventional no-scalpel vasectomy approach to be taken for separating and isolating the

vas under the skin prior to vasectomy. It also preserves the urologist's field-of-view so he can directly visually monitor the skin surface during subsurface heating of the vas and prevent the formation of scrotal skin burns. Second, it is possible to create circular lesions that match the geometry of the vas tube, while focused ultrasound typically creates acorn-shaped lesions with a higher depth-to-width ratio, more likely to damage tissue structures immediately surrounding the vas.

3.2 Materials and Methods

3.2.1 Tissue Studies

Scrotal skin and vas tissue was harvested from male dogs immediately after sacrifice for unrelated experiments. The tissue was used in an *ex vivo* vasectomy model. The tissue was partially submerged in a temperature-controlled saline bath, placed on a hotplate, and maintained at approximately 37 °C. A 4.0-mm-inner diameter vasectomy clamp was then used to tightly grasp the vas and surrounding scrotal skin. Table 3 provides a comparison between the normal thickness of the tissue layers and the thicknesses after compression between the vasectomy clamp, as measured using both standard calipers and an optical coherence tomography system.

Table 3. Canine Tissue Dimensions (mm)

Normal scrotal skin thickness	1.8
Compressed scrotal skin thickness	1.0
Uncompressed vas wall thickness	0.55
Total vas thickness	1.3
Vas lumen	0.2

3.2.2 Laser and Cooling Parameters

A 50-W CW Ytterbium fiber laser emitted radiation with a wavelength of 1075 nm that was focused with a 300-mm-FL lens into a 400- μ m silica fiber optic patchcord. A function generator was used to modulate the fiber laser, producing an average output power of 11.7 W, 1-s pulse duration, 0.5 Hz pulse rate, and 3-mm-diameter spot at the scrotal skin surface. Average power is defined as the total power seen by the tissue over the course of the procedure.

A dynamic cooling device was used to deliver the cryogen to the tissue surface through a solenoid valve. The solenoid valve was externally triggered with a 50-ms-long pulse from a function generator, and an oscilloscope was used to view the pulse characteristics. A total of 2 cryogen pulses were used to pre-cool the tissue surface prior to irradiation. During irradiation, the cryogen spray was delivered intermittently between laser pulses with a pulse duration of 60 ms, pulse repetition rate of 0.333 Hz, and a 2-cm-diameter spot size concentric with the laser spot. A summary of the treatment parameters is provided in Table 4, and diagrams of the experimental setup are shown in Figure 9.

Table 4. Summary of Laser and Cooling Parameters

Laser Parameters		Cooling Parameters	
Wavelength (nm)	1075	Pulse Duration (ms)	60
Average Power (W)	11.7	Pulse Repetition Rate (Hz)	0.33
Pulse Duration (s)	1.0	Spot Diameter (mm)	20
Pulse Repetition Rate (Hz)	0.5	Number of Pre-Cooling Pulses	2
Duty Cycle	1:1	Total Number of Pulses	23
1/e ² Spot Diameter (mm)	3.0	Total Treatment Time (s)	66

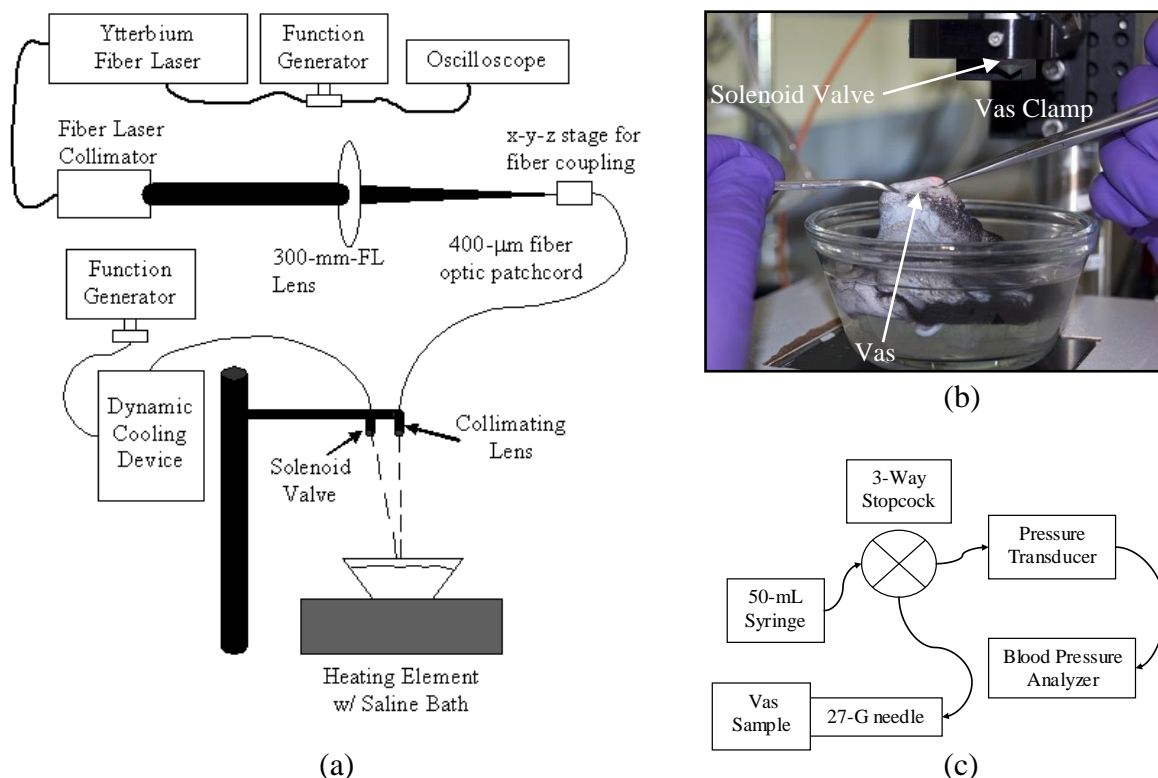


Figure 9. Experimental setup (Noninvasive laser vascectomy showing burst pressure setup). (a) Experimental setup for laser vascectomy; (b) Image of alignment of laser beam and cryogen spray on the surface of the scrotal skin and clamped vas; (c) Experimental setup for vas burst pressure measurements.

3.2.3 Tissue Temperature Measurements

Temperature measurements were conducted during the pre-ablation cooling phase using insulated micro-thermocouples interfaced to a personal computer with automated acquisition of temperature vs. time data. The thermocouples were placed at the skin surface and inside the vas lumen at approximately 1.5 mm below the skin surface. Temperature measurements were recorded during the pre-ablation cooling phase at a sampling rate of 1 s.

3.2.4 Burst Pressure Measurements

Vas burst pressure measurements were performed to quantify the degree of closure of the thermally coagulated vas. The ports of a 3-way stopcock were connected to a 50 mL syringe, pressure transducer, and hypodermic needle. The syringe was filled with water which was also distributed throughout the entire system. The vas was attached to a 27-G (406- μ m-OD) hypodermic needle and clamped with hemostats. A pressure analyzer unit was calibrated to zero setting. Saline from the syringe was then slowly pumped into the vas tube, resulting in a pressure reading that elevated over a 20 s time period until the vas burst open and the pressure dropped precipitously.

3.2.5 Statistical Analysis

A total of 20 vas were thermally coagulated with 10 vas processed for histologic measurements and 10 vas used for burst pressure measurements. The mean \pm standard deviation (S.D.) was calculated for each parameter measured.

3.3 Results

3.3.1 Thermal Coagulation of the Vas

Thermal coagulation and occlusion of the vas was achieved in all samples with one exception. If the 3-mm-diameter laser beam was not correctly centered within the 4-mm-ID ring of the vasectomy clamp, skin burns were observed from absorption and scattering of the laser radiation off of the steel clamp, and the vas was incompletely coagulated. Gross measurements and histologic analysis were both used to assess the thermal lesion dimensions on the vas. Gross analysis was more accurate due to the difficulty in achieving precise longitudinal histologic sections through the vas lumen. Vas lesion dimensions measured 2.0 ± 0.3 mm diameter by 3.0 ± 0.9 mm length, without any

visual evidence of skin damage (Table 5). Analysis of histologic cross-sections and longitudinal sections of the vas demonstrated complete closure of the vas lumen (Figure 10). The targeted area of the vas consistently demonstrated significant blanching, hardening, and shrinkage, all characteristic indicators of thermally coagulated tissue.

Table 5. Dimensions of Thermal Lesions in the Canine Vas

Native Vas Width (mm)	2.8 ± 0.3
Coagulated Vas Diameter (mm)	2.0 ± 0.3
Reduction in Vas Diameter (%)	30 ± 8
Vas Lesion Length (mm)	3.0 ± 0.9

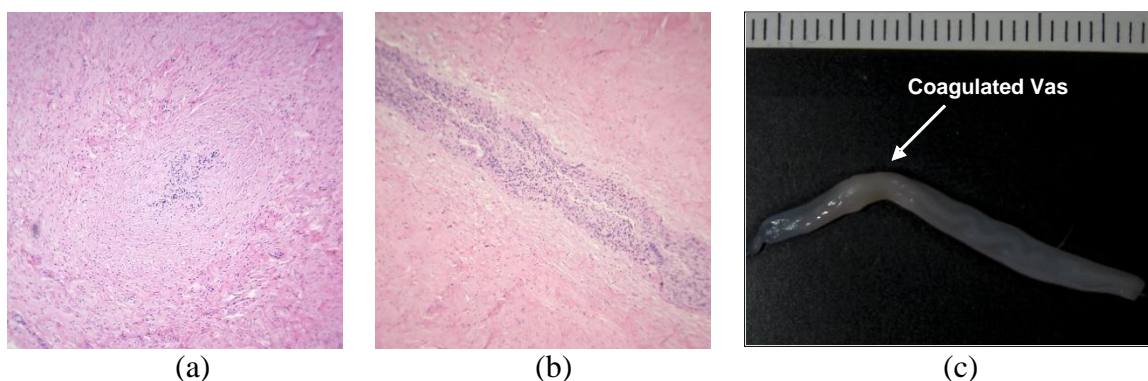


Figure 10. Gross and histology images of coagulated vas deferens. H&E-stained histological cross-section and (b) longitudinal section of vas after laser coagulation, demonstrating complete vas occlusion. (c) Gross image of the thermally coagulated region of the vas lesion (ruler bar = 1 mm increments).

3.3.2 Tissue Temperature Measurements

Figure 11 shows temperature versus time data for the scrotal skin surface and vas during the pre-ablation cooling phase of the study, with the first 0.33 Hz pulse of cooling occurring at 4 seconds. The scrotal skin surface cools down to approximately 20 °C, while the vas remains at 35 °C. This separation in temperatures provides a therapeutic

window in which to heat and coagulate the vas without causing thermal damage to the scrotal skin surface.

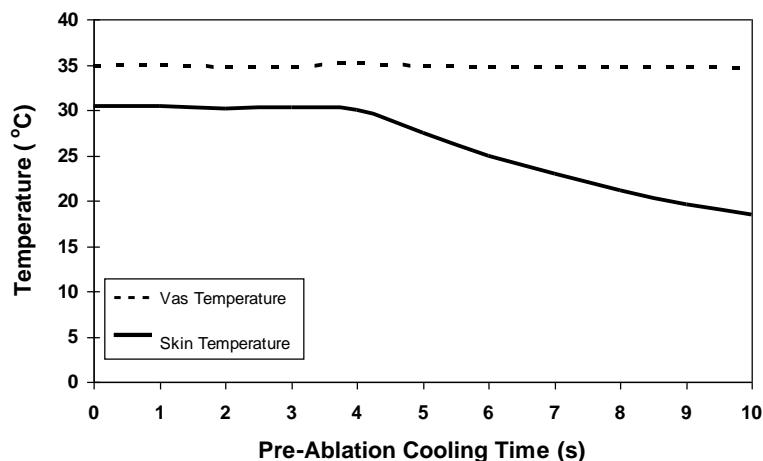


Figure 11. Temperature vs. time graph for scrotal skin surface (solid line) and vas (dotted line) during pre-ablation cooling phase. The scrotal skin surface cools down to approximately 20°C, while the vas remains at 35 °C. This separation in temperatures provides a therapeutic window in which to heat and coagulate the vas without causing thermal damage to the skin surface.

3.3.3 Burst Pressure Measurements

The resting intravasal pressure (IVP) of the vas is approximately 5 ± 1 mm Hg and the IVP during ejaculation reaches 136 ± 29 mm Hg [37]. The bursting pressure of the coagulated vas samples averaged 295 ± 72 mm Hg, significantly above the resting and ejaculation pressures that the vas physiologically experiences.

3.4 Discussion

This preliminary study explores the application of lasers for noninvasive thermal coagulation and occlusion of the vas in an *ex vivo* canine model. A compact, Ytterbium fiber laser with a wavelength of 1075 nm was chosen to provide deep penetration of the laser energy through the skin to the targeted vas deferens. Cryogen spray cooling of the tissue surface prevented scrotal skin burns during the procedure. Both the laser radiation

and cryogen spray were delivered in a non-contact mode to the tissue. This approach allowed a conventional no-scalpel vasectomy method to be applied for separating and isolating the vas under the scrotal skin prior to vasectomy, using a standard vasectomy clamp. This procedure also preserved the surgical field-of-view, potentially allowing the urologist to visually monitor the skin surface during subsurface heating of the vas and prevent the formation of scrotal skin burns.

Several indicators were used to confirm thermal occlusion of the vas, including gross and histologic analysis of the vas and burst pressure measurements. Thermal lesions in the vas measured approximately 2 mm diameter by 3 mm length, without any evidence of scrotal skin burns. Burst pressures for the coagulated vas measured about 300 mm Hg, over twice as high as the approximately 140 mm Hg that the vas experiences during ejaculation.

3.5 Conclusions

Noninvasive laser coagulation and occlusion of the vas deferens is possible in a canine tissue model, *ex vivo*. Gross and histologic measurements as well as burst pressure measurements confirm that the vas can be consistently thermally occluded in a noninvasive manner without evidence of thermal damage to the scrotal skin surface. This technique can easily be integrated into the no-scalpel vasectomy technique currently in clinical practice. Chronic *in vivo* animal studies will first be necessary to optimize the laser/cooling treatment parameters and confirm long-term vas occlusion with absence of sperm in the ejaculate.

CHAPTER 4: NEAR-INFRARED WAVELENGTHS FOR NONINVASIVE LASER VASECTOMY

4.1 Introduction

We have reported successful targeting, thermal occlusion, and scarring of the vas in an *ex vivo* canine model [38]. However, the therapeutic window for treatment is relatively narrow. This study determines the dependence of vas thermal coagulation on laser wavelength for development of a noninvasive laser vasectomy procedure. Three commonly available near-infrared laser wavelengths were studied, including, 808, 980, and 1075 nm.

4.2 Methods

4.2.1 Laser Parameters

Three near-infrared lasers were compared for this study: a CW, 30 W, 808 nm diode laser (Model # P30-808-6OEM, Apollo Instruments, Irvine, CA); a CW, 60 W, 980 nm diode laser (Model #60980 Optiwave 980, Edwards Lifesciences, Irvine, CA); and a 50 W, 1075 nm, Ytterbium fiber laser (Model #YLR-50-1075, IPG Photonics, Oxford, CA), shown in Figure 12. Each laser delivered an average power of 9.2 W, 500-ms pulse duration, pulse rate of 1.0-Hz, and 3.2-mm diameter laser spot to the tissue, through a 400- μ m silica fiber optic patch-cord, for a total treatment time of 60 s.

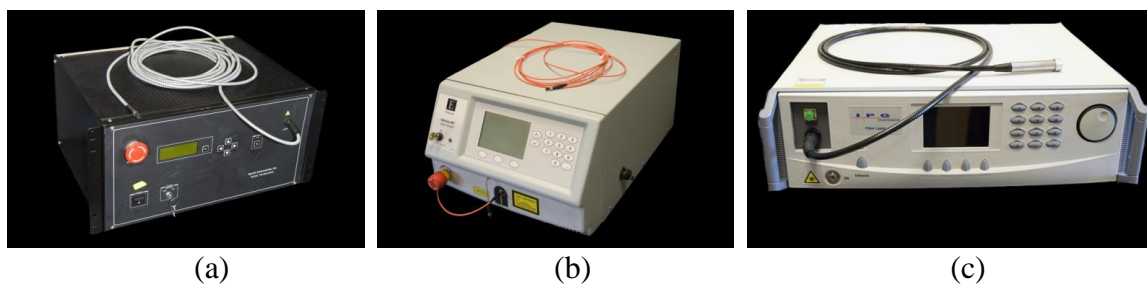


Figure 12. Images of the three tabletop, near-infrared lasers used in this study, (a) 808 nm, (b) 980 nm, (c) 1075 nm.

4.2.2 Cryogen Cooling System

A dynamic cooling device (DCD, Candela Laser Corporation, Wayland, MA) was used to deliver the cryogen (halocarbon 134a, 1,1,1,2-tetrafluoroethane, boiling point = -26 °C) to the tissue surface through a solenoid valve. The solenoid valve was externally triggered using a function generator and an oscilloscope to view the pulse characteristics. Two cryogen pulses were applied to pre-cool the skin surface prior to irradiation. During irradiation, the cryogen spray was delivered intermittently between laser pulses with pulse duration of 60 ms, pulse rate of 0.333 Hz, and a 1-cm-diameter spot concentric with the laser spot. Table 6 summarizes the treatment parameters used in this study.

Table 6. Summary of treatment parameters

Laser Parameters		Cooling Parameters	
Wavelength (nm):	808, 980, 1075	Pulse Duration (ms):	60
Average Power (W):	9.2	Pulse Rate (Hz):	0.33
Pulse Duration (ms):	500	Spot Diameter (mm):	10
Pulse Rate (Hz):	1.0	Cooling Time (s):	60
Spot Diameter (mm):	3.2		
Irradiation Time (s):	60		

4.2.3 Burst Press Measurements

Vas burst pressure measurements were performed to quantify the degree of closure of the thermally coagulated vas in a manner identical to that previously reported in chapter 3 (Figure 13).

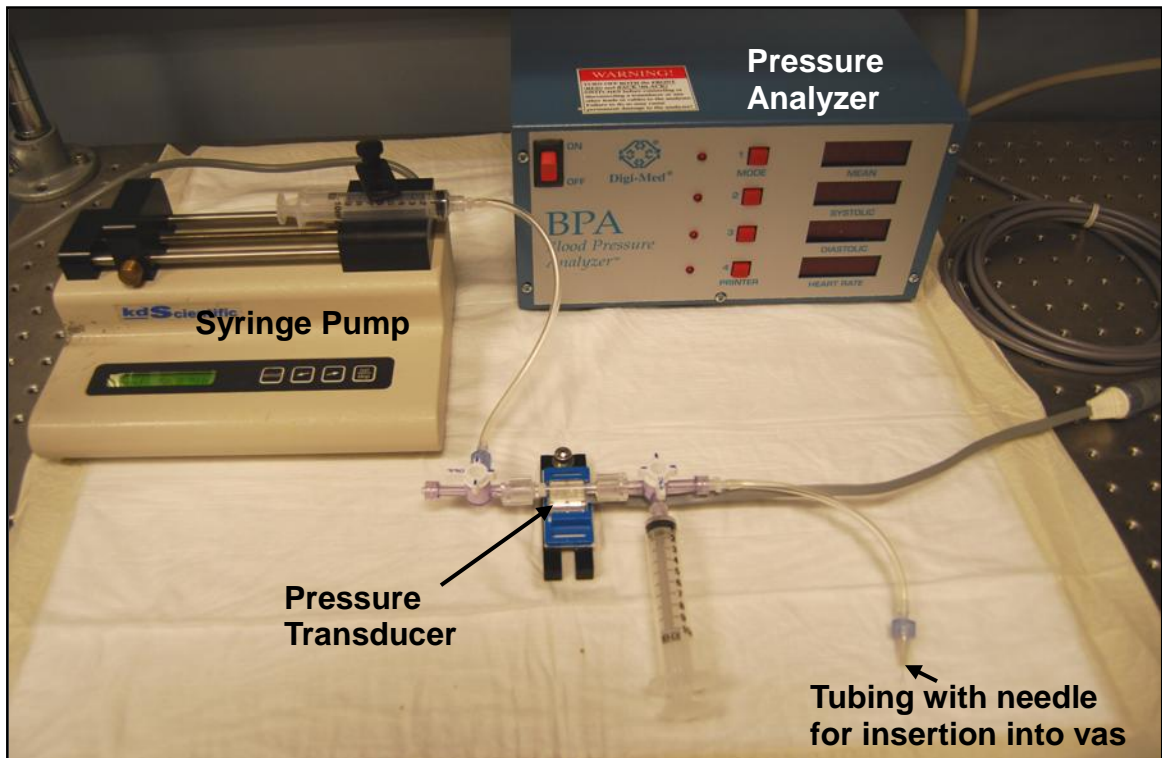


Figure 13. Photograph of experimental setup for measuring vas burst pressures, consisting of a pressure transducer, pressure analyzer unit, and syringe pump.

4.2.4 Statistical Analysis

Multiple vas tissue samples were used for each laser data set. Burst pressure measurements were conducted, and the mean \pm standard deviation (S.D.) was calculated for each parameter measured.

4.3 Results

Several indicators were used to determine successful noninvasive thermal coagulation of the vas, including vas burst pressure measurements, gross observation of

vas coagulation, and monitoring of the scrotal skin surface for evidence of burns. Table 7 summarizes the vas burst pressure results and probability of skin burns. The 808 nm laser wavelength produced thermal occlusion of the vas without frequent skin burns. However, the burst pressures were not significantly greater than normal ejaculation pressures typically experienced by the vas [37]. The 980 nm laser wavelength produced very weak vas burst pressures and always resulted in skin burns. Only the 1075 nm laser wavelength was able to produce vas burst pressures significantly greater than typical vas ejaculation pressures, without the formation of scrotal skin burns.

Table 7. Burst pressure and skin burn results for the three near-IR lasers

Wavelength (nm)	Burst Pressure (mmHg)	Scrotal Skin Burns	N
808	141 ± 61	1/12 (8%)	12
980	89 ± 58	8/8 (100%)	8
1075	288 ± 28	0/9 (0%)	9
Ejaculation (control) [9]	136 ± 29		

Representative images of the canine vas deferens, after noninvasive laser coagulation was performed, *ex vivo*, are shown in Figure 14. Typical indicators of vas thermal coagulation and occlusion, including blanching and shrinkage of the vas in the area of treatment, are clearly observed for the 808 and 1075 nm wavelengths. However, no visual evidence of thermal coagulation of the vas for the 980 nm can be observed.

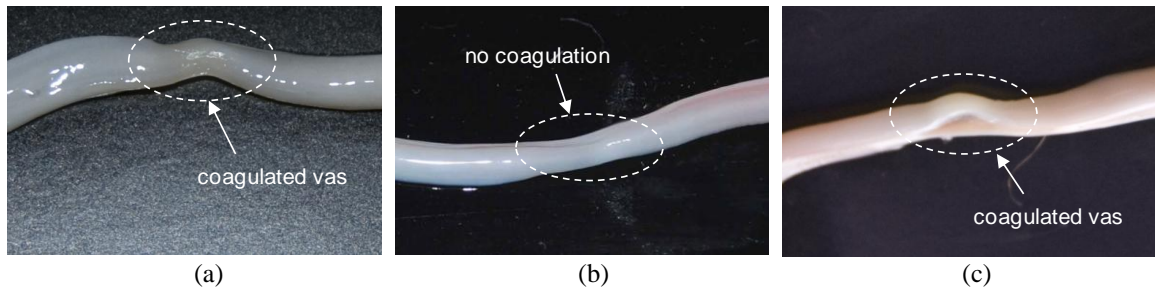


Figure 14. Representative images of the canine vas deferens taken immediately after noninvasive thermal coagulation of the vas, *ex vivo*, using (a) 808, (b) 980, and (c) 1075 nm lasers. Evidence of thermal coagulation of the vas, such as tissue blanching and shrinkage was observed after irradiation with 808 and 1075 nm lasers, but not with the 980 nm laser.

Representative images of the scrotal skin surface, after the procedure, are shown in Figure 15. Temporary compression marks in the skin caused by the vasectomy ring clamp were observed during all of the procedures but typically disappeared soon after the procedure. For the 808 and 1075 lasers, the treatment area did not show any signs of thermal coagulation that could lead to scrotal skin burns during a procedure, *in vivo*. For the 980 nm wavelength, however, thermal coagulation of the scrotal skin surface was always observed after each procedure.

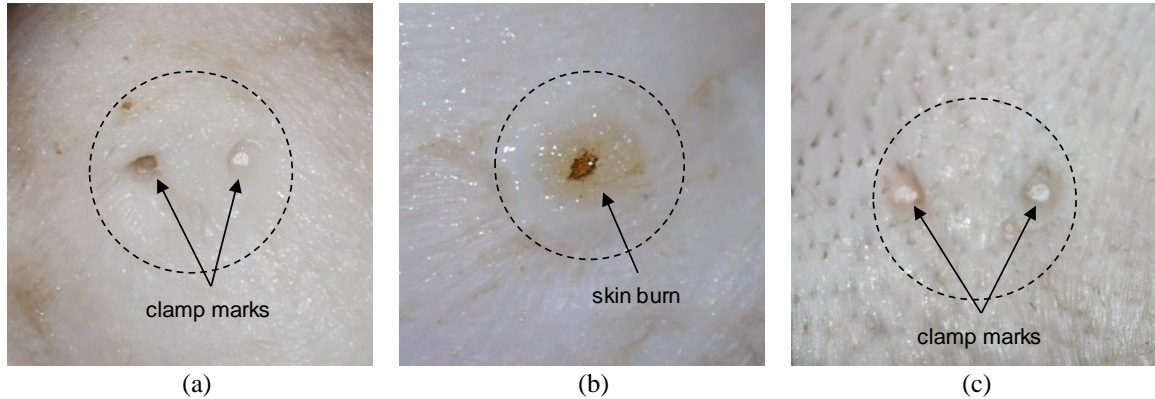


Figure 15. Representative images of the canine scrotal skin surface taken immediately after noninvasive thermal coagulation of the canine vas deferens, *ex vivo*, using (a) 808, (b) 980, and (c) 1075 nm lasers. The vasectomy ring clamp compression marks typically disappear soon after the procedure. Thermal coagulation that may lead to severe scrotal skin burns during a procedure, *in vivo*, was consistently observed for the 980 nm laser wavelength.

4.4 Discussion

In summary, the 808 nm laser wavelength produced thermal occlusion of the vas without skin burns. However, the vas burst pressures were not strong enough to withstand typical vas ejaculation pressures. The 980 nm laser wavelength produced very weak vas burst pressures while creating severe scrotal skin burns. The 1075 nm laser wavelength was able to produce vas burst pressures significantly greater than typical vas ejaculation pressures without formation of skin burns.

In order to interpret these results, the optical penetration depth of these three laser wavelengths in skin needs to be compared. Figure 16a plots the optical penetration depth in human skin for the wavelength range of 400 - 2000 nm [39]. Although the canine model is the most commonly accepted large animal model for surgical vasectomy research studies, there is a significant difference in the optical properties of canine and human skin. Nevertheless, the trends between the two models should be similar. The graph shows a roughly similar optical penetration depth for 808 and 980 nm, of about 2.3

mm, and a near optimal penetration depth for 1075 nm, of about 3.5 mm. The peak penetration depth in human skin occurs at a wavelength of 1090 nm, close to the 1075 nm wavelength used in this study [39]. This observation may explain the superior results for vas bursting pressures achieved at 1075 nm and the absence of skin burns.

However, the data in Figure 16a does not predict the large difference in results between the 808 and 980 nm wavelengths that were observed in this experimental study. In order to understand why the 980 nm wavelength produced severe skin burns, while the 808 and 1075 nm wavelengths did not, the role of water absorption during our procedure needs to be discussed as well. In Figure 16b, the water absorption coefficient is plotted as a function of wavelength in the range from 800 - 1100 nm [40]. While water absorption is relatively low at 808 and 1075 nm, there is a water absorption peak near 980 nm. This graph explains why severe skin burns are observed and form at the scrotal skin surface during 980 nm laser irradiation of the scrotal skin. Residual water layers present on the skin surface from the cryogen spray cooling during the procedure strongly absorb the 980 nm laser radiation, resulting in a much higher temperature rise on the skin surface than for the 808 and 1075 nm wavelengths.

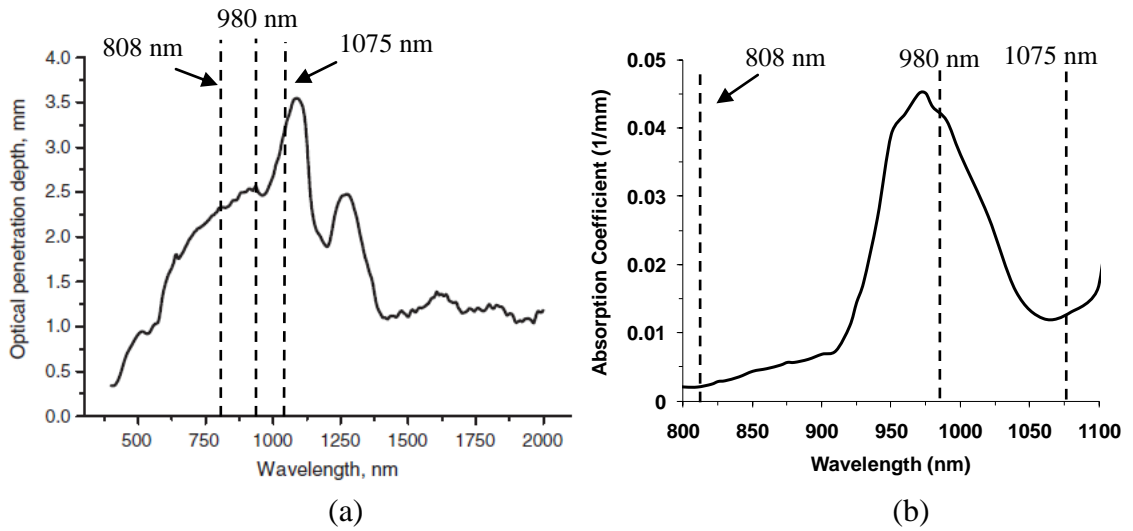


Figure 16. (a) Optical penetration depth of light into human skin over the wavelength range of 400 - 2000 nm [39]; (b) Water absorption coefficients in the near-infrared range of 800 - 1100 nm [40].

4.5 Conclusions

The 1075 nm laser wavelength was the only near-IR wavelength studied that consistently resulted in thermal coagulation and occlusion of the canine vas deferens without the formation of scrotal skin burns in a canine vasectomy tissue model, *ex vivo*.

CHAPTER 5: NONINVASIVE LASER COAGULATION OF THE CANINE VAS DEFERENS, *IN VIVO*

5.1 Introduction

We have developed a novel noninvasive vasectomy technique utilizing near-infrared laser irradiation in conjunction with cryogen spray cooling of the scrotal skin surface for successful thermal coagulation and occlusion of the vas deferens while minimizing scrotal skin injury in an *ex vivo* model [38]. Previous studies report that laser, cooling and wavelength parameters have been optimized in an *ex vivo* model and can now be tested in an *in vivo* model. In this study, we report our initial *in vivo* experience of noninvasive laser vasectomy in a canine model.

5.2 Materials and Methods

5.2.1 Animal Studies

All procedures were conducted at Johns Hopkins Hospital (Baltimore, MD) under an animal protocol approved by the Johns Hopkins Animal Review Committee. Noninvasive thermal occlusion of the vas was performed bilaterally in a total of 8 dogs (n = 16 vasa). The study was divided into two groups. In Group 1, the vas tissue from four dogs (n = 8 vasa) was harvested immediately after the procedure to provide acute data at Day 0. In Group 2, another four dogs were allowed to recover for 21 days post-operatively in a short-term chronic study before the vas tissue was harvested. The animals were monitored on a daily basis for any signs of distress. All of the dogs used

for this study were neutered after either Day 0 or Day 21 of the procedure and then adopted out to caring homes.

5.2.2 Laser Parameters

A 50-W, CW Ytterbium fiber laser (Model TLR1075-50, IPG Photonics, Oxford, MA) emitted radiation at a wavelength of 1075 nm which was then focused with a 300-mm-FL lens into a 400- μ m fiber optic patch-cord. A lens at the end of the patch-cord delivered a collimated laser beam to the tissue. A function generator was used to electronically modulate the fiber laser for pulsed delivery of the laser radiation, producing an average output power of 11.2 W, 500-ms pulse duration, 0.5 Hz pulse rate, and 3-mm-diameter spot at the scrotal skin surface (Figure 17).

5.2.3 Cooling Parameters

A dynamic cooling device (DCD, Candela Laser Corporation, Wayland, MA) was used to deliver the cryogen (halocarbon 134a, 1,1,1,2-tetrafluoroethane, boiling point = -26 °C) to the tissue surface through a solenoid valve. The solenoid valve was externally triggered using a function generator and an oscilloscope was used to view the pulse characteristics. Three cryogen pulses were applied to pre-cool the skin surface prior to laser irradiation. During irradiation, the cryogen spray was delivered intermittently between laser pulses with 60-ms pulse duration, pulse rate of 0.333 Hz, and a 2-cm-diameter spot concentric with the laser spot.

5.2.4 Indicators of Vas Occlusion

Vas burst pressure measurements were performed in a manner identical to that previously reported in chapter 3.

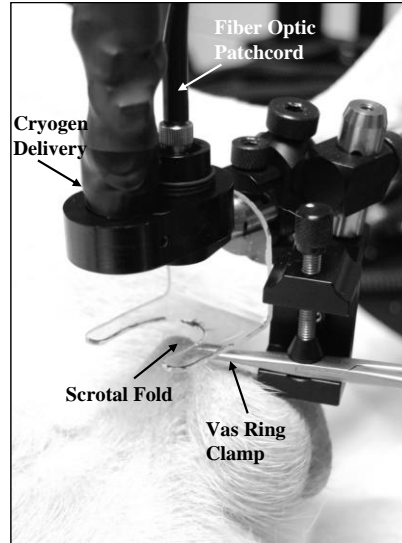


Figure 17. Image of the experimental setup. A standard no-scalpel vasectomy ring clamp is used to isolate the vas within the scrotal fold. A flexible fiber optic patch-cord with integrated lens delivers a 3-mm-diameter collimated laser beam to the skin surface. A solenoid valve delivers the cryogen coolant to the skin surface co-linear with the laser spot. A Plexiglas spacer maintains the working distance for the laser and cryogen spots.

5.3 Results

Thermal coagulation and occlusion of the vas was achieved in 15/16 vasa (94%). One vas was not present due to an anatomical defect. In 14/15 of the vasa (93%), burst pressures recorded were above typical ejaculation pressures. The coagulated vas bursting pressure averaged 283 ± 34 mmHg at Day 0 and 260 ± 77 mmHg at Day 21, significantly higher than reported vas ejaculation pressures of 136 ± 29 mmHg [15] (Table 8). Two of the lowest burst pressures were observed in Dog #7, where our urologists recorded having difficulty isolating the vasa. These low burst pressures may have been due to poor alignment of the vas with the laser, and only partial vas occlusion.

Table 8. Acute and chronic burst pressure measurements of coagulated canine vas.

Dog #	Vas	Pressure (mmHg)
Control (Ejaculation Pressure)		136 ± 29
Acute (Day 0)		
1	Left	305
	Right	203
2	Left	305
	Right	305
3	Left	305
	Right	232
4	Left	305
	Right	275
Average		283 ± 34
Chronic (Day 21)		
5	Left	305
	Right	305
6	Left	No Vas
	Right	305
7	Left	216
	Right	103
8	Left	283
	Right	305
Average		260 ± 77

At Day 0, the excised vas exhibited the characteristic indicators of thermal coagulation (blanching, hardening, and shrinkage of vas) with the full-thickness lesion extending 3 mm along the vas (Figure 18a). After 21 days, the vasa exhibited full-thickness scarring with the scar also extending 3 mm along the vas. (Figure 18b). The 3-mm-length of the coagulated and scarred vasa corresponded to the 3-mm-diameter laser spot used in the study. The only significant complication of the procedure was the presence of small scrotal skin burns. The burns coincided with where the laser beam overlapped the metal tips of the vas clamp. Both mechanical compression of the scrotal skin and small pin point burns were observed. These burns healed rapidly over the 21-day recovery period (Figure 19).

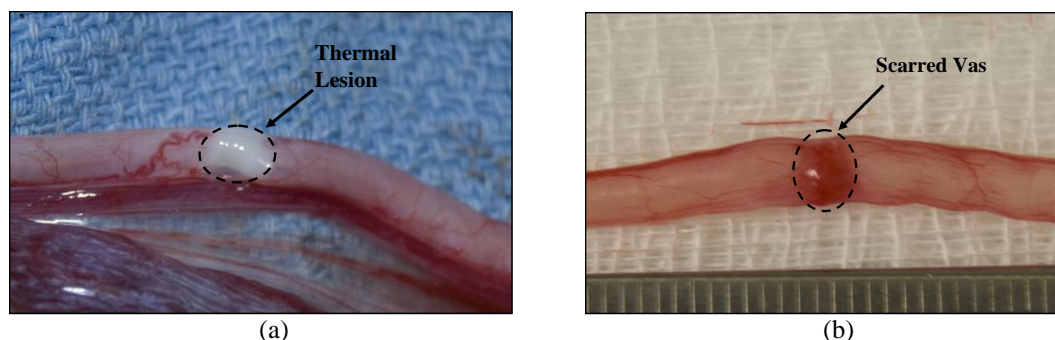


Figure 18. Representative images of canine vas deferens at a) Day 0 and b) Day 21; demonstrating successful thermal occlusion and scarring of the vas. The thermal lesion and scar tissue is full-thickness and 3 mm long, matching the 3 mm diameter laser spot used in the study.

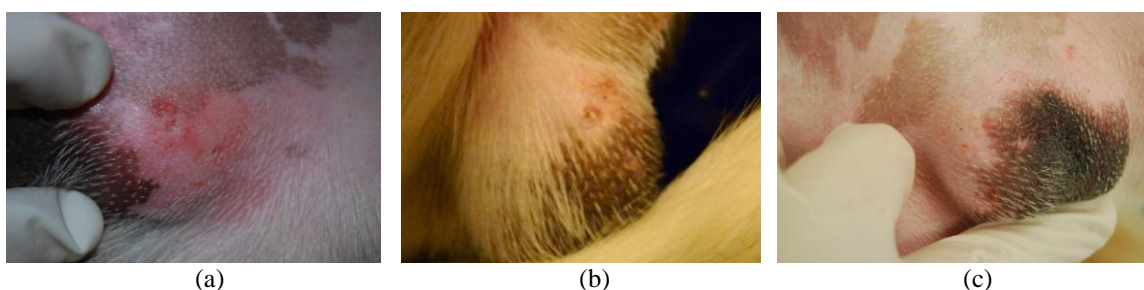


Figure 19. Photographs of scrotal skin at Days 0 (a), 12 (b), and 21 (c), showing development of minor scrotal skin burns. At Day 0, a small area of reddening is seen, corresponding to both laser heating and mechanical compression of the scrotal skin from the vas clamp. The larger area corresponds to a superficial freeze burn from the cryogen spray. By Day 21, the skin has completely healed.

5.4 Discussion

This study explores the application of near-IR laser radiation in conjunction with cryogen spray cooling for noninvasive thermal coagulation and occlusion of the canine vas, *in vivo*. Near-IR laser radiation with a wavelength of 1075 nm was chosen because it provides the deepest and most uniform penetration of the laser energy through the skin to the targeted vas deferens. Simultaneous application of cryogen spray cooling preferentially cooled the skin surface, preventing the development of serious scrotal skin burns during the procedure.

Several indicators were used to confirm thermal occlusion of the vas, including gross and histologic analysis of the vas and burst pressure measurements. Full thickness thermal lesions and scarring of the vas measuring about 3 mm in length, were achieved without any evidence of scrotal skin burns. Burst pressures for the coagulated vas measured about 300 mm Hg, over twice as high as the vas experiences during normal ejaculation [37].

The 93% success rate for vas occlusion is promising, considering that the canine model is a more difficult model than the human for vasectomy in several respects. First, the canine vas is more difficult to isolate than the human vas. Second, canine scrotal skin is thicker than human scrotal skin, making it not only more difficult for the laser radiation to penetrate the skin and reach the vas, but also resulting in a higher probability of skin burns. Finally, canine scrotal skin contains more hair which needs to be removed without skin irritation, so the hair follicles do not serve as absorption and burn sites for the laser radiation.

Although minor skin burns were observed during the procedure, our laboratory has since taken several steps to reduce this complication. First, the standard vasectomy clamp has been coated with an FEP Teflon material which is optically transparent in the near-infrared and thermally insulating, thus providing a buffer between the scrotal skin and vas clamp during the procedure. A cryogen mask has also been introduced to minimize skin irritation and reddening from splattering of the cryogen spray on the skin surface. Finally, removal of the canine scrotal skin hair with chemical depilators (e.g. Nair) and a razor blade has been replaced by a depilating gel.

Finally, it should be noted that near-IR laser radiation in conjunction with cryogen spray cooling may have several advantages over other technologies being explored for noninvasive vasectomy, such as high-frequency ultrasound (HIFU) [32, 33]. First, our success rate for targeting, thermal coagulation, and occlusion of the vas without skin burns approaches 100%, which has not been achieved previously in a noninvasive manner. Second, the scrotal skin burn complications observed in this study appear minor in scope compared with those observed using HIFU. Third, unlike HIFU, laser radiation and cryogen spray can be delivered in a non-contact mode, allowing the urologist to monitor the skin surface during the procedure. Fourth, noninvasive laser vasectomy utilizes a vas ring clamp for isolation of the vas, and can therefore easily be integrated into the no-scalpel clinical procedure currently used.

Despite initial success with development of noninvasive laser vasectomy, additional steps are needed to address the rare occurrence of skin burns such as implementing an optical clearing agent to reduce optical scattering. Additionally, long-term azoospermia and recanalization studies in a canine model need to be performed as definitive indicators of success for permanent male sterilization.

5.5 Conclusions

Noninvasive laser thermal coagulation and occlusion of the vas deferens was achieved in a canine animal model, *in vivo*, with a 93% success rate. Burst pressure measurements and gross observation of the vas were used as short-term indicators of success. Minor scrotal skin burns were observed, but healed rapidly over the 21-day recovery period. However, further chronic *in vivo* animal studies will be necessary to optimize the laser/cooling treatment parameters and confirm long-term vas occlusion

with absence of sperm in the ejaculate, before clinical application. The use of more advanced techniques such as optically clearing the skin could also help eliminate scrotal skin burns.

CHAPTER 6: USE OF AN OPTICAL CLEARING AGENT DURING NONINVASIVE LASER VASECTOMY

6.1 Introduction

Optical clearing agents (OCA) have been explored over the past decade with great interest by numerous investigators for reducing light scattering in skin and increasing the optical transmission through skin for both therapeutic and diagnostic light-based procedures [41-54]. Although the mechanism of optical skin clearing is still being studied, the basic affect is understood. OCA's typically have higher indices of refraction (n) than the skin components. For example, glycerol has an $n=1.47$. Common skin constituents, collagen ($n=1.42$), stratum corneum ($n=1.55$), and water ($n=1.33$) have different n values. As the water content in the skin is reduced due to diffusion driven by the osmotic stress induced by the OCA, skin constituents with higher n 's become more closely packed and form a homogenous medium. As the OCA diffuses into the tissue, it further matches the tissue matrix, leading to a significant reduction in light scattering, and a corresponding increase in optical transmission [48].

Common OCA's include Dimethyl Sulfoxide (DMSO), glycerol, glucose, and other sugar compounds. In this study, we used a DMSO/glycerol mixture, taking advantage of the excellent transport properties of DMSO while minimizing its concentration due to toxicity concerns, and relying on glycerol for optical clearing of the scrotal skin.

The Madajet, a device marketed for noninvasive delivery of local anesthesia through the scrotal skin during conventional no-scalpel vasectomy, was used in this study for delivery of the OCA. The device provides a less invasive means of temporarily breaching the stratum corneum than previously reported mechanical and optical methods (e.g. needle injection, tape stripping, sandpaper, micro-needle rollers, flashlamp irradiation of carbon dots, and laser perforation) [46-48, 52]. The Madajet also allows delivery of much smaller quantities of OCA (0.4 ml) than our preliminary studies with conventional syringe needle injection (4 ml). This is significant because it allows use of an order of magnitude less volume of DMSO, thus reducing the potential risks of tissue toxicity.

The purpose of this study is to explore the use of an optical clearing agent (OCA) to increase the transparency of the scrotal skin, thus reducing the laser power necessary for successful thermal coagulation of the canine vas deferens and completely eliminating the formation of minor scrotal skin burns, observed during previous studies.

6.2 Methods

6.2.1 Optical Clearing Agent (OCA)

A 1:3 ratio of dimethyl sulfoxide (DMSO) and glycerol was used as an OCA in both *ex vivo* and *in vivo* tissue. DMSO was chosen because of its transport properties in tissue. However, the concentration of DMSO was minimized due to concerns about its toxicity. Glycerol was chosen because it is biocompatible and has been shown to increase skin transparency. The OCA was delivered to the skin using a pneumatic jet device (Madajet, AMI, Flushing, NY) normally used for noninvasive delivery of anesthesia during the conventional no-scalpel vasectomy procedure. A total of four sites

on the skin surface were treated with the OCA, corresponding to a diamond configuration immediately bordering the targeted vas area. Each of the four sites received 0.1 ml of the OCA in the same 1:3 DMSO/glycerol ratio, resulting in a total of 0.4 ml delivered to the skin per a vas. The skin was then allowed to sit for 30 min, providing sufficient time for the OCA to diffuse into the treatment site and increase the transparency of the scrotal skin. The treatment site was not directly treated with the Madajet, so as to avoid unnecessary tissue swelling which may otherwise interfere with the delivery path of the laser radiation to the underlying vas.

6.2.2 *Ex Vivo* Tissue Studies

Scrotal skin and vas tissue was harvested from male dogs immediately after sacrifice for unrelated experiments. The tissue was then partially submerged in a temperature-controlled saline bath, placed on a hotplate, and maintained at approximately 37 °C. A standard 4.0-mm-ID vasectomy clamp (VE-1, AMI), custom coated with FEP Teflon tubing for thermal insulation, was then used to tightly grasp the vas and surrounding scrotal skin. These studies provided a strong basis for choosing the proper *in vivo* parameters

6.2.3 *In Vivo* Animal Studies

All procedures were conducted under an animal protocol approved by the Johns Hopkins Animal Review Committee. Noninvasive thermal occlusion of the vas was performed bilaterally in a total of 5 dogs (n = 10 vasa). The study was divided into two groups. In Group 1, noninvasive laser vasectomy was performed at an average power of 9.2 W and cryogen cooling rate of 0.25 Hz without application of an OCA. In Group 2, noninvasive laser vasectomy was also performed but at an average power of 7.0 W and

cryogen cooling rate of 0.20 Hz with application of an OCA. These parameters were chosen based on the success of previous *ex vivo* tissue studies. Figure 20 shows the experimental setup for the *in vivo* canine studies. For both groups, after completion of the procedure, the vas tissue was harvested, and burst pressure measurements were performed. All of the dogs used for this study were neutered immediately after the procedure and then adopted out to caring homes.

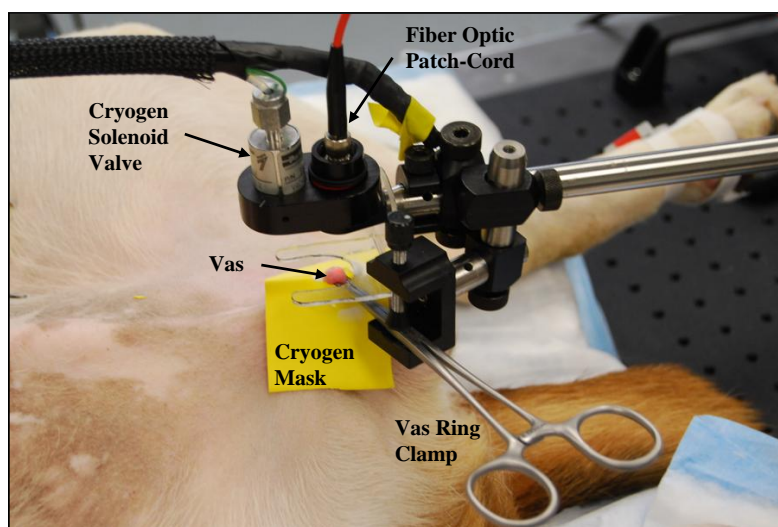


Figure 20. Experimental setup for noninvasive laser vasectomy in dogs, *in vivo*.

6.2.4 Laser Parameters

A 50-W Ytterbium fiber laser (TLR1075-50, IPG Photonics, Oxford, MA) emitted radiation with a wavelength of 1075 nm which was then focused with a 300-mm-FL lens into a 400- μm fiber optic patch-cord. A lens at the end of the fiber patch-cord provided a collimated laser beam to the tissue surface. A function generator was used to electronically modulate the fiber laser for operation in pulsed mode, producing an average output power of 7.0-11.7 W, 500-ms pulse duration, 0.5 Hz pulse rate, and 3-mm-diameter spot at the scrotal skin surface.

6.2.5 Cooling Parameters

A dynamic cooling device (DCD, Candela Laser Corp., Wayland, MA) was used to deliver the cryogen (halocarbon 134a, 1,1,1,2-tetrafluoroethane, BP = - 26 °C) to the tissue surface through a solenoid valve. Three cryogen pulses were applied to pre-cool the skin surface prior to laser irradiation. During laser irradiation, the cryogen spray was delivered with a 60-ms pulse duration, pulse rate of 0.20-0.33 Hz, and a 2-cm-diameter spot concentric with the laser spot. A cryogen mask was used to thermally insulate adjacent skin from the cryogen spray and avoid superficial freeze burns observed during previous studies.

6.2.6 Indicators of Vas Occlusion

Vas burst pressure measurements were performed to quantify closure of the thermally coagulated vas. A 3-way stopcock was connected to a 50 mL syringe, pressure transducer, and hypodermic needle. The syringe was filled with saline which was also distributed throughout the system. The vas was attached to a 27-G hypodermic needle and clamped with hemostats. Saline was then slowly pumped into the vas lumen using a syringe pump at a rate of 0.01 ml/s, resulting in an elevated pressure, as measured by a pressure analyzer unit, until the vas burst open.

6.3 Results

6.3.1 Transmission Studies

Transmission studies performed in canine scrotal skin samples, *ex vivo*, by placing a power detector at the position of the vas and recording the transmitted power of a low power beam, demonstrated that application of the OCA for 30 min improved skin transparency by $26 \pm 5 \%$, as shown in Figure 21. These values were used to calculate the laser power necessary for the noninvasive laser vasectomy studies. Although optical transmission continued to increase beyond 30 min, these studies were not extended beyond 30 min because of concern that longer surgical preparation times would not be suitable for vasectomy, which is already a brief clinical procedure.

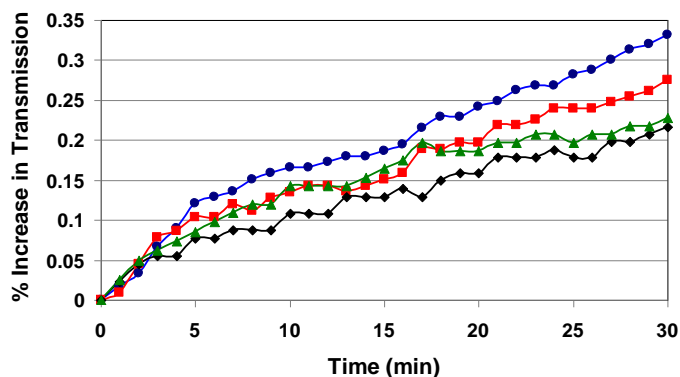


Figure 21. Optical transmission studies performed in canine scrotal skin, *ex vivo*, after application of an optical clearing agent using the Madajet. Percent increase ($n=4$ samples) in optical transmission is plotted as a function of time. Measurements were taken every minute immediately behind 1 mm of scrotal skin, in the vicinity of where the vas rests.

6.3.2 Noninvasive Laser Vasectomy Studies

Burst pressure results as a function of the laser/cooling parameters for both the *ex vivo* and *in vivo* noninvasive laser vasectomy procedures performed in this study, as well as in previous studies [38, 55], are compared in Table 9. The average power necessary for successful noninvasive laser vasectomy was reduced from 9.2 W without OCA (BP =

291 ± 31 mmHg) to 7.0 W with OCA (BP = 292 ± 19 mmHg). Control studies without OCA at 7.0 W failed to coagulate the vas with burst pressures (82 ± 28 mmHg) significantly below typical ejaculation pressures (136 ± 29 mmHg) [37]. These lower power settings also eliminated the formation of minor scrotal skin burns previously observed using higher average powers to the tissue.

Table 9. Comparison of burst pressure results for *ex vivo* and *in vivo* noninvasive laser vasectomy studies performed with and without an optical clearing agent (OCA).

Study	Laser Power (W)	Cooling Rate (Hz)	Burst Pressure (mmHg)	N
Control Ejaculation Pressure [37]			136 ± 29	
<i>Ex Vivo</i> [38]	11.7	0.33	295 ± 72	10
<i>In Vivo</i> [55]	11.2	0.33	283 ± 34	8
<i>Ex Vivo</i>	9.2	0.25	296 ± 18	5
<i>In Vivo</i>	9.2	0.25	291 ± 31	5
<i>Ex Vivo</i>	7.0	0.20	82 ± 28	5
<i>Ex Vivo</i> w/ OCA	7.0	0.20	298 ± 15	5
<i>In Vivo</i> w/ OCA	7.0	0.20	292 ± 19	5

Images of the canine vas and scrotal skin immediately after the *in vivo* noninvasive laser vasectomy procedure are shown in Figure 22a. Thermally coagulated sections of the canine vas demonstrated characteristic signatures of blanching and shrinkage along an approximately 3 mm long segment, corresponding to the laser spot diameter (Figure 22a and 22c). Grossly, thermal effects were similar when the vas was coagulated using 9.2 W, 0.25 Hz w/o OCA or when 7.0 W, 0.20 Hz, and OCA were used (Figures 22a and c, respectively). Figures 22b and 22d show the scrotal skin surface in the region of the procedure both with and without the use of OCA, respectively. In Figure 22b, the blanched area corresponds to where the optical clearing agent was applied, and the two compression marks correspond to where the vas ring clamp was closed down on the scrotal fold (7.0 W, 0.20 Hz, w/ OCA). In comparison to Figure 22d

(which shows the scrotal skin surface after the procedure at 9.2 W and 0.25 Hz without OCA), the scrotal skin after use of OCA (represented in Figure 22b) appeared to have more acute tissue trauma. This was, in part, due to the need to leave the vas ring clamp on the skin for a prolonged period of time as the OCA needed 30 min to diffuse into the skin. This complication may be eliminated in a human model, where the vas is much easier to grasp and the OCA timing and vas surgical preparation can more easily be coordinated.

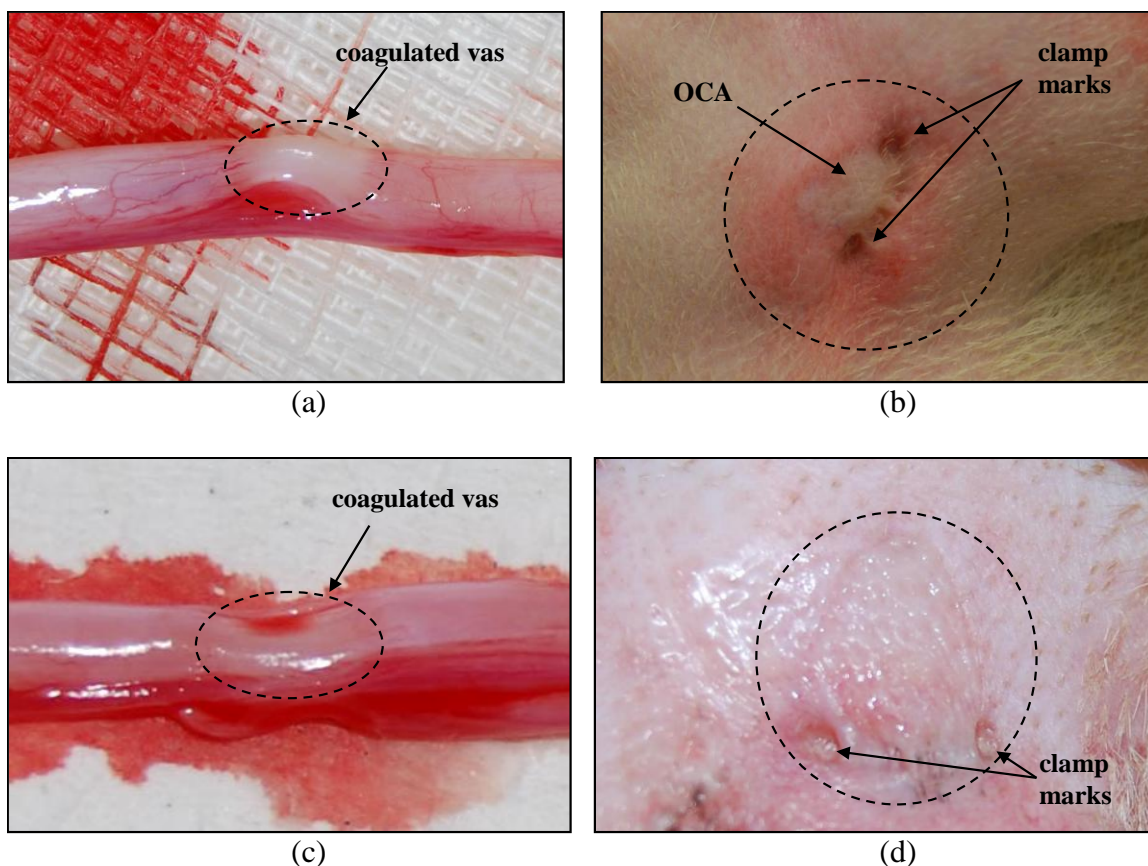


Figure 22. Gross analysis of the vas and scrotal skin conducted immediately after the noninvasive laser vasectomy procedure on dogs, *in vivo*. (a) Thermally coagulated section of the canine vas (dotted circle) demonstrating characteristic signatures of blanching and shrinkage along an approximately 3 mm long segment corresponding to the laser spot diameter (7.0 W, 0.20 Hz, w/ OCA). (b) Scrotal skin surface in the region of the procedure (dotted circle). The swollen area corresponds to where the optical clearing agent was applied. (c) Thermally coagulated section of the canine vas (dotted circle) demonstrating characteristic signatures of blanching and shrinkage along an approximately 3 mm long segment corresponding to the laser spot diameter (9.2 W, 0.25 Hz, w/o OCA). (d) Scrotal skin surface after procedure without OCA (9.2 W, 0.25 Hz, w/o OCA).

6.4 Discussion

Higher laser power is associated with increased local tissue trauma. Indeed, in this study, by recalibrating our laser, we were able to decrease the power setting (from 11.2 W to 9.2 W) with equivalent or superior occlusive results to our previous studies while minimizing skin injury [55]. In addition, this study demonstrates that it is possible

to decrease the average power even further to 7 W if the procedure is combined with noninvasive delivery of an optical clearing agent to the scrotal skin, which increases skin transparency. Using this technique, the vas was consistently thermally coagulated and occluded as indicated by the high vas burst pressure measurements, and indicators of minor scrotal skin burns observed during previous procedures were also completely eliminated.

Although the noninvasive aspect of our laser vasectomy procedure remains the primary attraction of this technique, cost is an important factor as well. It should be noted that the cost of surgical lasers usually scales with output power. Thus, any approach that results in a net reduction in laser power for noninvasive vasectomy may directly translate into a less expensive procedure. This is important because the current, conventional no-scalpel vasectomy procedure is already a short, inexpensive procedure.

6.5 Conclusions

Application of an optical clearing agent reduced the average power necessary for successful noninvasive laser coagulation of the vas deferens by approximately 25%. This technique may result in the use of a less expensive laser system and eliminate the formation of scrotal skin burns during the procedure.

CHAPTER 7: OPTICAL AND THERMAL SIMULATIONS OF HUMAN VAS DURING LASER VASECTOMY

7.1 Introduction

Although the canine is the most commonly accepted large animal model for surgical vasectomy research studies, there is a significant difference in the optical and thermal properties of canine and human skin. The objective of the study is to map the thermal and light transport properties in human tissue so a more simple clinical transition can be made. Since the matrix of laser and cooling parameters is too large to completely explore in experiments, computer simulations are used to predict the optimal set of laser and cooling parameters for a successful noninvasive laser vasectomy procedure. In this study, results from a Monte Carlo model of light transport in tissue are used as the input for a heat transfer model to map temperatures in the human scrotal skin and vas during noninvasive laser vasectomy.

7.2 Methods

7.2.1 Monte Carlo Model of Light Transport in Tissue

A previously reported Monte Carlo (MC) program was adapted for these studies [56]. This program was used to model photon transport through tissue layers having plane parallel geometry. This assumption is generally an acceptable condition since the geometry of the tissue in the vicinity of the infinitely thin “pencil” photon beam used by the MC program can be treated as planar even though it may be slightly curved, such as in our application. We can compensate for the overall curvature of the tissue, which is

small at the interaction site, by assuming that the interaction site is a series of planar cylinders corresponding to the tissue layers. Even though we cannot model photon propagation around the curvature of the tissue, the attenuation of the beam at the depth of the vas deferens is such that the energy distribution will be minimally affected by the curvature.

One million photons were used in the MC program to achieve a sufficiently thorough distribution of photons in the tissue. The simulations were run on an Intel based personal computer with an Intel® Core™2 Duo P8600 processor and 4 gigabytes of RAM. Each run of 1 million photons took approximately 100 seconds. A previously reported convolution program was used to fit the results to an actual laser beam of known power, profile, and beam size [57]. In our study, these results were convolved for a Gaussian laser beam of 3.0-mm-diameter for average laser powers of 5-9 W.

The overall dimensions of the tissue model, and the dimensions of the individual tissue layers (Figure 23), were chosen to match known thicknesses for human scrotal skin and vas deferens [58]. The final tissue model incorporated a skin layer which curved back on itself and enclosed the vas deferens in an effort to simulate the clinical procedure used to clamp and isolate the vas deferens with a vasectomy ring clamp. The total tissue dimensions modeled measured 4.44 mm depth and 4.50 mm in the radial direction. The MC model was divided into 50 equally spaced bins in radial direction, 100 bins in z-direction, and 30 bins in theta direction. Since the model was axisymmetric about the z-axis, this was considered to be a 2D model and the angular direction could be neglected. The overall spatial resolution of the MC model was 44 μm in z-direction and 90 μm in radial direction.

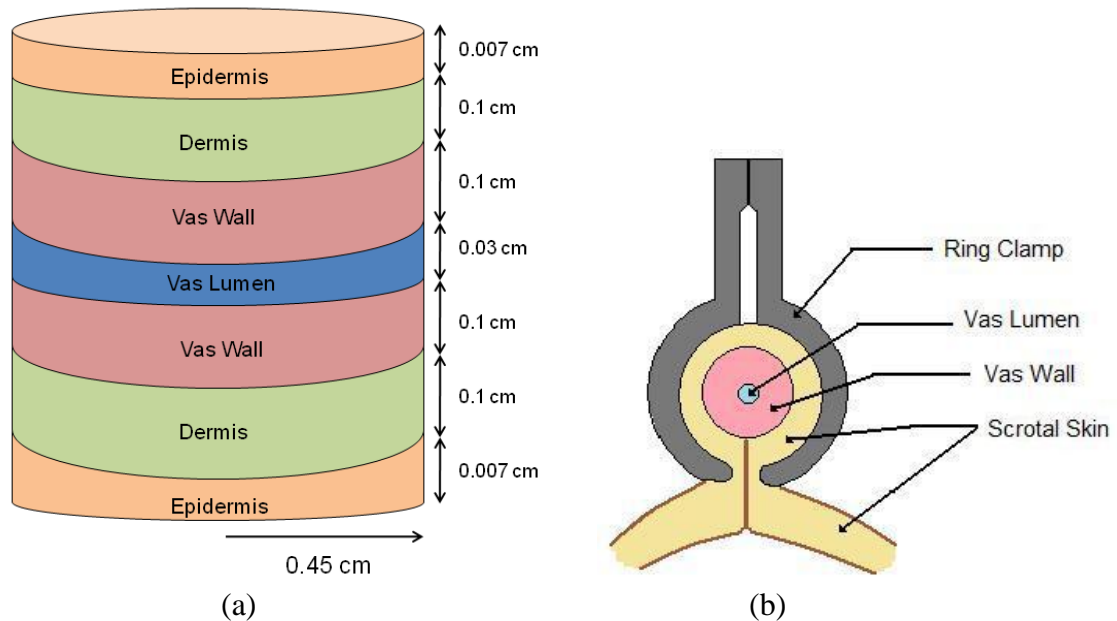


Figure 23. (a) Geometry of tissue layers used for Monte Carlo and heat transfer simulations. The epidermis and dermis layers of the skin appear both above and below the vas in an effort to incorporate the folded tissue into a planar model when it is placed inside a conventional vasectomy ring clamp, as shown in (b).

The optical properties (absorption, scattering, anisotropy) of the skin layers (epidermis and dermis) were compiled from the literature [39, 59, 60]. The optical properties of the vas wall were modeled as similar to muscle tissue as a good approximation[61]. The vas lumen was modeled as water [40]. The index of refraction (n) for all tissue layers except epidermis and lumen was set to $n=1.37$. The epidermis was set to $n=1.42$, based on previous reports [59]. The anisotropy factor, g , was set to 0.9 for all tissue layers [62] except the vas lumen. Table 10 summarizes the values for optical properties of the human tissue layers used in the MC model.

Table 10. Optical properties of human tissues at 1064 nm.

	Scattering (cm^{-1})	Absorption (cm^{-1})	Anisotropy Factor	Index of Refraction	Layer Thickness (cm)
Epidermis	300	0.200	0.9	1.42	0.007
Dermis	188	0.490	0.9	1.37	0.100
Vas Wall	60	0.500	0.9	1.37	0.100
Vas Lumen	0.0001	0.128	0.0	1.327	0.030

The effect of application of an optical clearing agent (OCA) to the human skin on transmission was also incorporated into the MC model. Our laboratory has previously reported successful application of an OCA (Glycerol/Dimethyl Sulfoxide) during preclinical studies, resulting in a 25% increase in optical transmission in skin during noninvasive laser coagulation of the canine vas [63]. Recently, other research groups developing the latest generation of OCA's (e.g. PEG400/Thiazone and PEG400/DMSO) have demonstrated much greater than 50% increase in optical transmission in skin [64, 65]. Based on these previous reports, three cases were considered: (1) a 25% increase in transmission produced by a reduction in scattering, (2) a 25% increase in transmission produced by a reduction in both absorption and scattering, and (3) a 50% increase in transmission produced by a reduction in both absorption and scattering. Table 11 summarizes the new optical property values of skin for these three cases.

Table 11. Optical properties of human skin at 1064 nm after application of an OCA.

	Scattering (cm^{-1})	Absorption (cm^{-1})	Index of Refraction
Case 1: 25% increase in transmission by reduction of scattering only			
Epidermis	170	0.20	1.42
Dermis	105	0.49	1.37
Case 2: 25% increase in transmission by reduction of absorption and scattering			
Epidermis	200	0.15	1.42
Dermis	125	0.30	1.40
Case 3: 50% increase in transmission by reduction of absorption and scattering			
Epidermis	135	0.10	1.42
Dermis	75	0.20	1.40

7.2.2 Heat Transfer Model

Tissue temperatures were calculated using ANSYS Version 11.0 (UP20070125), which is a general purpose commercial finite element package used to solve thermal problems. The heat transfer model was matched to the MC model dimensions, and the mesh set to equally spaced areas of $44 \times 90 \mu\text{m}$. Four-node axisymmetric elements were used in the mesh. Each layer of tissue was represented in the mesh and given thermal properties consistent with human tissue, with the values compiled from several sources [66-68]. Table 12 summarizes the values for the thermal properties of the human tissue layers used in the heat transfer model.

Table 12. Thermal properties of human tissues.

	Specific Heat [J/kgK]	Thermal Conductivity [W/mK]	Density [kg/m ³]
Epidermis	3590	0.240	1070
Dermis	3300	0.450	1070
Vas Wall	3639	0.568	1050
Vas Lumen	4178	0.580	994.1

To simulate laser pulses, the absorption data output from the convolved MC model was converted to the input of the heat transfer model since the absorption data represents how much energy is present in each bin due to the laser. No data manipulation was necessary other than converting the spatial heat source from J/cm^3 to J/m^3 and converting the data structure from a 1D linear array to a 2D matrix where each matrix element corresponded to a mesh element.

A cryogen spray cooling system, using 1,1,1,2 tetrafluoroethane (R-134a), was used to minimize surface tissue damage in previous experiments [69, 70]. This was modeled in the simulation with a convective heat transfer coefficient of $2400 \text{ W/m}^2\text{K}$ and

a bulk temperature of $-26\text{ }^{\circ}\text{C}$ present on the skin surface and penetrating the skin up to $100\text{ }\mu\text{m}$, corresponding to previous reports [71]. Convective heat transfer occurred on the surfaces of the model that were exposed to air. The convective film coefficient of air was set to 40 W/m^2 and room temperature was set to $20\text{ }^{\circ}\text{C}$ [72]. The initial temperature of the model was set at normal scrotal skin temperature of $33\text{ }^{\circ}\text{C}$.

The laser simulations were conducted using a laser pulse duration of 500 ms and a laser pulse repetition rate of 1 Hz. Cryogen spray cooling simulations were conducted with pulse durations of 60-100 ms (plus 300 ms of time necessary for the cryogen to completely evaporate, as previously reported [71]) and pulse repetition rates of 0.5 - 1.0 Hz. The entire simulation was conducted for a total of 60 s and the final temperatures for each element were reported in a color map contour graph. Temperature vs. time data was also obtained for each node in the mesh. A summary of the laser and cooling parameters is provided in Table 13.

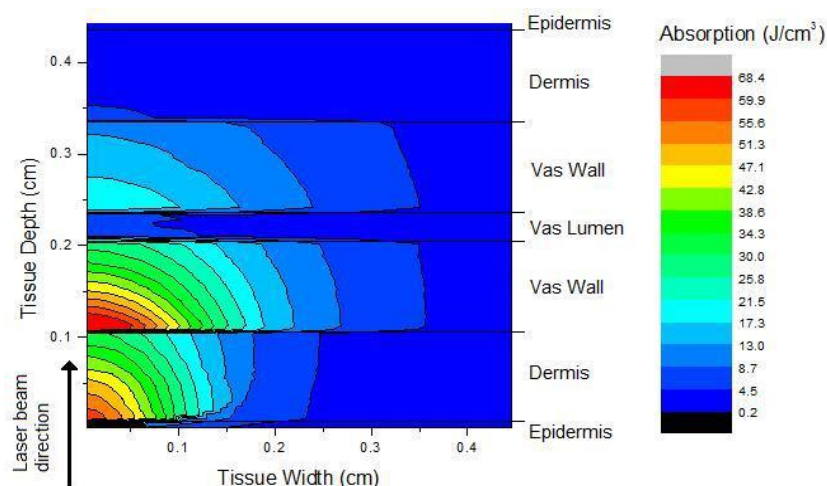
Table 13. Laser and cooling parameters used in this study.

Laser Parameters		Cooling Parameters	
Wavelength (nm):	1064	Pulse Duration (ms):	60 - 100
Average Power (W):	5 - 9	Pulse Rate (Hz):	0.5 - 1.0
Pulse Duration (ms):	500	Spot Diameter (mm):	10
Pulse Rate (Hz):	1.0	Cooling Time (s):	60
Spot Diameter (mm):	3.0	Boiling Point ($^{\circ}\text{C}$):	-26
Irradiation Time (s):	60	Convection ($\text{W/m}^2\text{k}$):	2400

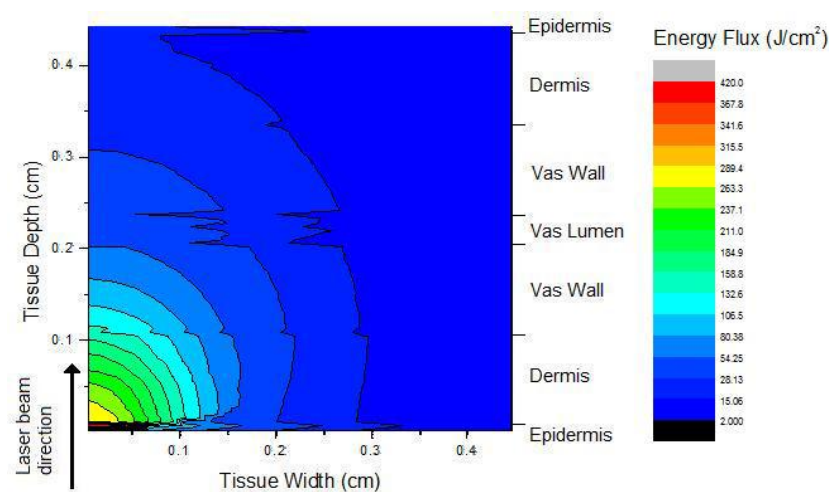
7.3 Results

A Monte Carlo 2D color plot of both photon absorption and energy flux contour lines for the optimal set of laser and cooling parameters used in this study (Wavelength = 1064 nm, Average power = 6 W, Laser spot diameter = 3 mm, Optical clearing = 50%) is shown in Figure 24. This plot only shows the right half of the tissue (assuming

symmetry) with a laser beam radius of 1.5 mm incident on the bottom of the tissue. In this simulation, the vas deferens absorbed ~ 25% of the total number of photons, while the epidermis and dermis layers of the skin absorbed ~ 11% of the total number of photons. As the laser energy travels through the tissue it is absorbed more heavily in the vas walls due to the higher absorption coefficient of the tissue. The difference in the optical properties effectively changes the energy profile as it travels through the tissue, and this causes the apparent discontinuities in absorption across tissue layers observed in Figure 24a, while the radiant exposure (flux) plotted in Figure 24b remains continuous.



(a)



(b)

Figure 24. Representative map of photon (a) absorption and (b) energy flux in the tissue for the Monte Carlo model of light transport, for the optimal laser parameters (Wavelength = 1064 nm, Power = 6 W, Laser spot = 3 mm, Optical clearing = 50%).

A 2D thermal map with temperature contour lines is shown in Figure 25 for the optimal set of laser parameters listed above and the optimal cooling parameters (Cryogen pulse duration = 60 ms, Cryogen pulse rate = 1 Hz), near the end of the procedure ($t = 60$ s). The red temperature region corresponds to thermal coagulation temperatures of ~ 60 °C through the entire vas wall and lumen, while the other color regions (blue, green, and yellow) correspond to safe tissue temperatures below ~ 52 °C. The orange region

represents a borderline area in which tissue coagulation is possible. This may be of concern, since the orange region in the dermis above the vas wall (corresponding to the bottom of the scrotal fold) is relatively large. This presents the possibility that although the skin surface is preserved during the procedure, scrotal skin burns have the potential to occur on the underside of the scrotal fold.

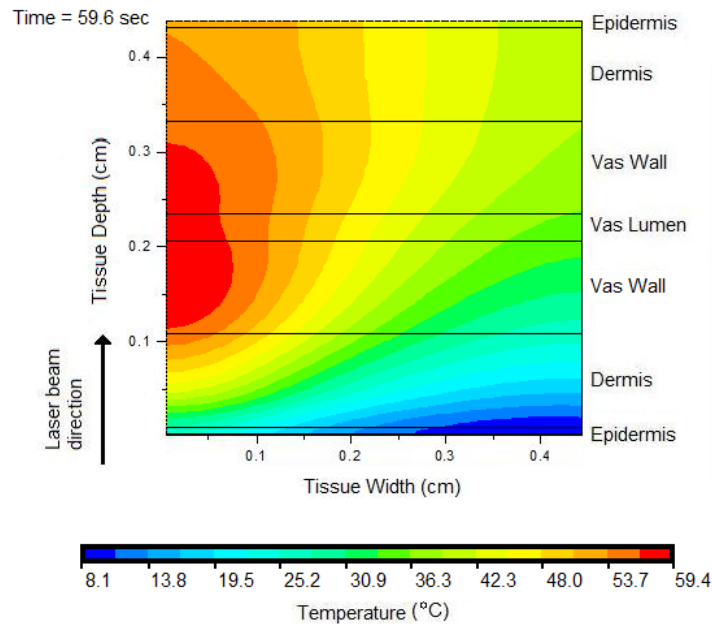


Figure 25. Map of tissue temperatures observed for heat transfer model. The laser beam is incident on skin surface from the bottom, and the temperature map only shows right half of laser beam and tissue due to symmetry. This map was taken near the end of the procedure ($t = 60$ s), for optimal treatment parameters (Wavelength = 1064 nm, Power = 6 W, Laser pulse duration = 500 ms, Laser pulse repetition rate = 1 Hz, Laser spot = 3 mm. Cryogen pulse duration = 60 ms, Cryogen pulse rate = 1 Hz).

Temperature versus time data for epidermis, dermis, and vas, taken along the central axis of the thermal map (from Figure 25) is plotted in Figure 26. Temperatures above 52 °C are reached in the vas after 20 s, leading to thermal coagulation and occlusion of the vas, while the epidermis and dermis layers of the skin remain safely below 52 °C for the entire procedure, thus preventing the formation of scrotal skin burns.

The cyclical nature of the epidermis and dermis temperatures matches that of the cryogen cooling pulse rate of 1 Hz. The initial temperature of the epidermis ($-50\text{ }^{\circ}\text{C}$) is caused by the first cryogen cooling pulse, which causes the skin to cool further before the laser starts heating the tissue. This effect has been previously reported, in which the cryogen spray cools considerably when traveling to the skin surface [71], due to the high convective film coefficient of the coolant.

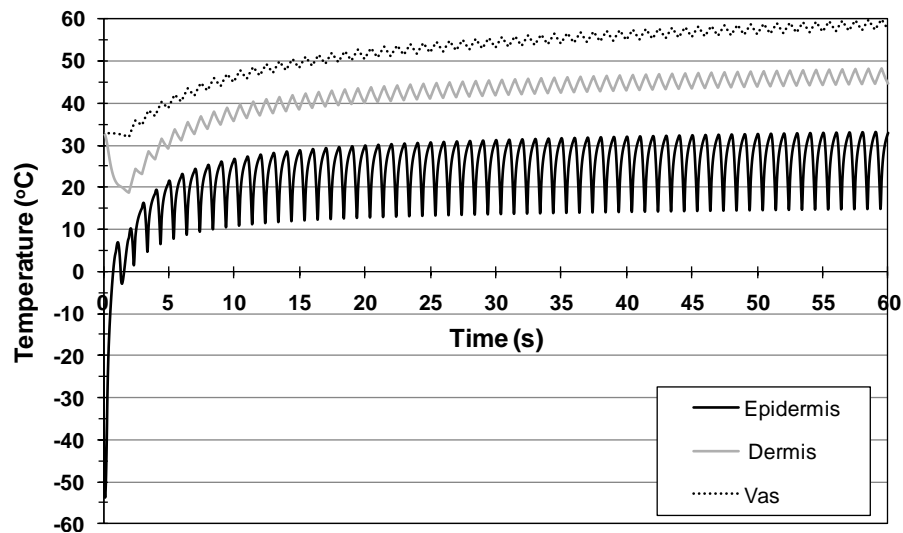


Figure 26. Temperature versus time data for the epidermis, dermis, and vas, taken along the central axis of the thermal plot in Figure 23, is shown. Temperatures above $52\text{ }^{\circ}\text{C}$ are reached in the vas after about 20 s leading to thermal coagulation and occlusion of the vas, while the epidermis and dermis layers of the skin remain safely below $52\text{ }^{\circ}\text{C}$ for the entire procedure, thus preventing the formation of scrotal skin burns.

In the simulations where the optical properties of the vas deferens are varied we observe a slight difference in the absorption distribution. When the optical absorption and scattering are set to +20% of the assumed value we see that the vas layers absorb almost 29% of the total energy. In this case we expect, and do see, an increase in the temperature of the vas and immediate surrounding tissues by a maximum of $5\text{ }^{\circ}\text{C}$. When the optical properties of the vas are estimated at -20% of the assumed value we see that

the vas layers absorb only 21% of the total energy, and this corresponds to a temperature decrease in the vas layers and immediate surrounding tissue by approximately 7 °C.

7.4 Discussion

The availability of a rapid, cost-effective, straightforward, and noninvasive technique for male sterilization is likely to improve the popularity of vasectomy. We have reported successful targeting, thermal occlusion, and scarring of the vas while minimizing scrotal skin injury in both *ex vivo* and *in vivo* canine models [38, 63]. However, there is a significant difference in the optical and thermal parameters between canine and human skin. It is necessary to use computer simulations of Monte Carlo light transport in tissue and heat transfer simulations to simplify the large matrix of laser and cooling parameters involved in the procedure and provide some predictions on the optimal set of treatment parameters for noninvasive laser vasectomy in humans.

Previous studies have shown that for time scales on the order of tens of seconds, a critical temperature above approximately 52 °C is necessary to achieve thermal coagulation of skin [73]. This study demonstrates that it should be possible to achieve the temperatures necessary in the human vas deferens for thermal coagulation and occlusion of the vas, while preventing adverse side-effects, such as the formation of burns in the epidermal and dermal layers of the scrotal skin, by keeping these tissue layers at safe temperatures below 52 °C. The results of the thermal map also show that it is possible to obtain uniform heating and thermal coagulation across the vas walls and lumen, while preserving the epidermis and dermis to a depth of approximately 1 mm. It should be noted that preservation of such a large skin thickness is not unprecedented, and

that similar results have been previously reported for experiments using both canine and porcine skin models [3, 4, 56, 63].

The results of this study also demonstrate the importance of the application of optical clearing agents (OCA) to the scrotal skin prior to the procedure. Application of an OCA is critical to the success of the procedure because human skin has significantly higher absorption and scattering properties than animal skin, leading to a decrease in optical transmission. The OCA reverses this trend by reducing absorption and scattering in the human skin, resulting in higher optical transmission and less probability of skin burns. The results of this study indicate that at least a 50% increase in transmission is needed from the OCA for a successful procedure.

The results of these MC and heat transfer models provide valuable insight into the effect of individual laser and cooling parameters on tissue temperatures. Considering the large matrix of treatment parameters, such information is vital for helping to predict the optimal set of treatment parameters for transitioning from preclinical to clinical studies. However, as with any computer model, there are several assumptions and limitations of the models used in this study that need to be mentioned: this model did not incorporate the curvature of the scrotal skin fold within the vasectomy clamp, but instead, for simplicity, a planar geometry was used; changes in the optical properties of the tissue layers due to compression and thermal coagulation were not included in the MC model; and the effect of blood perfusion in the tissues was not incorporated into the heat transfer model.

7.5 Conclusions

Monte Carlo and heat transfer simulations indicate that it is possible to noninvasively thermally coagulate the human vas without adverse effects (e.g. scrotal skin burns) if an optical clearing agent is applied to the skin prior to the procedure.

CHAPTER 8: ULTRASOUND IMAGING OF THE CANINE VAS DEFERENS

8.1 Introduction

During conventional vasectomy the damage to the vas is visually confirmed by the performing surgeon. However, our noninvasive laser vasectomy technique, by definition, does not provide the urologist with any tissue to confirm successful closure of the vas. A diagnostic method that can noninvasively and quantitatively confirm successful vas closure is necessary to confirm consistent and reproducible results. The current no scalpel vasectomy method has very high success rates so the noninvasive vasectomy must meet or exceed these high standards. High-frequency diagnostic ultrasound has recently been used to measure the anatomy of the normal vas deferens [58]. In this study, ultrasound is introduced as a noninvasive diagnostic method for confirming successful thermal occlusion and scarring of the canine vas after noninvasive laser vasectomy. This study also builds upon previous acute studies, by demonstrating, for the first time, successful noninvasive laser coagulation and occlusion of the canine vas in a short-term, *in vivo* model without any adverse complications such as scrotal skin burns. This was primarily due to a first iteration of a modified vasectomy prototype ring clamp that was used to manually isolate the vas beneath the scrotal skin surface for co-location with the cryogen and laser spots (Figure 27).



Figure 27. First iteration of the noninvasive vasectomy prototype clamp, using standard NSV clamp.

8.2 Methods

8.2.1 Animal Studies

All procedures were conducted under an animal protocol approved by the Johns Hopkins Animal Review Committee. Noninvasive thermal occlusion of the vas was performed bilaterally in a total of nine dogs. Vas were harvested and used for burst pressure measurements at Day 0 (3 dogs) and Day 28 (6 dogs). The animals were monitored on a daily basis for signs of distress during the study and then neutered and adopted out to caring homes at the completion of the study.

8.2.2 Laser Parameters

A 50-W, CW Ytterbium fiber laser (Model TLR1075-50, IPG Photonics, Oxford, MA) emitted radiation at a wavelength of 1075 nm which was then focused with a 300-mm-FL lens into a 400- μ m fiber optic patch-cord. A lens at the end of the patch-cord delivered a collimated laser beam to the tissue. A function generator was used to electronically modulate the fiber laser for pulsed delivery of the laser radiation,

producing an average output power varied between 6-9W, 500-ms pulse duration, 1 Hz pulse rate, and 3-mm-diameter spot at the scrotal skin surface.

8.2.3 Cooling Parameters

A dynamic cooling device (DCD, Candela Laser Corporation, Wayland, MA) was used to deliver the cryogen (halocarbon 134a, 1,1,1,2-tetrafluoroethane, boiling point = -26 °C) to the tissue surface through a solenoid valve. The solenoid valve was externally triggered using a function generator and an oscilloscope was used to view the pulse characteristics. Three cryogen pulses were applied to pre-cool the skin surface prior to laser irradiation. During irradiation, the cryogen spray was delivered intermittently between laser pulses with a 60-ms pulse duration, pulse rate of 0.2 Hz, and a 2-cm-diameter spot concentric with the laser spot.

8.2.4 Ultrasound Imaging

A clinical ultrasound console (SSD-Alpha 7, Aloka, Wallingford, CT) with 13.2 MHz high-frequency linear array transducer (UST-5411, Aloka) was used to image the native vas at Day 0, the thermally coagulated vas at Day0, and the scarred vas at Day 28. This transducer provided an axial image resolution of approximately 200 μm and an imaging depth of 2 cm. Simultaneous application of Doppler US at a frequency of 6.15 MHz helped to distinguish between the vas and spermatic cord. A standard US gel was applied to the canine scrotum and the vas was identified using Doppler imaging to locate the spermatic cord and nerve bundle. Doppler US was also used to indicate whether there was normal blood flow through the testicular artery after the procedure and confirm the absence of collateral thermal damage to proximal tissue structures.

8.3 Results

8.3.1 Noninvasive Laser Vasectomy

Day 0 burst pressures (291 ± 31 mmHg) for the thermally coagulated vas did not differ significantly from Day 28 burst pressures (297 ± 26 mmHg) for the scarred vas. However, both of these vas burst pressures were significantly higher than burst pressures that the canine vas typically experiences during ejaculation (136 ± 29 mmHg) [37], thus demonstrating strong vas occlusion. High-frequency ultrasound images of the vas were taken at Day 0 before and after the procedure to confirm successful thermal coagulation of the vas, and again at Day 28 to identify the scarred region of the vas (Figure 28). These images showed an increased, hyperechoic signal and a disruption of the vas structure in the laser-treated region. The sonographic length of the coagulated vas at Day 0 measured 4.1 ± 0.7 mm, and the length of the scarred vas measured 3.7 ± 0.5 mm. These measurements roughly correspond to the 3-mm-diameter laser spot used, with a slightly larger increase in coagulated vas length due to both light scattering and thermal diffusion that occurs in the tissue during the procedure.

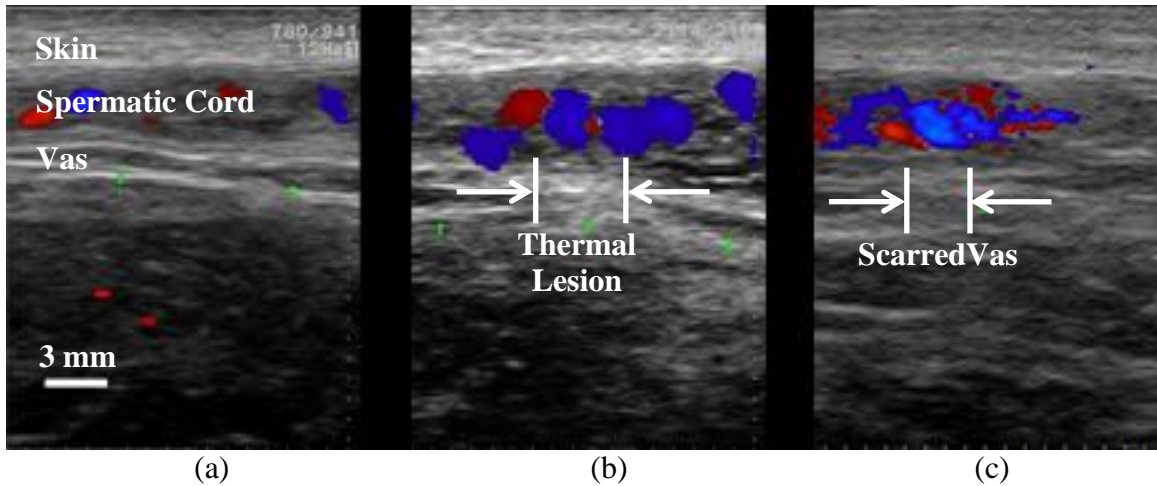


Figure 28. (a) Un-occluded vas prior to noninvasive laser vasectomy. (b) Occluded vas after noninvasive laser vasectomy. (c) 28 day trials show the scarring noticed on the vas may appear in high frequency ultrasound imaging.

The thermally coagulated and scarred vas were excised for examination to verify the ultrasound images (Figure 29).

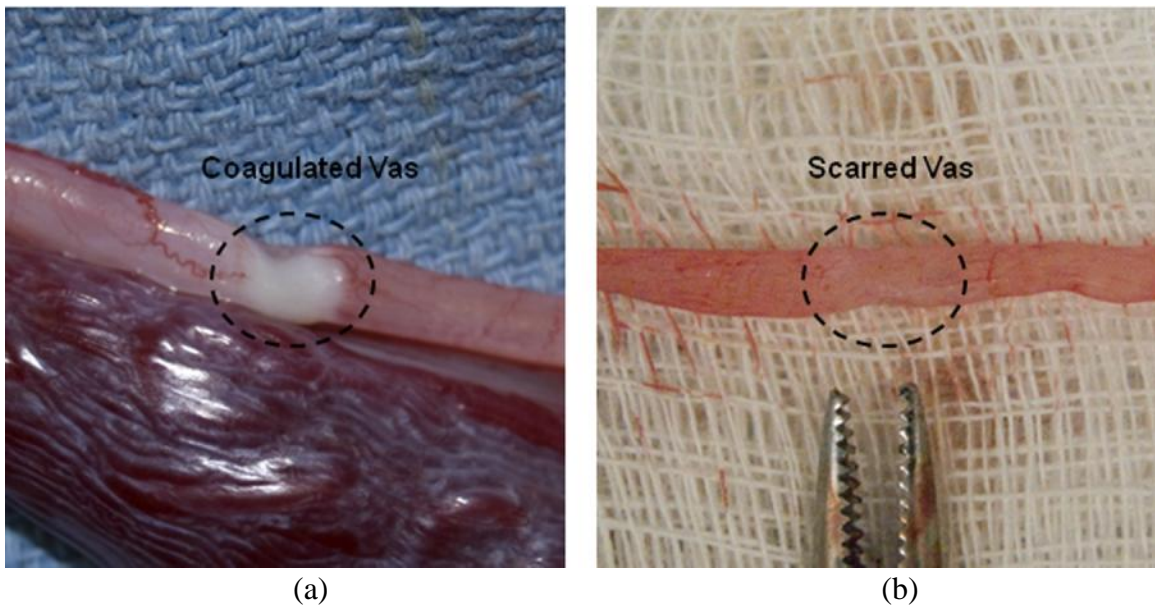


Figure 29. Representative images of the excised canine vas: (a) At Day 0 immediately after the procedure, showing the thermally coagulated zone; and (b) at Day 28, showing the scarred region of the vas.

The thermally coagulated vas segment was identified by several indicators including blanching and shrinkage of the vas wall. The scarred vas, although less distinct, also showed discoloration and shrinkage in the treated area. Both the thermally coagulated and scarred vas segments tended to bulge, indicative of blockage at the treatment site, during burst pressure studies. While our previous noninvasive laser vasectomy studies have noted the formation of minor scrotal skin burns with the use of higher laser powers [55], there was no evidence of skin burns in this study. Figure 30 shows the scrotal skin surface at Day 0 before and after the procedure and at Day 28. Only temporary skin irritation and reddening was observed due to the blunt trauma of the vasectomy ring clamp tips on the skin. Such trauma caused by the vas ring clamp is normal for the conventional vasectomy technique as well. This irritation disappeared approximately 15 minutes after the clamp was removed and the procedure completed. One dog experienced some melena and diarrhea, unrelated to the laser procedure, which was successfully treated with medication. Otherwise, the dogs were monitored on a daily basis and showed no visual signs of skin damage, or discomfort with the treatment site in the scrotal region.

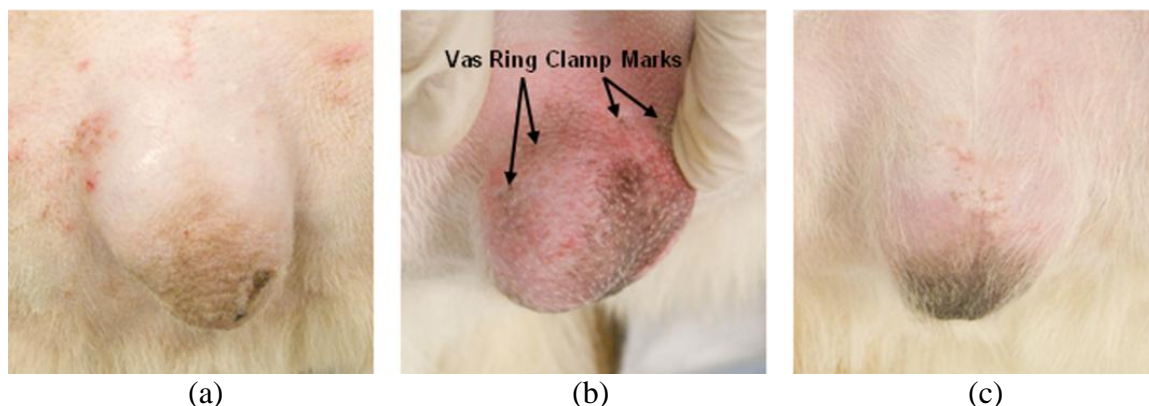


Figure 30. Representative images of the canine scrotal skin surface: (a) At Day 0 before the procedure; (b) at Day 0 immediately after the procedure; and (c) At Day 28 at the completion of the study. Note that much of the skin irritation observed immediately after the procedure is due to the vasectomy ring clamp used to isolate the vas underneath the skin. This irritation is temporary and disappears soon after the procedure.

The average bursting pressure for the ten dogs compared well with previous studies that were performed. Acute burst pressures (291 ± 31 mmHg) for the thermally coagulated vas did not differ significantly from chronic burst pressures (297 ± 26 mmHg) for the scarred vas. However, both acute and chronic vas burst pressures were significantly higher than burst pressures that the canine vas typically experiences during ejaculation (136 ± 29 mmHg) [37], demonstrating strong and lasting vas occlusion.

8.4 Discussion

During previous studies, we have reported successful laser thermal occlusion and scarring of the vas while minimizing scrotal skin injury in *ex vivo* and *in vivo* canine models [38, 55, 63]. The results of this study demonstrate that the canine vas becomes scarred and remains occluded, confirmed by the burst pressure measurements, in a short-term study. High-frequency ultrasound served as a useful noninvasive diagnostic tool for qualitatively confirming successful thermal occlusion and scarring of the vas, indicated by a hyperechoic signal and disrupted vas structure in the laser treated region. It may be possible to further improve the ultrasound resolution (at the expense of shallower

imaging depth) by using a higher frequency ultrasound transducer than the 13.3 MHz transducer used in this study. However, this transducer was chosen initially because it is the highest frequency transducer used with a standard clinical ultrasound system commonly available to physicians. While the use of burst pressure measurements is not the definitive indicator of a successful vasectomy, it does provide a reliable quantitative source of feedback to determine the degree of vas closure with comparison to typical vas ejaculation pressures. Our results show that the vas burst pressures after both thermal coagulation at Day 0 and scarring at Day 28 were over twice that of previously reported canine vas ejaculation pressures, thus demonstrating a robust, short-term closure of the vas in this canine model. However, once the noninvasive laser vasectomy system and treatment parameters have been fully optimized, it will be necessary to perform more definitive and longer-term chronic canine studies. These studies will include examining recanalization and azoospermia rates, with comparison of surgical vasectomy and noninvasive laser vasectomy, prior to clinical studies. It should also be noted that our 100% success rate for thermal occlusion and scarring of the vas, with no adverse complications, is promising, considering that the canine model is a more difficult model than the human for vasectomy as previously reported in chapter 5. Finally, although this was not intended to be a cost comparison study, it is worth considering some of the costs involved with noninvasive laser vasectomy versus conventional surgical vasectomy. It is well known that the cost of a conventional surgical vasectomy is relatively low (approximately \$500–1,000 per procedure). For noninvasive laser vasectomy, there are significant capital costs associated with the purchase of the laser and cryogen systems, although it should be noted that laser rentals are a viable and popular option for laser

surgical procedures. The ultrasound system, if used in a clinical setting, is portable and readily available for shared use, and therefore may not add significant cost to the procedure. The cost of the cryogen spray used for cooling the scrotal skin during the procedure was calculated to be almost negligible (adding less than \$2 per procedure). Additionally, some supplies currently used during surgical vasectomy (e.g., surgical tray, clips, sutures, etc.) would not be needed for noninvasive laser vasectomy. It is also possible that a patient would be willing to pay a slightly higher fee associated with a noninvasive vasectomy compared to surgical vasectomy.

The results of this study further demonstrate that the canine vas becomes scarred and remains occluded, confirmed by the burst pressure measurements, in a short-term chronic study. High-frequency ultrasound served as a useful noninvasive diagnostic tool for confirming successful targeting, thermal occlusion, and scarring of the vas, indicated by a hyperechoic signal and disrupted vas structure in the laser treated region.

It may be possible to further improve the ultrasound resolution (at the expense of shallower imaging depth) by using a higher frequency ultrasound transducer than the 13.3 MHz transducer used in this study. However, this transducer was chosen because it is the highest frequency transducer used with a standard clinical ultrasound system commonly available to physicians, and as such, does not introduce more costly specialized ultrasound equipment for use in an inexpensive vasectomy procedure.

8.5 Conclusions

Ultrasound may be used as a diagnostic tool to assist in determining successful laser thermal coagulation and scarring of the vas during noninvasive laser vasectomy.

CHAPTER 9: OCT AND HIGH FREQUENCY US IMAGING OF THE CANINE VAS DEFERENS

9.1 Introduction

Optical coherence tomography (OCT) and high-frequency diagnostic ultrasound (HFUS) have recently been used to measure the anatomy of the normal human vas deferens [58, 74]. Our laboratory has also used US (with a 13 MHz probe) for imaging the canine vas before and after laser thermal coagulation [75]. This study aims to improve on these previous studies by using a higher frequency (20 MHz) probe capable of improved resolution and to compare HFUS with another high resolution imaging modality, optical coherence tomography (OCT), for imaging the canine vas before and after laser thermal coagulation. Both imaging modalities are safe, compact, and inexpensive, and are therefore evaluated as possible choices for potential use in laser vasectomy during this pre-clinical study. However, each imaging modality serves a slightly different purpose: US provides deep imaging with intermediate scale resolution while OCT provides high resolution but is limited in its superficial imaging depth. Additionally, a modified vasectomy ring clamp was used to manually isolate the vas beneath the scrotal skin surface for co-location with the cryogen and laser spots (Figure 31).

9.2 Methods

9.2.1 Animal Studies

All procedures were conducted under an animal protocol approved by the Johns Hopkins Animal Review Committee. Noninvasive thermal occlusion of the vas was performed bilaterally in a total of 6 dogs (n = 12 vasa). After completion of the procedure, all vasa were harvested and processed for histology with H&E staining. The animals were neutered, monitored for a few days during recovery, and then adopted out to caring homes.

9.2.2 Laser Parameters

A compact, tabletop, 50-Watt Ytterbium fiber laser (Model TLR1075-50, IPG Photonics, Oxford, MA) emitted near-infrared radiation with a wavelength of 1075 nm which was focused with a lens into a 400- μm -core fiber optic patch-cord (Thorlabs, Newton, NJ). Another lens at the end of the patch-cord delivered a collimated laser beam to the tissue surface. The laser was externally triggered by a function generator (DS345, Stanford Research Systems, Sunnyvale, CA) to operate in long-pulse mode, with an average incident power of 9.0 W, 500-ms pulse duration, 1 Hz pulse rate, and 3-mm-diameter ($1/e^2$) spot at the scrotal skin surface.

9.2.3 Cooling Parameters

A Dynamic Cooling Device (DCD, Candela Laser Corporation, Wayland, MA) was used to deliver cryogen (1,1,1,2-tetrafluoroethane, boiling point = - 26 °C) to the scrotal skin surface through a solenoid valve to prevent overheating and formation of skin burns during the procedure. Three cryogen pulses were applied to pre-cool the skin prior to laser irradiation over a period of eight seconds. For all of the procedures, laser

irradiation was performed for a period of 60 seconds for each vas. Cryogen spray was delivered intermittently between laser pulses with a 60-ms pulse duration, pulse rate of 0.25 Hz, and a 2-cm-diameter spot concentric with the laser spot. A cryogen mask was used to thermally insulate surrounding scrotal skin from cryogen spray to avoid superficial freeze burns. Details of the experimental setup have been previously reported [63]. A modified, 4-mm-OD, vasectomy ring clamp was used to manually isolate the vas beneath the scrotal skin surface for co-location with the cryogen and laser spots (Figure 31). It should be noted that although a modified vasectomy ring clamp design was used for these procedures, the base of the clamp (hemostat) is essentially the same as the instrument currently used during a standard no scalpel vasectomy procedure.

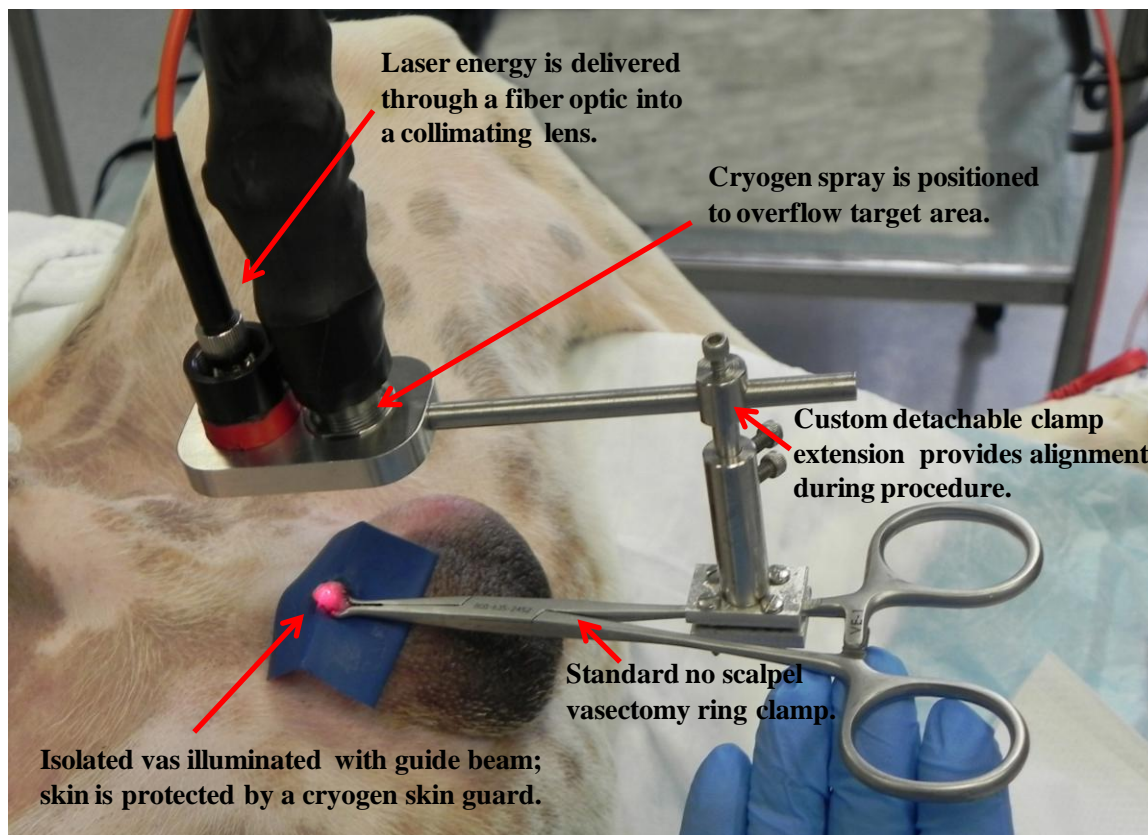


Figure 31. A conventional no scalpel vasectomy ring clamp was used to isolate the vas deferens beneath the scrotal skin surface, and then a detachable customized clamp extension was used to safely co-locate both the cryogen spray spot and laser spot on the tissue surface inside the ring.

9.2.4 OCT Parameters

A compact, tabletop, inexpensive, FDA-approved, endoscopic, optical coherence tomography system (Niris II, Imalux, Cleveland, OH) with a handheld 8-Fr (2.7-mm-OD) probe was used (Figure 32a). The OCT system acquired real-time images at 8 frames/swith $\sim 11 \mu\text{m}$ axial resolution and $\sim 25 \mu\text{m}$ lateral resolution in tissue with a lateral scan length of 2 mm and an imaging depth of 1.6 mm. The OCT system was used for superficial imaging of the canine vas once it was compressed inside the vas ring clamp, immediately before and after laser irradiation. This approach to OCT imaging of the vas is entirely feasible during a clinical procedure.

9.2.5 High Frequency Ultrasound Parameters

A compact, tabletop, inexpensive, FDA-approved high frequency ultrasound system (Episcan-I-200, Longport International, Silchester, United Kingdom) with 20-MHz linear scanning transducer was used for comparison with OCT (Figure 32b). This transducer provided a scan length of 15 mm, an axial image resolution of $\sim 100 \mu\text{m}$, and an imaging depth of $\sim 1 \text{ cm}$. The HFUS transducer was used to provide deeper imaging of the canine vas when it was held manually within a scrotal fold immediately before and after application of the vas ring clamp.

Several indicators were used to determine successful laser thermal coagulation and occlusion of the canine vas, including OCT, HFUS, gross analysis, and histology.

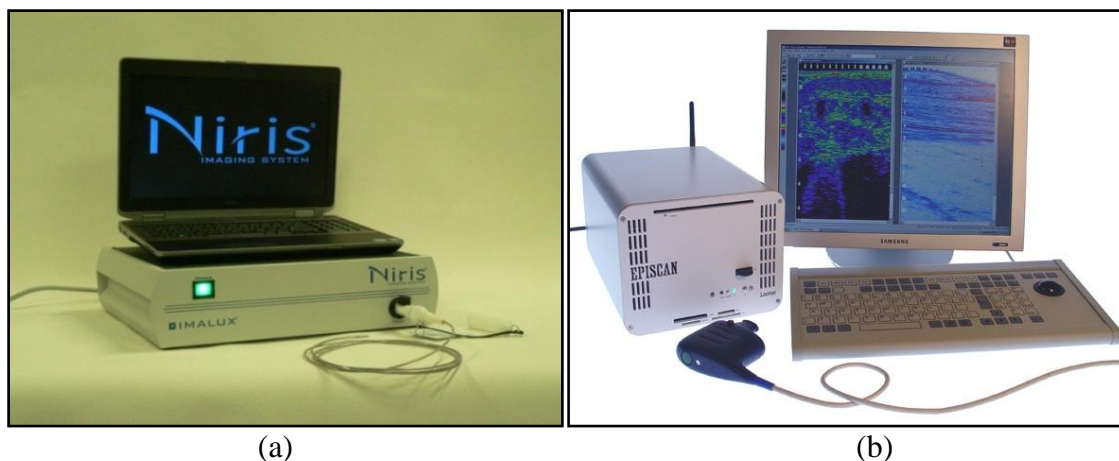


Figure 32. (a) Photograph of the optical coherence tomography system and probe used in these studies; (b) Photograph of the high-frequency ultrasound system and probe used in these studies.

9.3 Results

9.3.1 OCT Results

Longitudinal and cross-sectional OCT images of the vas were taken, *in vivo*, before and after the procedure to confirm successful thermal coagulation of the vas (Figure 33abc). OCT images of the excised vas were also taken, *ex vivo*, immediately after the procedure for comparison (Figure 33def). The native vas appeared with a dark, fluid-filled lumen (absent of reflected signal intensity), while the thermal lesion was represented by a lighter region (indicative of enhanced reflected signal intensity). This is consistent with a significant increase in the scattering coefficient of soft tissue once it has been thermally denatured. It should also be noted that since the thermal lesion length along the vas (3.58 ± 0.36 mm) was longer than the OCT lateral scanning distance of 2 mm, it was impossible to capture the entire lesion in a single image. Furthermore, the vas was not a straight tube, but rather traveled in and out of the OCT (and US) image plane.

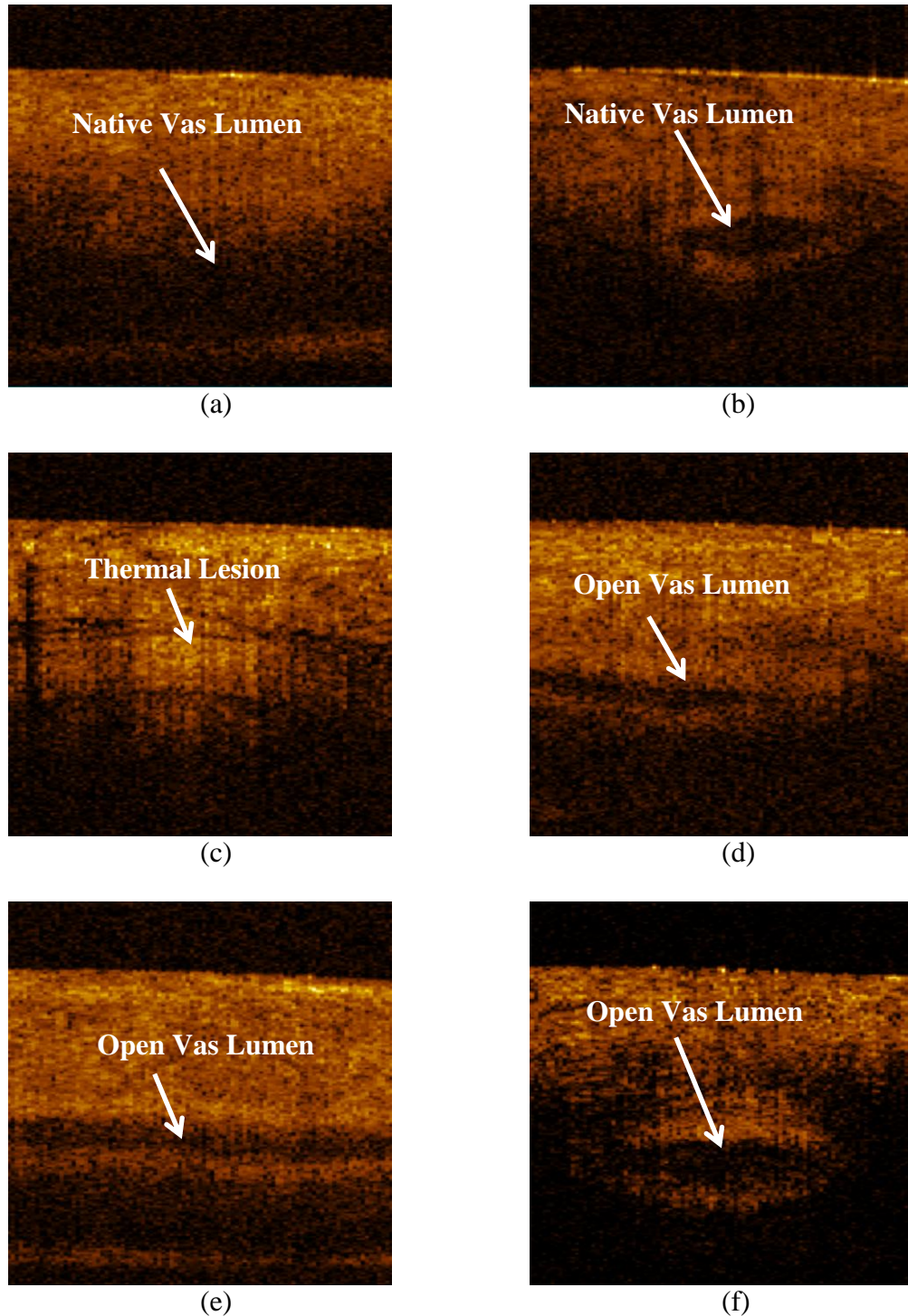


Figure 33. (a,b) Longitudinal and cross-sectional OCT images of the native canine vas acquired prior to the procedure. (c) Longitudinal OCT image of the thermally coagulated canine vas acquired while the vas and scrotal skin were compressed inside the vas ring clamp after the procedure. (d) Longitudinal OCT image of the thermally coagulated canine vas acquired *ex vivo* after the vas tissue was harvested; (e,f) Longitudinal and cross-sectional OCT images of the native canine vas acquired *ex vivo* after the tissue was harvested. All OCT images measure 1.6 x 1.6 mm (depth x width).

9.3.2 High Frequency Ultrasound Results

Longitudinal and cross-sectional HFUS images of the vas were also taken, *in vivo*, before and after the procedure to confirm successful thermal coagulation of the vas (Figure 34). In the native vas images, the fluid-filled lumen also appears dark (with an absence of reflected signal intensity), while the thermally denatured vas appears lighter (again indicative of increased reflected signal intensity). Using HFUS, the average vas lumen diameter, vas wall thickness, and vas thermal lesion length were measured to be 0.27 ± 0.07 mm (n=6), 1.09 ± 0.06 mm (n=6), and 3.58 ± 0.36 mm (n=9), respectively. These lumen diameter and wall dimensions are within a similar range to that previously reported for the native human vas deferens [58]. The canine vas deferens in general is known to have similar dimensions to that of the human vas deferens [76]. The thermal lesion length is strongly correlated with the 3-mm-diameter laser spot used in these studies, and is also similar to measurements reported in previous studies [38, 55, 63, 75].

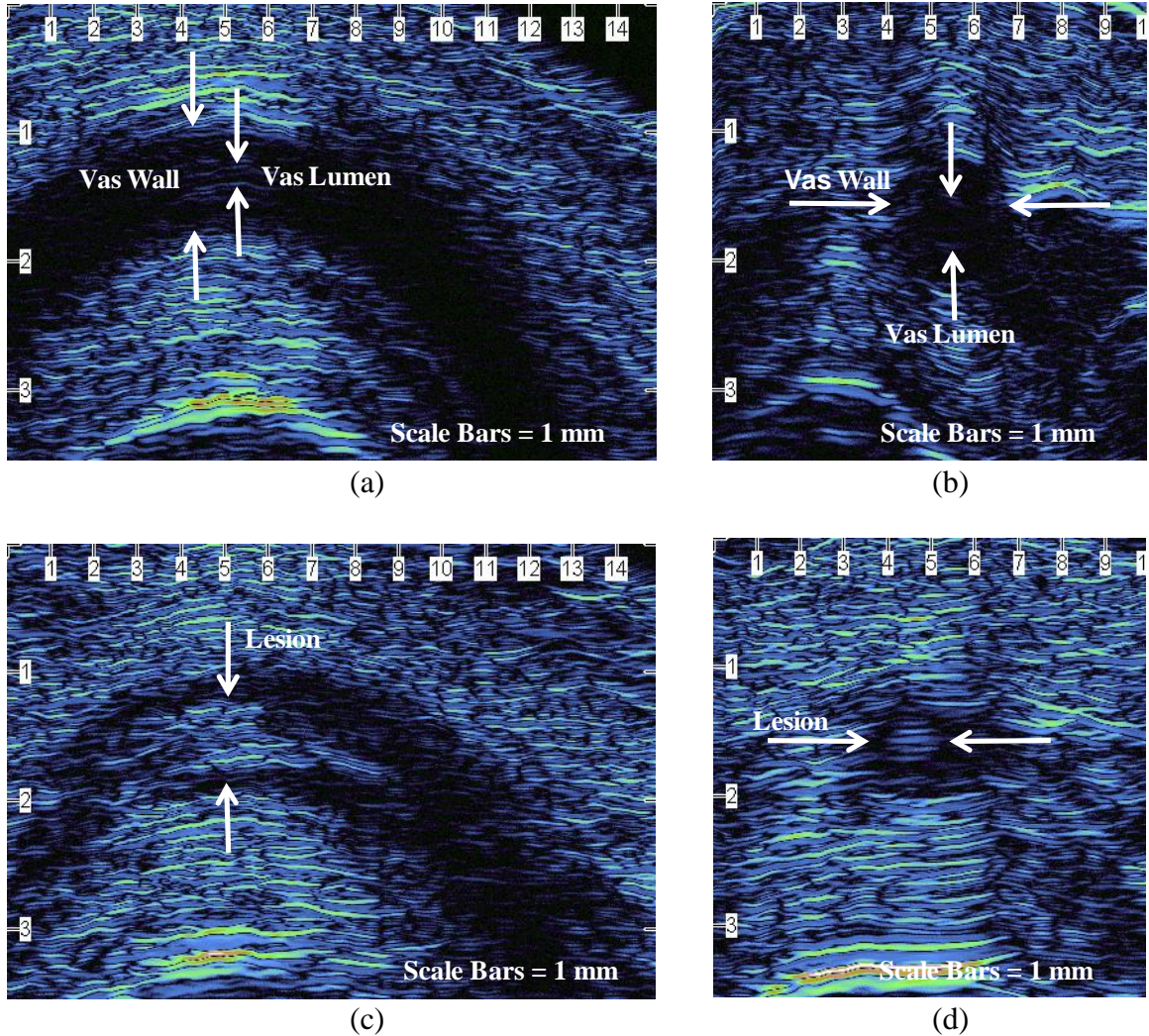


Figure 34. (a,b) Longitudinal and cross-sectional US images of the native canine vas, acquired by manually isolating the vas within the scrotal skin fold prior to placement of the vas ring clamp. The vas wall and lumen can be identified. (c,d) Longitudinal and cross-sectional US images of the thermally coagulated canine vas acquired by manually isolating the vas within the scrotal skin fold after removal of the vas ring clamp. A thermal lesion encompassing both the vas wall and lumen is observed.

The thermally coagulated vas was excised for examination to verify the OCT and HFUS images. Figure 35 shows a representative image of the thermally coagulated vas segment, which can be identified by several indicators including blanching and shrinkage of the vas wall.

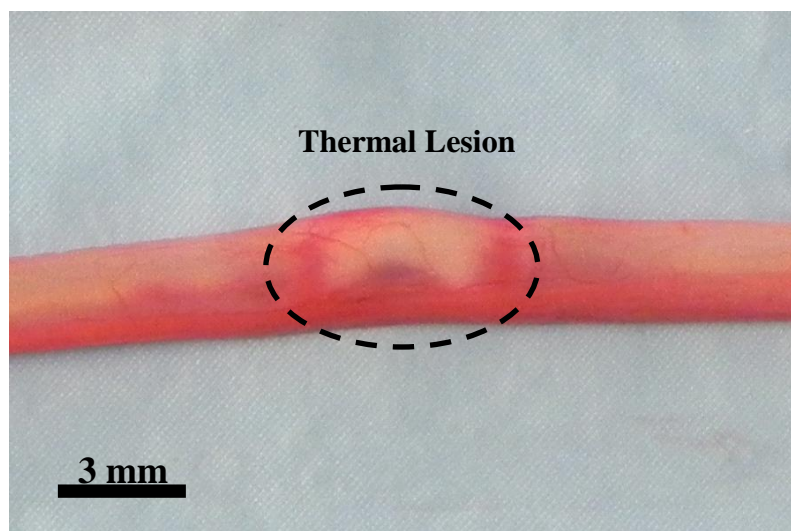


Figure 35. Gross image of the thermally coagulated vas segment showing significant blanching and shrinkage of the vas wall.

9.3.3 Histology Results

The vas samples were then processed for histology using standard techniques. For each dog, serial sectioning of the vas was performed in both the longitudinal and cross-sectional directions (one orientation for each vas – left and right sides) through the entire vas sample at 100 μm intervals. Figure 36 provides representative longitudinal and cross-sectional histologic sections of the canine vas with open lumen sections (taken beyond the thermally coagulated segment) also provided for comparison.

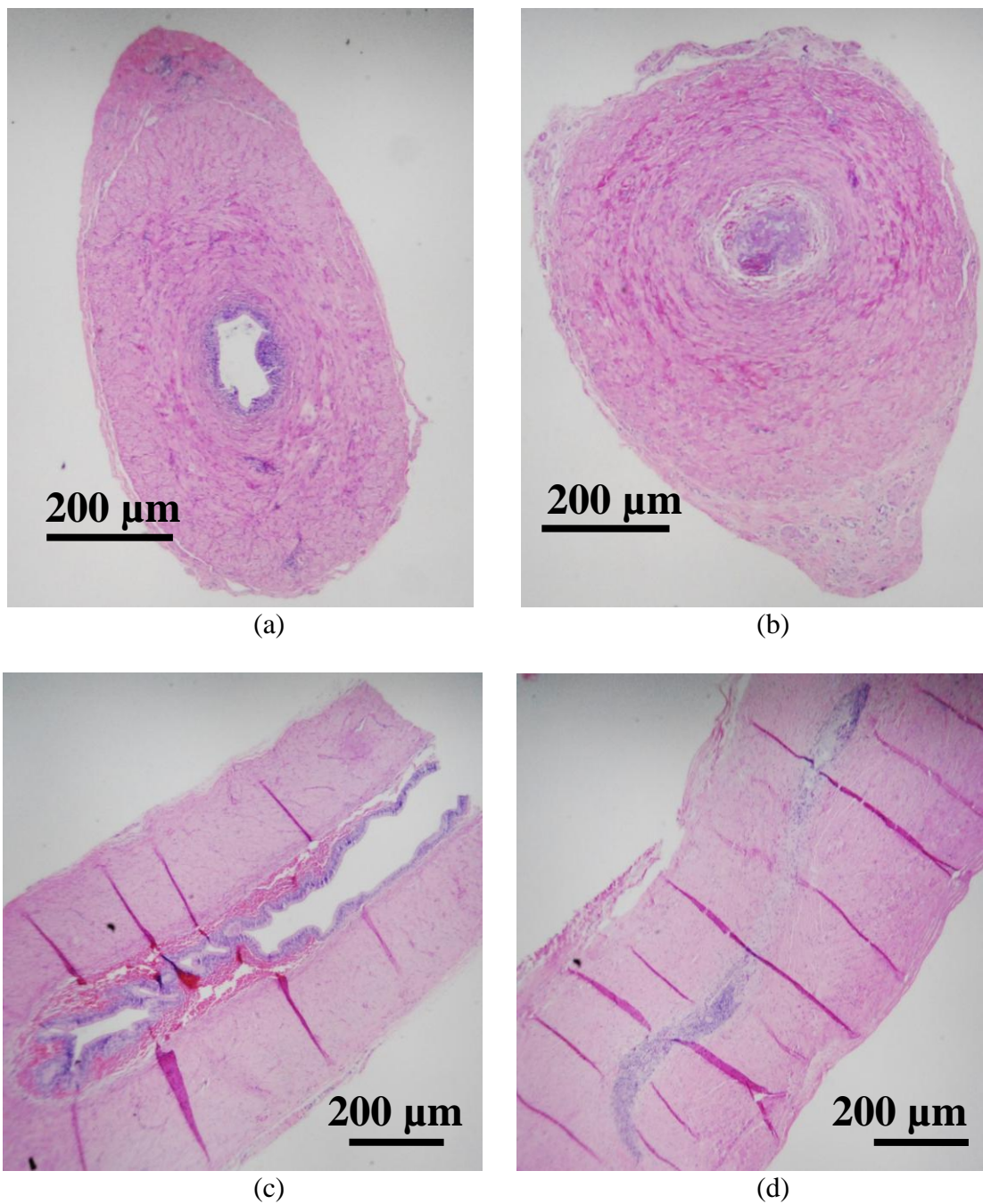


Figure 36. H&E-stained histologic sections of the vas: (a) Cross-section of open lumen; (b) Cross-section of thermally occluded lumen; (c) Longitudinal section of open lumen; (d) Longitudinal section of thermally occluded lumen.

9.4 Discussion

Vasectomy is a safe, simple, effective, and inexpensive surgical procedure for male sterilization. Despite the low morbidity of this procedure, societal pressures, psychological factors such as the perception of the loss of “manhood”, and male fear of surgery are reasons frequently cited by couples choosing other forms of contraception. A noninvasive laser vasectomy technique may eliminate many of these concerns and increase male acceptance of vasectomy. While some of our earlier noninvasive laser vasectomy studies have noted the formation of minor scrotal skin burns with the use of higher laser powers [55], there was no evidence of skin burns in this study. Only temporary skin irritation and reddening was observed due to the blunt trauma of the vasectomy ring clamp tips on the skin. Such trauma caused by the vas ring clamp is normal for the conventional vasectomy technique as well. This irritation disappeared approximately 15 min after the clamp was removed and the procedure completed.

The development of any completely noninvasive therapeutic procedure may benefit from the introduction of a diagnostic modality to confirm success since no tissue is removed for analysis during the noninvasive procedure. OCT and HFUS are obvious choices for use in vas imaging during noninvasive laser vasectomy because they are both relatively compact, inexpensive imaging modalities that provide sufficient image resolution and depth to view the vas deferens, which has a lumen and wall thickness of $\sim 300\ \mu\text{m}$ and $\sim 1\ \text{mm}$, respectively.

OCT has an order of magnitude better resolution and an order of magnitude worse imaging depth than HFUS. Therefore, OCT was limited in these studies to imaging the vas once it was fixed and compressed beneath the scrotal skin inside the 4-mm-diameter

vas ring clamp. However, while the native vas was easily visible during OCT imaging before the procedure, it was more difficult to identify the thermally coagulated vas segment after the procedure. Only longitudinal sections were obtained, and cross-sectional images of the thermally coagulated vas could not easily be confirmed. It may be that the need to perform OCT imaging of the compressed vas and scrotal skin within the clamp resulted in a distorted view of the anatomy which in turn made interpretation of the OCT images more difficult. HFUS imaging of the vas was more successful, with longitudinal and cross-sectional images of the native and thermally coagulated vas obtained while the vas was held manually within a scrotal fold, both before and after removal of the vas from the ring clamp.

However, it should be noted that the limited imaging depth of the HFUS system required manual isolation of the vas prior to measurement. This made locating the region of interest during postoperative imaging of the thermal lesion more difficult and resulted in a slightly lower vas sample set for evaluation. In some vas, it was also difficult to differentiate the lumen from the wall before the procedure and provide two distinct measurements for these two structures. This may have been due to suboptimal probe placement, or the method of manual isolation causing excessive pressure and flattening of the vas. It may be possible in future studies to design the imaging probe tip and vas clamp to minimize these limitations.

From a clinical perspective, it is also worth briefly mentioning the costs associated with noninvasive laser vasectomy, since surgical vasectomy is currently a low-cost procedure (~\$500-1000). For noninvasive laser vasectomy, there are capital costs associated with purchase of the laser (~\$20,000) and cryogen (~\$5,000) systems. The

compact, portable, tabletop, time-domain OCT system and probe used in this study is relatively inexpensive (~\$40,000), in comparison to other OCT systems. The compact, tabletop HFUS system and probe used in this study is also relative inexpensive (~\$20,000) in comparison with conventional clinical US consoles. However, a patient may be willing to pay a slightly higher fee for nonsurgical vasectomy.

Finally, more definitive and longer term chronic canine studies are currently being performed to examine vas recanalization and azoospermia rates, with comparison of surgical vasectomy and noninvasive laser vasectomy, prior to clinical studies. Both OCT and HFUS may be used in these chronic studies for imaging of the scarred vas.

9.5 Conclusions

High-frequency ultrasound may be used as a diagnostic tool to assist in determining successful laser thermal coagulation and scarring of the vas during noninvasive laser vasectomy. While optical coherence tomography also shows promise, further improvements are necessary before this imaging modality can be reliably used for evaluation of the thermally coagulated vas.

CHAPTER 10: CONCLUSION

Studies that show the efficacy of noninvasive laser vasectomy have been performed. Successful *ex vivo* tissue studies and short term acute and chronic *in vivo* animal studies have been successfully completed. Problems that have arisen (e.g. skin burns) have been eliminated by optimizing the laser and cooling treatment parameters during experimental studies. Optical clearing agents, while not yet approved by the FDA, have also been explored, which increase the optical penetration depth of near-infrared laser radiation through the scrotal skin and require less energy to achieve similar results in noninvasive laser vasectomy. Optical and thermal computer models, with the use of an optical clearing agent, have produced results predicting the successful transition from a pre-clinical canine model into human clinical studies. Both optical coherence tomography and high-resolution ultrasound imaging modalities have also been explored as a method for real-time, noninvasive confirmation of successful targeting, thermal occlusion, and scarring of the canine vas. Finally, a novel noninvasive vasectomy prototype clamp has developed to provide a robust, compact, and inexpensive component of the noninvasive laser vasectomy system for translation into clinical studies.

REFERENCES

- [1] J. S. Nelson, B. Majaron, and K. M. Kelly, "Active skin cooling in conjunction with laser dermatologic surgery," *Semin. Cutan. Med. Surg.*, vol. 19, pp. 253-266, 2000.
- [2] H. H. Zenzie, G. B. Altshuler, M. Z. Smirnov, and R. R. Anderson, "Evaluation of cooling methods for laser dermatology," *Lasers Surg. Med.*, vol. 26, pp. 130-144, 2000.
- [3] R. Ramli, D. Durand, and N. M. Fried, "Subsurface tissue lesions created using an Nd:YAG laser and cryogen cooling," *J. Endourol.*, vol. 17, pp. 923-926, 2003.
- [4] R. Ramli, C. C. Chung, N. M. Fried, N. Franco, and M. H. Hayman, "Subsurface tissue lesions created using an Nd:YAG laser with a sapphire contact cooling probe," *Lasers Surg. Med.*, vol. 35, pp. 392-396, 2004.
- [5] C. C. Chung, S. Permpongkosol, I. M. Varkarakis, G. Lima, N. Franco, M. H. Hayman, T. Nichol, and a. N. M. Fried, "Laser probes for noninvasive coagulation of subsurface tissues," *Proc. SPIE*, vol. 6078, pp. 1-5, 2006.
- [6] A. Chandra, "Sterilization in the United States: prevalence and statistics, 1965-1995.," *Vital Health Stat.*, vol. 23, pp. 1-41, 1998.
- [7] W. B. Miller, R. N. Shain, and D. J. Pasta, "Tubal sterilization or vasectomy: how do married couples make the choice," *Fertil. Steril.*, vol. 56, pp. 278-284, 1991.
- [8] N. W. Hendrix, S. P. Chauhan, and J. C. Morrison, "Sterilization and its consequences," *Obstet. Gynecol.*, vol. 54, pp. 766-777, 1999.
- [9] R. N. Shain, W. B. Miller, and A. E. Holden, "Factors associated with married women's selection of tubal sterilization and vasectomy," *Fertil. Steril.*, vol. 43, pp. 234-244, 1985.
- [10] M. Goldstein, "Surgical management of male infertility and other scrotal disorders," in *Campbell's Urology*. vol. 2, P. C. Walsh, A. B. Retik, E. D. Vaughan, and A. J. Wein, Eds., ed Philadelphia: W.B. Saunders, 1998, pp. 1338-1358.
- [11] W. H. Weiske, "Vasectomy," *Andrologia*, vol. 33, pp. 124-134, 2001.
- [12] G. L. Smith, G. P. Taylor, and K. F. Smith, "Comparative risks and costs of male and female sterilization," *Am. J. Public Health*, vol. 75, pp. 370-374, 1985.

- [13] L. T. Strauss, C. M. Huezo, D. G. Kramer, R. W. Rochat, P. Senanayake, and G. L. Rubin, "Sterilization-associated deaths: a global survey," *Int. J. Gynaecol. Obstet.*, vol. 22, pp. 67-75, 1984.
- [14] G. C. Denniston, "Vasectomy by electrocautery: outcomes in a series of 2,500 patients," *J. Fam. Pract.*, vol. 21, pp. 35-40, 1985.
- [15] P. M. Alderman, "Complications in a series of 1224 vasectomies," *J. Fam. Pract.*, vol. 33, pp. 579-584, 1991.
- [16] P. J. Schwingl and H. A. Guess, "Safety and effectiveness of vasectomy," *Fertil. Steril.*, vol. 73, pp. 923-936, 2000.
- [17] S. Li, M. Goldstein, J. Zhu, and D. Huber, "The no-scalpel vasectomy," *J. Urol.*, vol. 145, pp. 341-344, 1991.
- [18] S. L. Ban, "Sterility by vas injection method," *Hu Nan Med. J.*, vol. 5, pp. 49-50, 1980.
- [19] S. Li, "Percutaneous injection of vas deferens," *Chin. J. Urol.*, vol. 1, pp. 193-198, 1980.
- [20] T. Tao, "Vas deferens sterility by injection method," *Qeng Dao Med. J.*, vol. 5, pp. 65-68, 1980.
- [21] J. O. Esho, G. W. Ireland, and A. Cass, "Comparison of ligation and fulguration methods," *Urology*, vol. 3, pp. 337-338, 1974.
- [22] S. S. Schmidt and T. M. Minckler, "The vas after vasectomy: comparison of cauterization methods," *Urology*, vol. 40, pp. 468-470, 1992.
- [23] T. R. L. Black, D. S. Gates, K. Lavelly, and P. Lampzey, "The percutaneous electrocoagulation vasectomy technique – a comparative trial with the standard incision technique at Marie Stopes House, London," *Contraception*, vol. 39, pp. 359-368, 1989.
- [24] O. T. Tan, M. Motamedi, A. J. Welch, and A. K. Kurban, "Spotsize effects on guinea pig skin following pulsed irradiation.," *J Invest Dermatol*, vol. 90, pp. 877-881, 1988.
- [25] M. Keijzer, S. L. Jacques, S. A. Prahl, and A. J. Welch, "Light distribution in artery tissue: Monte Carlo simulations for finite laser beams.," *Lasers Surg Med*, vol. 9, pp. 148-154, 1989.
- [26] M. Keijzer, J. W. Pickering, and M. J. C. van Gemert, "Laser beam diameter for port wine stain treatment.," *Lasers Surg Med*, vol. 11, 1991.

- [27] N. M. Fried, V. C. Hung, and J. T. Walsh, "Laser tissue welding: laser spot size and beam profile studies.," *IEEE J. Sel. Top. Quant. Electron.*, vol. 5, pp. 1004-1012, 1999.
- [28] R. R. Anderson and J. A. Parish, "Selective photothermolysis: precise microsurgery by selective absorption of pulse radiation.," *Science*, vol. 220, pp. 524-527, 1983.
- [29] S. L. Jacques, "Role of tissue optics and pulse duration on tissue effects during high power laser radiation.," *Appl. Opt.*, vol. 32, pp. 2447-2454, 1993.
- [30] J. Roider, F. Hillenkamp, T. Flotte, and R. Birngruber, "Microphotocoagulation: selective effects of repetitive short laser pulses.," *Proc. Natl Acad Sci USA*, vol. 90, pp. 8643-8647, 1993.
- [31] B. Anvari, B. S. Tanenbaum, T. E. Milner, K. Tang, L. H. Liaw, K. Kalafus, S. Kimel, and J. S. Nelson, "Spatially selective photocoagulation of biological tissues: feasibility study utilizing cryogen spray cooling," *Appl. Opt.*, vol. 35, pp. 3314-3320, 1996.
- [32] N. M. Fried, Y. D. Sinelnikov, B. Pant, W. W. Roberts, and S. B. Solomon, "Noninvasive vasectomy using a focused ultrasound clip: thermal measurements and simulations," *IEEE Trans. Biomed. Eng.*, vol. 48, pp. 1453-1459, 2001.
- [33] W. W. Roberts, D. Y. Chan, N. M. Fried, E. J. Wright, T. Nicol, T. W. Jarrett, L. R. Kavoussi, and S. B. Solomon, "High intensity focused ultrasound ablation of the vas deferens in a canine model," *J. Urol.*, vol. 167, pp. 2613-2617, 2002.
- [34] M. Sotomayor and G. F. Bernal, "Transurethral delivery of radiofrequency energy for tissue micro-remodeling in the treatment of stress urinary incontinence," *Int. Urogynecol. J.*, vol. 14, pp. 373-379, 2003.
- [35] R. Dmochowski and R. A. Appell, "Advancements in minimally invasive treatments for female stress urinary incontinence: radiofrequency and bulking agents," *Curr. Urol.*, vol. 4, pp. 350-355, 2003.
- [36] S. Madersbacher, C. Kratzik, M. Susani, M. Pedevilla, and M. Marberger, "Transcutaneous high-intensity focused ultrasound and irradiation: an organ-preserving treatment of cancer in a solitary testis," *Eur. Urol.*, vol. 33, pp. 195-201, 1998.
- [37] A. Shafik, "Electrovasogram: a canine study of the electromechanical activity of the vas deferens," *Urology*, vol. 46, pp. 692-696, 1995.

- [38] C. M. Cilip, J. P. Jarow, and N. M. Fried, "Noninvasive laser vasectomy: preliminary ex vivo tissue studies," *Lasers Surg. Med.*, vol. 41, pp. 203-207, 2009.
- [39] A. N. Bashkatov, E. A. Genina, V. I. Kochubey, and V. V. Tuchin, "Optical properties of human skin, subcutaneous and mucous tissues in the wavelength range from 400 to 2000 nm," *Appl. Phys.*, vol. 38, pp. 2543-2555, 2005.
- [40] G. M. Hale and M. R. Querry, "Optical constants of water in the 200 nm to 200 μ m wavelength region," *Appl. Opt.*, vol. 12, pp. 555-563, 1973.
- [41] A. K. Bui, R. A. McClure, J. Chang, C. Stoianovici, J. Hirshburg, A. T. Yeh, and B. Choi, "Revisiting optical clearing with dimethyl sulfoxide (DMSO)," *Lasers in Surgery and Medicine*, vol. 41, pp. 142-148, 2009.
- [42] B. Choi, L. Tsu, E. Chen, T. S. Ishak, S. M. Iskandar, S. Chess, and J. S. Nelson, "Determination of chemical agent optical clearing potential using in vitro human skin," *Lasers in Surgery and Medicine*, vol. 36, pp. 72-75, 2005.
- [43] J. Hirshburg, B. Choi, J. S. Nelson, and A. T. Yeh, "Collagen solubility correlates with skin optical clearing," *Journal of Biomedical Optics*, vol. 11, pp. 040501-3, 2006.
- [44] M. Kinnunen, R. Myllyla, and S. Vainio, "Detecting glucose-induced changes in in vitro and in vivo experiments with optical coherence tomography," *Journal of Biomedical Optics*, vol. 13, pp. 021111-7, 2008.
- [45] Z. Mao, D. Zhu, Y. Hu, X. Wen, and Z. Han, "Influence of alcohols on the optical clearing effect of skin in vitro," *Journal of Biomedical Optics*, vol. 13, pp. 021104-6, 2008.
- [46] R. J. McNichols, M. A. Fox, A. Gowda, S. Tuya, B. Bell, and M. Motamedi, "Temporary dermal scatter reduction: Quantitative assessment and implications for improved laser tattoo removal," *Lasers in Surgery and Medicine*, vol. 36, pp. 289-296, 2005.
- [47] O. Stumpp, B. Chen, and A. J. Welch, "Using sandpaper for noninvasive transepidermal optical skin clearing agent delivery," *Journal of Biomedical Optics*, vol. 11, pp. 041118-9, 2006.
- [48] O. F. Stumpp, A. J. Welch, T. E. Milner, and J. Neev, "Enhancement of transepidermal skin clearing agent delivery using a 980 nm diode laser," *Lasers in Surgery and Medicine*, vol. 37, pp. 278-285, 2005.
- [49] V. V. Tuchin, "A Clear Vision for Laser Diagnostics (Review)," *Selected Topics in Quantum Electronics, IEEE Journal of*, vol. 13, pp. 1621-1628, 2007.

- [50] G. Vargas, E. K. Chan, J. K. Barton, H. G. R. III, and A. J. Welch, "Use of an agent to reduce scattering in skin," *Lasers in Surgery and Medicine*, vol. 24, pp. 133-141, 1999.
- [51] G. Vargas, K. F. Chan, S. L. Thomsen, and A. J. Welch, "Use of osmotically active agents to alter optical properties of tissue: Effects on the detected fluorescence signal measured through skin," *Lasers in Surgery and Medicine*, vol. 29, pp. 213-220, 2001.
- [52] J. Yoon, T. Son, E.-h. Choi, B. Choi, J. S. Nelson, and B. Jung, "Enhancement of optical skin clearing efficacy using a microneedle roller," *Journal of Biomedical Optics*, vol. 13, pp. 021103-5, 2008.
- [53] D. Zhu, J. Zhang, H. Cui, Z. Mao, P. Li, and Q. Luo, "Short-term and long-term effects of optical clearing agents on blood vessels in chick chorioallantoic membrane," *Journal of Biomedical Optics*, vol. 13, pp. 021106-8, 2008.
- [54] M. Zimmerley, R. A. McClure, B. Choi, and E. O. Potma, "Following dimethyl sulfoxide skin optical clearing dynamics with quantitative nonlinear multimodal microscopy," *Appl. Opt.*, vol. 48, pp. D79-D87, 2009.
- [55] C. M. Cilip, A. E. Ross, J. P. Jarow, and N. M. Fried, "Noninvasive laser coagulation of the canine vas deferens, in vivo," *Proc. SPIE*, 2010.
- [56] L. H. Wang, S. L. Jacques, and L. Q. Zheng, "MCML – Monte Carlo modeling of photon transport in multi-layered tissues," *Comput. Methods Programs Biomed.*, vol. 47, pp. 131-146, 1995.
- [57] L. H. Wang, S. L. Jacques, and L. Q. Zheng, "CONV – Convolution for responses to a finite diameter photon beam incident on multi-layered tissues," *Comput. Methods Programs Biomed.*, vol. 54, pp. 141-150, 1997.
- [58] W. D. Middleton, N. Dahiya, C. K. Naughton, S. A. Teefey, and C. A. Siegel, "High-resolution sonography of the normal extrapelvic vas deferens," *J. Ultrasound Med.*, vol. 28, pp. 839-846, 2009.
- [59] H. Ding, J. Q. Lu, W. A. Wooden, P. J. Kragel, and X. H. Hu, "Refractive indices of human skin tissues at eight wavelengths and estimated dispersion relations between 300 and 1600nm," *Phys. Med. Biol.*, vol. 51, pp. 1479-1489, 2006.
- [60] E. Salomatina, B. Jiang, J. Novak, and A. N. Yaroslavsky, "Optical properties of normal and cancerous human skin in the visible and near-infrared spectral range," *J. Biomed. Opt.*, vol. 11:064026, 2006.

- [61] C. R. Simpson, M. Kohl, M. Essenpreis, and M. Cope, "Near-infrared optical properties of ex vivo human skin and subcutaneous tissues measured using the Monte Carlo inversion technique," *Phys. Med. Biol.*, vol. 43, pp. 2465-2478, 1998.
- [62] T. L. Troy and S. N. Thennadil, "Optical properties of human skin in the near infrared wavelength range of 1000 to 2200nm," *J. Biomed. Opt.*, vol. 6, pp. 167-176, 2001.
- [63] C. M. Cilip, A. E. Ross, J. P. Jarow, and N. M. Fried, "Application of an optical clearing agent during noninvasive laser coagulation of the canine vas deferens," *J. Biomed. Opt.*, vol. 15, 2010.
- [64] J. Jingying, W. Chen, R. Wang, and K. Xu, "Availability of thiazone as an enhancer for optical clearing of skin tissue in vitro," *Proc. SPIE*, vol. 6858:68580N, 2008.
- [65] X. Ma, J. Q. Lu, H. Ding, and X. H. Hu, "Bulk optical properties of porcine skin dermis at eight wavelengths from 325 to 1557nm," *Opt. Lett.*, vol. 30, pp. 412-414, 2005.
- [66] D. A. Torvi, "Effects of thermal properties on skin burn predictions in longer duration protective clothing tests," *J. ASTM International*, vol. 2, pp. 1-13, 2005.
- [67] S. C. Jiang, N. Ma, H. J. Li, and X. X. Zhang, "Effects of thermal properties and geometrical dimensions on skin burn injuries," *Burns*, vol. 28, pp. 713-717, 2002.
- [68] G. M. J. Van Leeuwen, J. J. W. Lagendijk, B. J. A. M. Van Leersum, A. P. M. Zwamborn, S. N. Hornsleth, and A. N. T. J. Kotte, "Calculation of change in brain temperatures due to exposure to a mobile phone," *Phys. Med. Biol.*, vol. 44, pp. 2367-2379, 1999.
- [69] M. A. Barone, P. L. Hutchinson, C. H. Johnson, J. Hsia, and J. Wheeler, "Vasectomy in the United States, 2002," *J. Urol.*, vol. 176, pp. 232-236, 2006.
- [70] W. D. Mosher, G. M. Martinez, A. Chandra, J. C. Abma, and S. J. Wilson, "Use of contraception and use of family planning services in the United States: 1982-2002," *Adv. Data*, vol. 350, pp. 1-36, 2004.
- [71] J. H. Torres, J. S. Nelson, B. S. Tanenbaum, T. E. Milner, D. M. Goodman, and B. Anvari, "Estimation of internal skin temperatures in response to cryogen spray cooling: Implications for laser therapy of port wine stains," *IEEE J. Sel. Top. Quant. Electron.*, vol. 5, pp. 1058-1066, 1999.
- [72] F. Incropera, D. DeWitt, T. Bergman, and A. Lavine, *Fundamentals of Heat and Mass Transfer*. Hoboken, NJ: John Wiley, 2007.

- [73] A. J. Welch, "The thermal response of laser irradiated tissue," *IEEE J. Sel. Top. Quant. Electron.*, vol. 20, pp. 1471-1481, 1984.
- [74] C. Davis and W. Kuang, "Optical coherence tomography: a novel modality for scrotal imaging," *Canadian Urological Association Journal*, vol. 3, pp. 319-322, 2009.
- [75] C. M. Cilip, P. M. Pierorazio, A. E. Ross, M. E. Allaf, and N. M. Fried, "High-frequency ultrasound imaging of noninvasive laser coagulation of the canine vas deferens," *Lasers Surg Med*, vol. 43, pp. 838-842, 2011.
- [76] D. E. Leocadio, A. R. Kunselman, T. Cooper, J. H. Barrantes, and T. J. C., "Anatomical and histological equivalence of the human, canine, and bull vas deferens," *Canadian Urological Association Journal*, vol. 18, pp. 5699-5704, 2011.

APPENDIX A: TECHNOLOGICAL DEVELOPMENT OF A NOVEL VASECTOMY CLAMP

Introduction

Conventional vasectomy has a very high rate of success. The prior research done has proven the success and ability to obtain long term vas occlusion. However, difficulties have arisen (skin burns, misalignment, freeze burns) that have resulted in delays and aborted procedures during our animal studies. These difficulties must be addressed to maintain a high success rate, comparable with the current no-scalpel vasectomy (NSV) technique. Issues such as misalignment and ‘slipping’ of the clamp can be addressed by the development of a new surgical clamping device while issues of skin burning and misused parameters can be addressed by limiting the number of parameters available through electronic pre-programming. In this chapter, the technological development of noninvasive laser vasectomy is discussed. A prototype modified NSV clamp is integrated with laser and cryogen delivery. Additionally, a microelectronic prototype system will control the procedure while only allowing known working parameters to be applied.

Methods

Miniaturization of experimental setup

The current experimental setup is very bulky consisting of many separate individual components: a standard no scalpel vasectomy ring clamp, cryogen tubing, cryogen solenoid valve, laser fiber optics, and collimating lens are necessary components for achieving successful occlusion of the canine vas deferens. Additional components (Figure A-1) add unnecessary weight and interfere with the procedure by requiring the

surgeon to secure the clamp on the canine and then move the system in around the clamp. Integrating only the necessary parts (Figure A-2) into the clamp will allow for a simplified setup and help the surgeon maintain control of the device during noninvasive laser vasectomy.

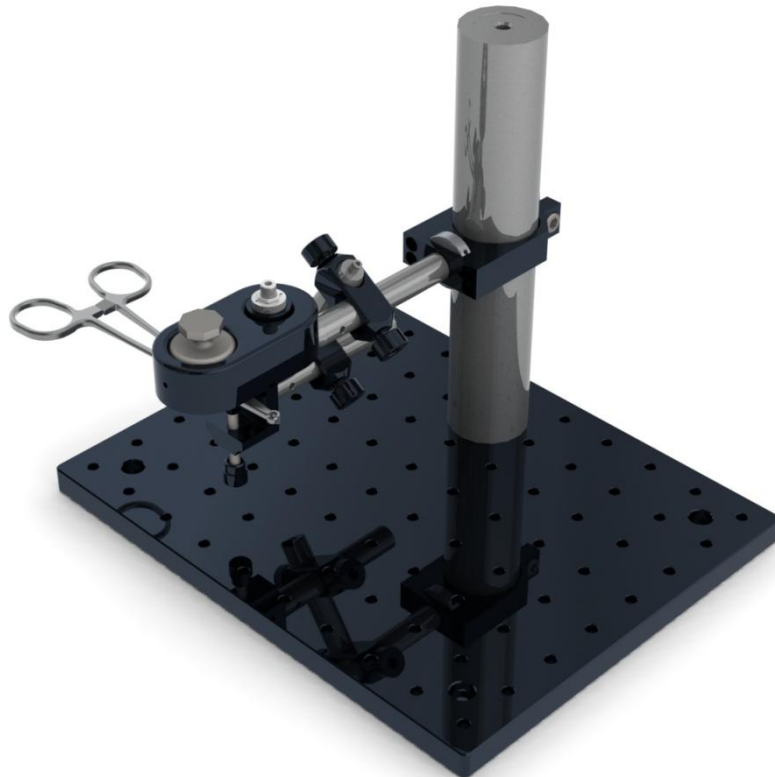


Figure A-1. Experimental setup; unwanted weight and limited motion arise from using bulky components.

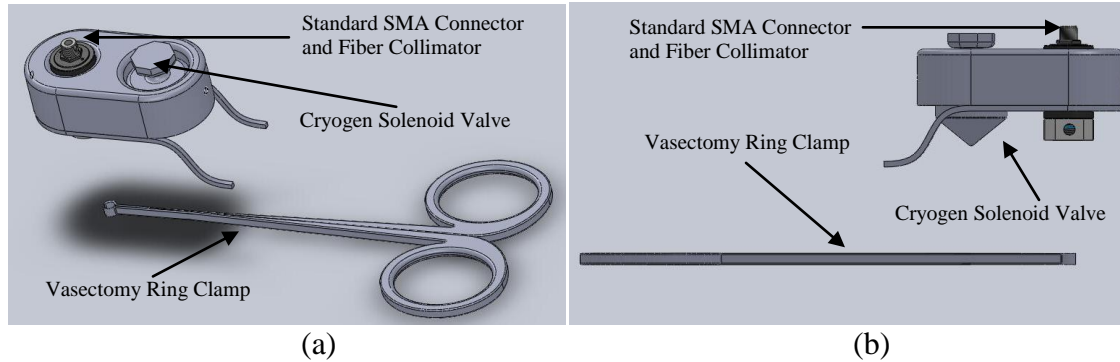


Figure A-2. Concept drawing with the necessary components for noninvasive laser vasectomy. (a) Isometric; (b) Side view.

Using a standard NSV clamp as the main axis of reference it is possible to achieve any orientation necessary for a successful procedure with only four degrees of freedom. Three orthogonal degrees of freedom allow the necessary components to be placed anywhere, spatially, in relation to the ring of the NSV clamp. An additional fourth degree of freedom, roll, provides the user with the ability to correct for any rotation of the clamp inside the secured device. By using a cylindrical coordinate system it is possible to minimize the material necessary to achieve all three orthogonal degrees of freedom (ρ, ϕ, z). Roll is then added by allowing the stabilizing arm which controls the ρ component to rotate freely before it is locked into place with a set screw. (FigureA-3)

Typically, surgical devices are made out of stainless steel, titanium or other alloys due to their oxidation properties and the ability to be autoclaved with minimal wear and tear. The machining capabilities available made stainless steel the only viable option and therefore minimizing the material used was very important due to the inherent weight of steel versus other softer lighter metals. Other future options include stainless alloys and titanium; however, this can be addressed during future product development.

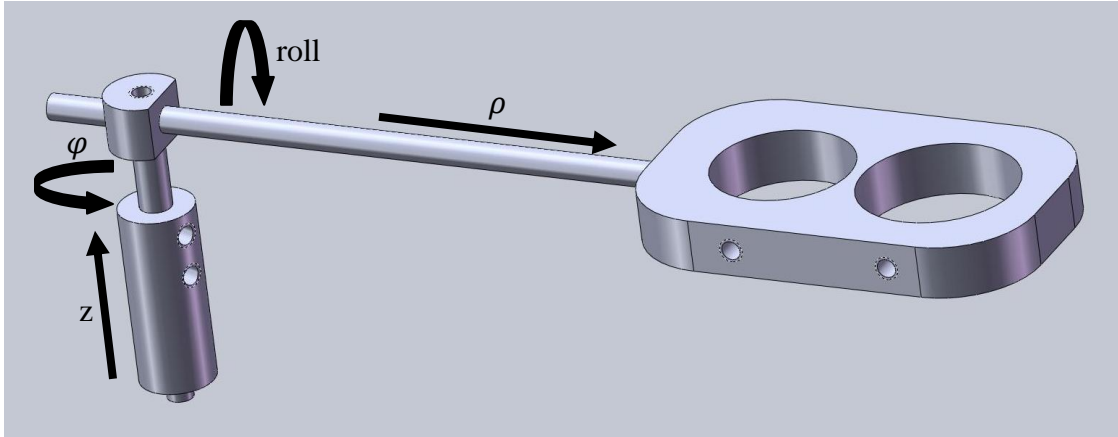


Figure A-3. Concept drawing of a clamp attachment with four degrees of freedom using a cylindrical coordinate system with integrated roll feature.

Miniaturization of control systems

The functionality of the laser and cryogen system is maintained by electronic modulation (differential TTL signal). The current setup consists of two signal generators (Stanford Research Systems) that allow full flexibility in choosing modulation parameters and an oscilloscope (Tektronix) which monitors the output of the entire system (Figure A-4 (a,b)). The laser will emit radiation during an active high pulse while the cryogen requires an active low pulse less than its set spray time (60 ms) to activate. The electronic modulation system should allow for some flexibility during the experimental phase, allowing the investigator to manipulate the parameters slightly however, the final iteration will be structured to allow only known working parameters.



Figure A-4. (a) Tektronix digital oscilloscope, (b) Stanford Research Systems signal generator.

Results

Development of miniaturize clamp system

Two iterations were done that streamlined the device into a system that includes two moving parts (Figure A-5, Appendix B), each secured into place with one set screw. A third set screw is present in the figure; however, this was added to increase the z direction motion without having to manufacture additional systems. Each part was turned on a lathe from standard 304 stainless steel bar stock with the exception of the laser and cryogen holder which was created using a CNC machine. The connecting rod was press fit into the laser/cryogen holder and requires no additional adhesive to prevent unwanted rotation. There is a clear disconnect between the designed system and the NSV clamp in figure A-5; the arm of the NSV clamped had to be planed off to create a clamping surface. During product development the lower junction of the system can be cast onto the actual NSV clamp during production, this will eliminate the junction device that was created to adhere to two devices.

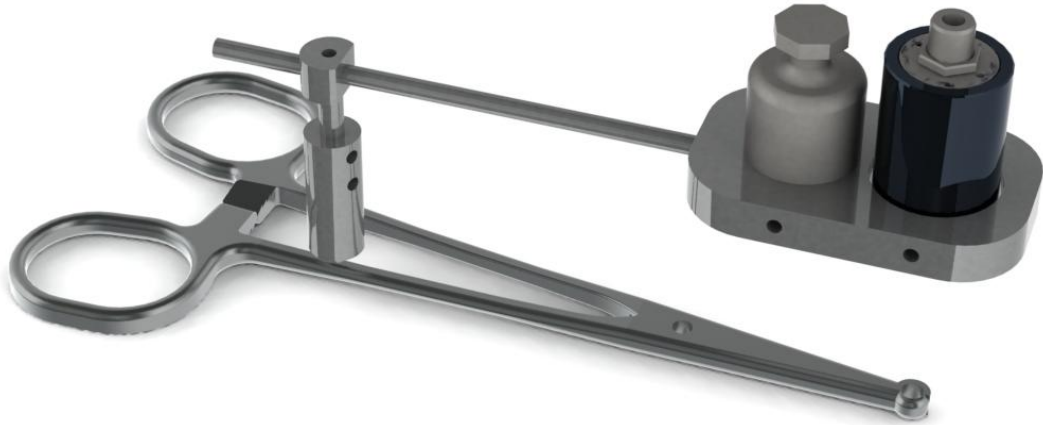


Figure A-5. Concept drawing of the second iteration of the noninvasive vasectomy clamp, using a NSV clamp.

Development of miniature control system

A Renesas prototype board was used to control multiple preset conditions for experimental testing (Appendix C). The laser parameter space was limited to 1, 2, and 4 Hz; there were additional conditions that allowed the laser to run in continuous wave mode for power calibration as well as be completely turned off for safety. The cryogen spray was set to allow frequencies 1/5, 1/4, 1/3 and 1/2 Hz settings which corresponded to previous parameters that have been tested in *ex vivo* and *in vivo* experiments. The miniature control system was button operated and packaged with BNC connectors allowing attachment of the laser and cryogen system (Figure A-6). The LCD readout on the board provided feedback on the current operating conditions (Figure A-7).



Figure A-6. Project box housing Renesas microcontroller board with BNC connectors



(a)



(b)

Figure A-7. Programmed Renesas microcontroller board showing (a) steady state, (b) working parameter space.

Discussion

Both iterations of a novel noninvasive laser vasectomy prototype clamp were previously tested experimentally. The development of a miniaturized system that was more robust than previous experimental systems helped control skin burning issues which have occurred due to misalignment of the laser/cryogen. Additionally, adapting bulky signal generators that are primarily useful in laboratory conditions to a more streamlined automated device allows for single user operation while maintaining flexibility to change between known working parameters.

Conclusion

This prototype is ready to undergo product development where physicians can be consulted to test and recommend personal changes based on their preference of technique. Further miniaturization of the microcontroller board can be accomplished with more streamlined packages such as the AT-Tiny microcontroller. An ergonomic plastic cover can be molded to fit over the metal components allowing a housing structure to support a small LCD screen for the option of easy viewing. The push button controls on the project box can be transitioned into the handle and the BNC connectors can be eliminated once the device is developed to have custom connections or hardwired to the laser/cryogen system. The final prototype design can be seen in Figure A-8.



Figure A-8. Final iteration of the noninvasive vasectomy prototype clamp.

APPENDIX B: SCHEMATICS OF NONINVASIVE LASER VASECTOMY
 PROTOTYPE CLAMP

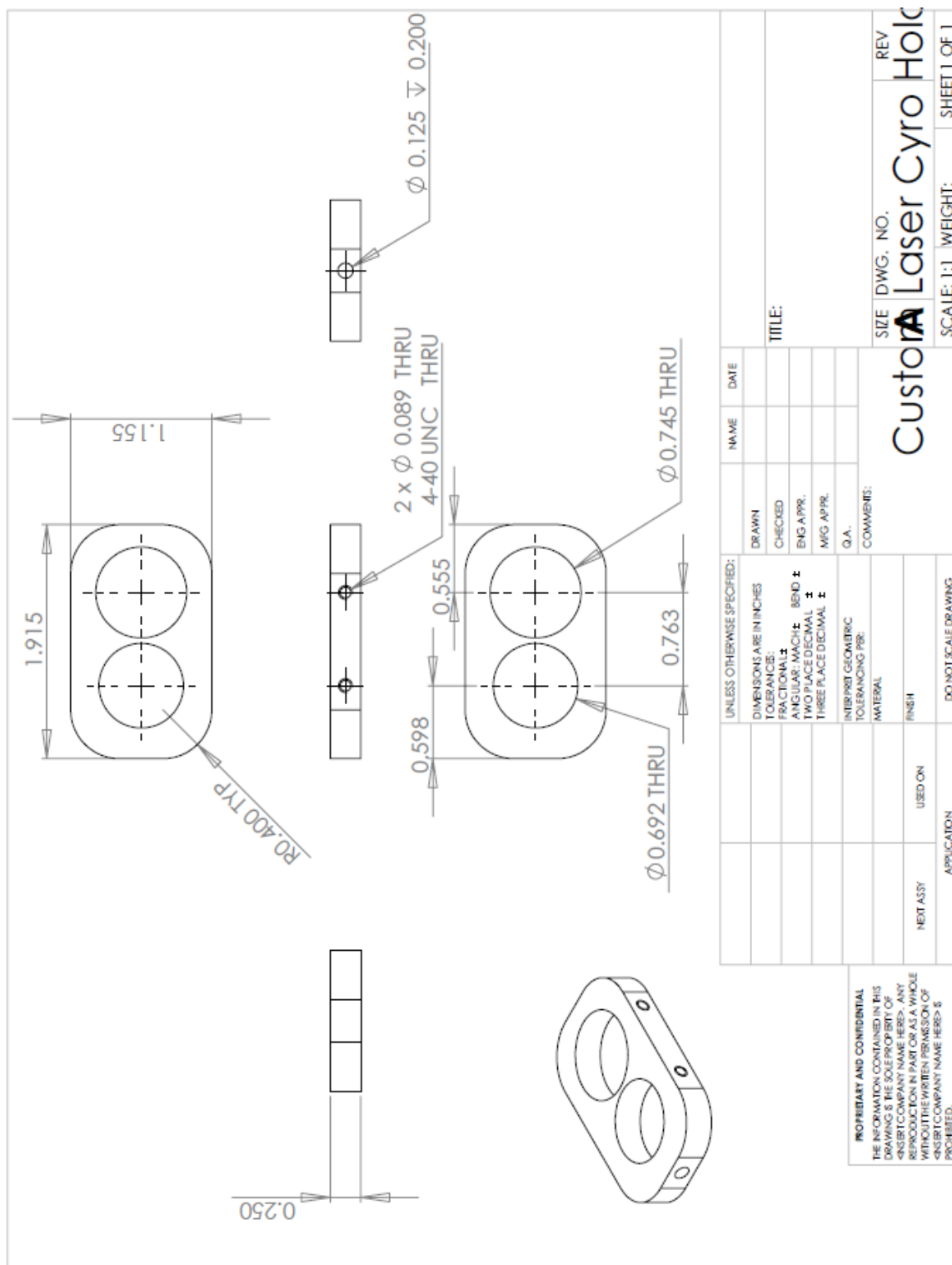


Figure B-1. Schematic of laser/cryogen holder for CNC machining.

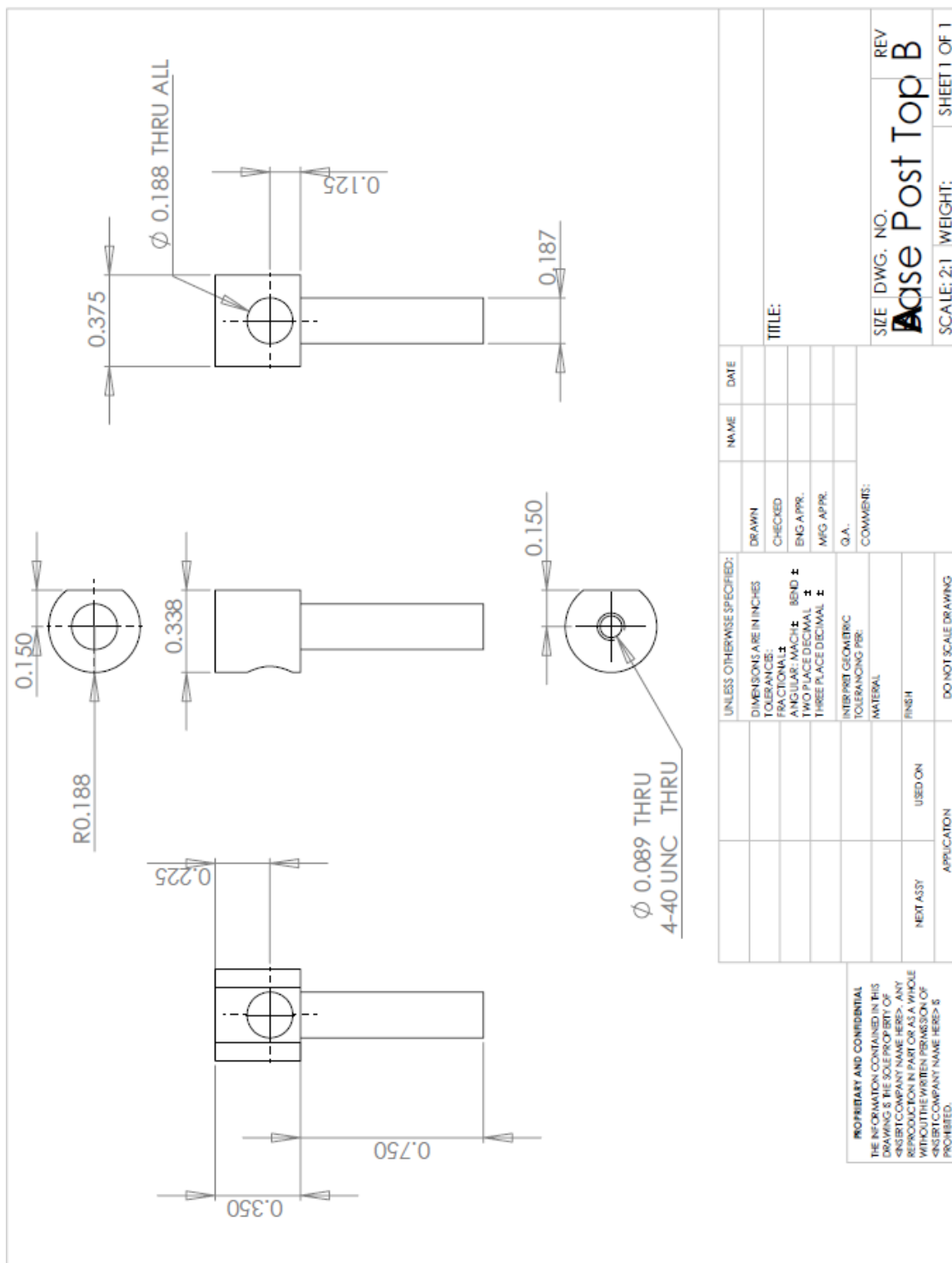


Figure B-2. Schematic of base post insert for machining.

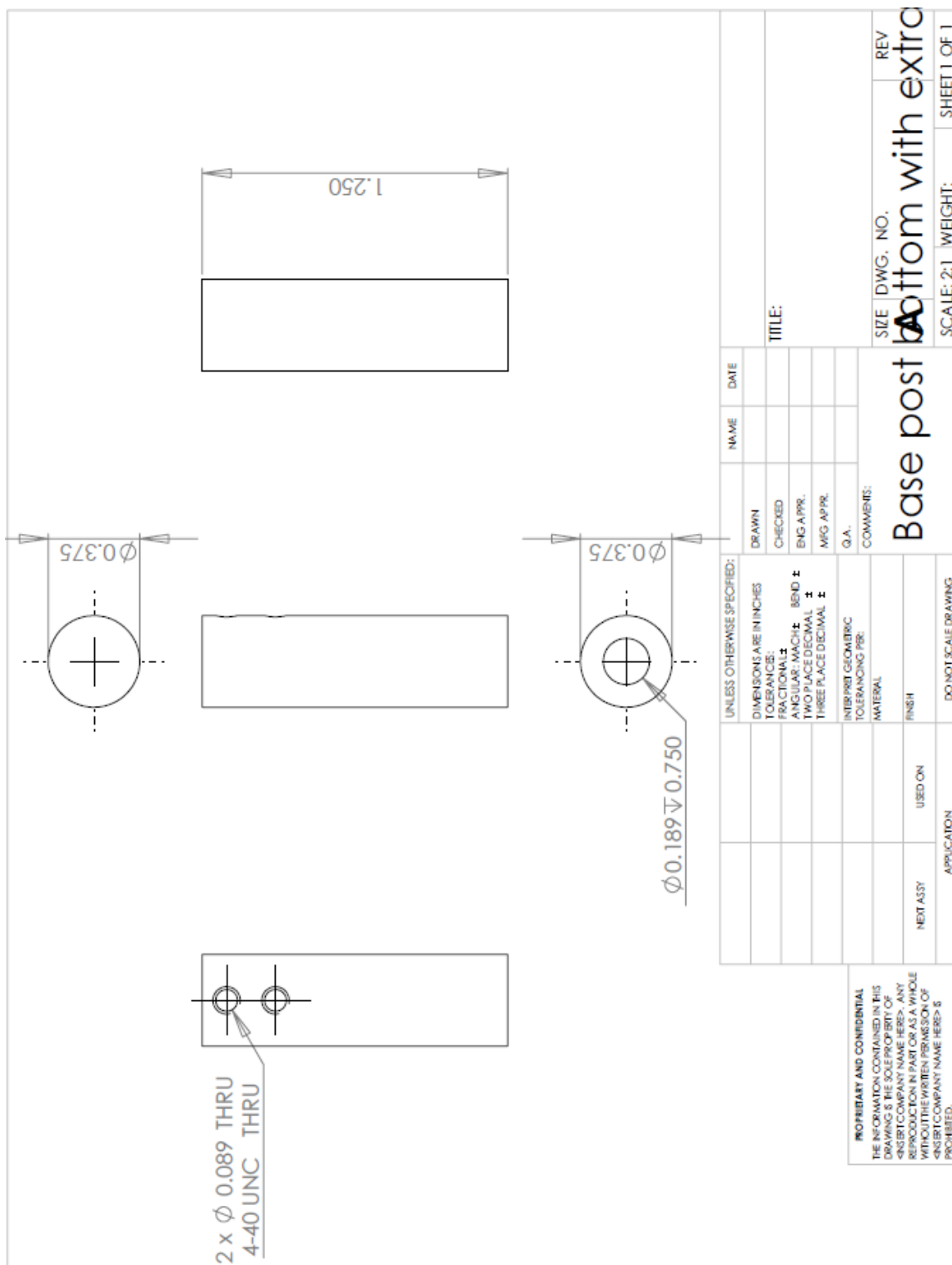


Figure B-3. Schematic of base post holder for machining.

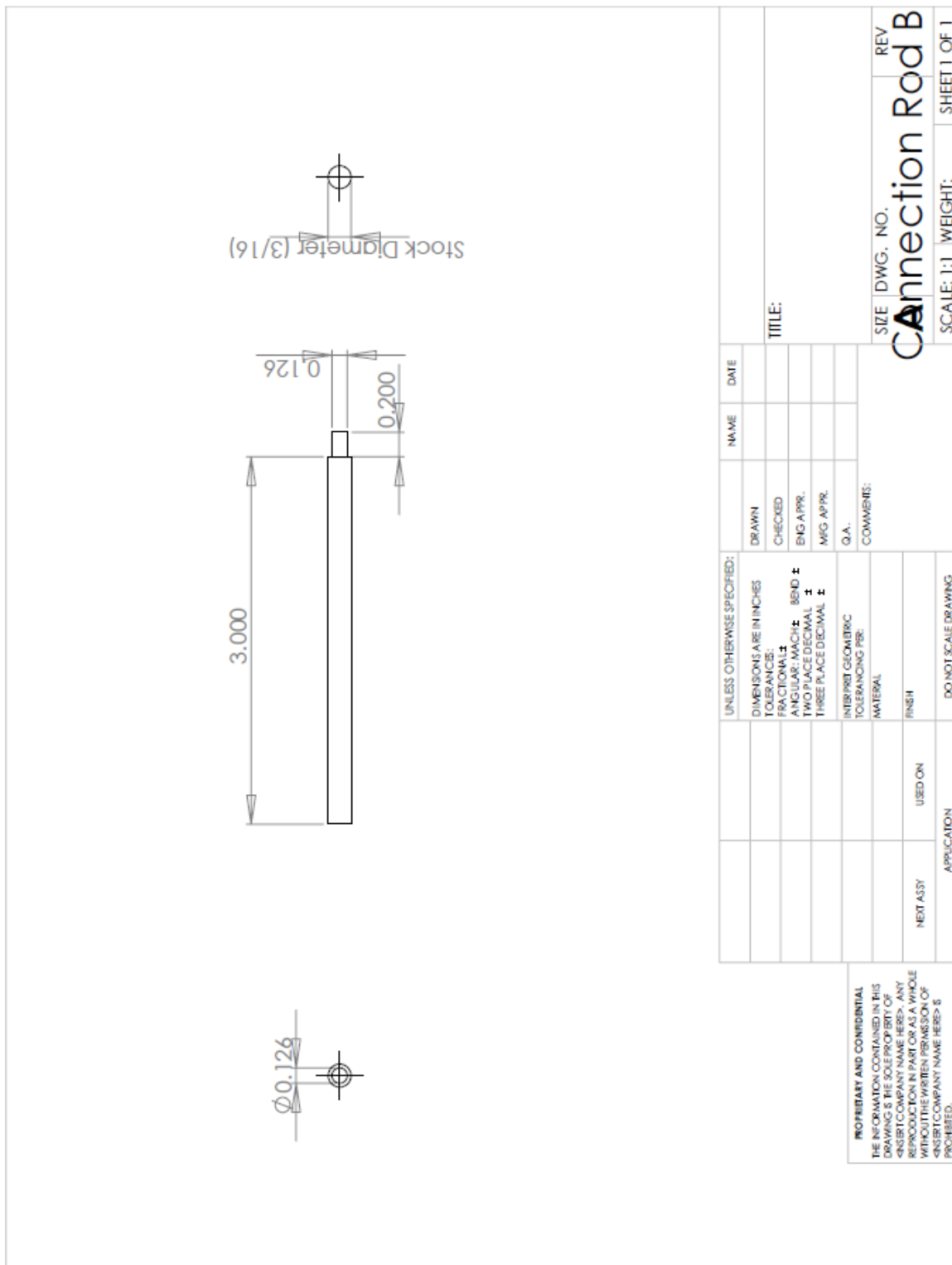


Figure B-4. Schematic of connection rod for press fitting.

UNLESS OTHERWISE SPECIFIED:		DRAWN	NAME	DATE
DIMENSIONS ARE IN INCHES		CHECKED		
TOLERANCES:		ENG. APPR.		
FRACTIONAL: ±		MFG. APPR.		
DECIMAL: ±		Q.A.		
ANGULAR: MACH ±		COMMENTS:		
TWO PLACE DECIMAL ±				
THREE PLACE DECIMAL ±				
INTERPRT GEOMETRIC TOLERANCING PER:				
MATERIAL				
FINISH				
APPLICATION	USED ON	DO NOT SCALE DRAWING		
NEXT ASSY				

PROPRIETARY AND CONFIDENTIAL
 THE INFORMATION CONTAINED IN THIS DRAWING IS THE SOLE PROPERTY OF <INSERT COMPANY NAME HERE>. ANY REPRODUCTION IN PART OR AS A WHOLE WITHOUT THE WRITTEN PERMISSION OF <INSERT COMPANY NAME HERE> IS PROHIBITED.

TITLE: _____
 SIZE DWG. NO. _____ REV _____
Connection Rod B
 SCALE: 1:1 | WEIGHT: _____ SHEET 1 OF 1

APPENDIX C-1: MAIN SIGNAL GENERATION PROGRAM

```

*DESCRIPTION: main routine for Timer - Pulse Output Mode

* PURPOSE: Outlines how to setup the M16C/62P Timer A in Pulseoutput
mode.*****

/* Include the required header files */

#include"qsk_bsp.h"           // include SKP board support package

#define TIME_CONFIG 0xC4

        /* 10000100 value to load into timer mode register

        Bit 0,1: TMOD0,TMOD1: TIMER MODE SELECTED

        Bit 2: MR0:PULSE OUTPUT

        Bit 3,4: MR1,MR2:GATE FUNCTION NOT SELECTED

        Bit 5: MR3:SET TO 0 IN TIMER MODE

        Bit 6,7:TCK0,TCK1:F DIVIDED BY 32 SELECTED gives 1 kHz clock*/

#define TIME2_CONFIG 0xCE

#define TIMER_CONFIG 0xD6

#define CNTR_IPL 0x00 // TA2 priority interrupt level: interrupts not required

char * IntToAsciiHex(char * dest_string,int min_digits,unsignedint value);

        //CONVERT HEXIDECIMAL VALUES TO ASCII FOR LCD

char * IntToAsciiDec(char * dest_string,int min_digits,unsignedint value);

        //CONVERT DECIMAL VALUES TO ASCII FOR LCD

char lcd_text[9];

        //9 CHARACTER ARRAY VARIABLE FOR OUTPUT DISPLAY USE

//prototypes

void tmr_init(void); //LOAD TIMER CLASS

void mcu_init(void); //LOAD CHIPSET CLASS

void lcd_init(void); //LOAD LCD CLASS

```

```

/*****

```

Name: main()

Parameters: none

Returns: nothing

Description: initializes variables and LED port. Then does nothing but wait for TA0 interrupts.

```

*****/

```

```

void main (void)                                //PROGRAM IS WRITTEN IN THE MAIN CLASS
{
    unsignedchar button1flag;                   //Variable to holdLaser State
    unsignedchar button2flag;                   //Variable to holdCryogen State
    unsignedint x, y;                            //DELAY VARIABLES
    int time_cnt;
    pd6 = 0xFF;
    mcu_init();                                 //initialize processor clock
    lcd_init();                                 //initialize LCD display
    tmr_init();                                 //initialize timer
    button1flag=0;                              //initialize variable to
    button2flag=0;
    while (1){                                  // square wave output is free running
        if (p8_3 == 0 && button1flag==0)        //if laser button is pressed (active low) and
        {                                       //the case is at start state (0), then
            for (x=0; x<0x7ff; x++){           //run 1Hz signal to laser
                _asm("NOP");
            }
            for (y=0; y<0x1ff; y++){           //for loop is for switch debouncing
                _asm("NOP");}
            button1flag = 1;                    //set the condition for next press
        }
    }
}

```

```

    p6_2 = 0;

    ta1s = 0;

    ta1 = (unsignedint) (511);           // 511 = (1024/2) if zero bit is used

    ta1s = 1;

    DisplayString(LCD_LINE1, " L: 1Hz ");
}

if (p8_3 == 0 && button1flag == 1 )    //drives to laser case 2: 2Hz
{
    for (x=0; x<0x7ff; x++){           //for loop is for switch debouncing
        _asm("NOP");
    }
    for (y=0; y<0x1ff; y++){
        _asm("NOP");}
    button1flag = 2;

    p6_2 = 1;

    ta1s = 0;

    ta1 = (unsignedint) (255);

    ta1s = 1;

    DisplayString(LCD_LINE1, " L: 2Hz ");
}

if (p8_3 == 0 && button1flag == 2 )    //drives to laser case 3: 4Hz
{
    for (x=0; x<0x7ff; x++){           //for loop is for switch debouncing
        _asm("NOP");
    }
    for (y=0; y<0x1ff; y++){
        _asm("NOP");}
    button1flag = 3;

    ta1s = 1;

    ta1 = (unsignedint) (127);
}

```

```

        ta1s = 1;

        DisplayString(LCD_LINE1, " L: 4Hz ");
    }

    if (p8_3 == 0 && button1flag == 3 )           //drives to laser case 4: continous wave
    {                                             //This is used for power calibration

        for (x=0; x<0x7ff; x++){               //for loop is for switch debouncing

            _asm("NOP");

            for (y=0; y<0x1ff; y++)

                _asm("NOP");

            button1flag = 4;

            ta1s = 0;

            ta1 = (unsignedint) (1);

            ta1s = 1;

            DisplayString(LCD_LINE1, "trigger");

        }

    if (p8_3 == 0 && button1flag == 4 )           //drives to laser case 5: OFF
    {

        for (x=0; x<0x7ff; x++){               //for loop is for switch debouncing

            _asm("NOP");

            for (y=0; y<0x1ff; y++)

                _asm("NOP");

            button1flag = 0;

            ta1s = 0;

            DisplayString(LCD_LINE1, "LASEROFF");

            for (x=0; x<0x7ff; x++){

                _asm("NOP");

                for (y=0; y<0x1ff; y++)

                    _asm("NOP");
            }
        }
    }

```

```

}
if (p8_1 == 1 && button2flag == 0 )           //drives to cryogen case 1: .5Hz
{
    for (x=0; x<0x7ff; x++){                 //for loop is for switch debouncing
        _asm("NOP");
    }
    for (y=0; y<0x1ff; y++){
        _asm("NOP");}
    button2flag = 1;
    ta2 = (unsignedint) (2047);
    ta3 = (unsignedint) (2017);
    ta2s = 1;
    ta3s = 1;
    ta2os = 1;
    DisplayString(LCD_LINE2,"C:.5Hz");
}
if (p8_1 == 1 && button2flag == 1 )           //drives to cryogen case 2: .33Hz
{
    for (x=0; x<0x7ff; x++){                 //for loop is for switch debouncing
        _asm("NOP");
    }
    for (y=0; y<0x1ff; y++){
        _asm("NOP");}
    button2flag = 2;
    ta2 = (unsignedint) (3071);
    ta3 = (unsignedint) (3041);
    ta2s = 1;
    ta3s = 1;
    ta2os = 1;
    DisplayString(LCD_LINE2,"C:.33Hz");
}

```

```

    }
if (p8_1 == 1 && button2flag == 2 )           //drives to cryogen case 3: .25Hz
{
    for (x=0; x<0x7ff; x++){                 //for loop is for switch debouncing
        _asm("NOP");
    for (y=0; y<0x1ff; y++)
        _asm("NOP");}
    button2flag = 3;
    ta2 = (unsignedint) (4095);
    ta3 = (unsignedint) (4065);
    ta2s = 1;
    ta3s = 1;
    ta2os = 1;
    DisplayString(LCD_LINE2, "C:.25Hz");
}
if (p8_1 == 1 && button2flag == 3 )           //drives to cryogen case 4: .2Hz
{
    for (x=0; x<0x7ff; x++){                 //for loop is for switch debouncing
        _asm("NOP");
    for (y=0; y<0x1ff; y++)
        _asm("NOP");}
    button2flag = 0;
    ta2 = (unsignedint) (5119);
    ta3 = (unsignedint) (5089);
    ta2s = 1;
    ta3s = 1;
    ta2os = 1;
    DisplayString(LCD_LINE2, "C:.2Hz");}}

```

```
/******
```

Name: tmr_init()

Parameters: none

Returns: nothing

Description: Setup timer A2 setup for Pulse Output Mode (in timer mode).

BCLK is set to f1 (divide by 1) in the nrt0 startup file.

```
***** */
```

```
void tmr_init(void)
```

```
{
```

```
    DISABLE_IRQ
```

```
    ta1mr = TIME_CONFIG;
```

```
    ta0mr = TIME2_CONFIG;
```

```
    tabsr = 0x04;
```

```
    ta3 = (unsignedint) (0);
```

```
    ta2 = (unsignedint) (0);
```

```
    trgsr = 0x20;
```

```
    ta2mr = TIME_CONFIG;
```

```
    ta3mr = TIMER_CONFIG;
```

```
    ta2ic = CNTR_IPL;
```

```
    ta3ic = CNTR_IPL;
```

```
    ENABLE_IRQ
```

```
}
```

```
/******  
Name    : lcd_init  
Parameters : none  
Returns  : nothing  
Description: initializes the LCD  
*****/  
void lcd_init(void)  
{  
    InitDisplay();           // Initialize LCD  
    DisplayString(LCD_LINE1," Laser "); //System start condition  
    DisplayString(LCD_LINE2,"Cryogen");  
}
```

```

/*****

```

Name: IntToAsciiHex

Returns: A pointer to the string's NULL character in the string that was just created.

Description: This function is used to convert a passed unsigned int into a ASCII string represented in Hexidecimal format.

```

*****/

```

```

char * IntToAsciiHex(char * dest_string,int min_digits,unsignedint value)

```

```

{
    unsignedint i, total_digits = 0;
    char buff[4];

    for(i=0;i<4;i++) {
        buff[i] = (char)(value & 0x0F);
        value = value >> 4;
        if( buff[i] <= 9)
            buff[i] += '0';
        else
            buff[i] = (char)(buff[i] - 0xA + 'A');

        if(buff[i] != '0')
            total_digits = i+1;
    }

    if( total_digits < min_digits)
        total_digits = min_digits;

    i = total_digits;

```

```
while(i) {  
    *dest_string++ = buff[i-1];  
    i--;  
}  
  
*dest_string = 0;  
  
return dest_string;  
}
```

```

/*****

```

Name: IntToAsciiDec

Returns: A pointer to the string's NULL character in the string that was just created.

Description: This function is used to convert a passed unsigned int into a ASCII string represented in base 10 decimal format.

```

*****/

```

```

char * IntToAsciiDec(char * dest_string,int min_digits,unsignedint value)

```

```

{

```

```

    constunsignedlong base10[] = {1,10,100,1000,10000,100000};

```

```

    unsignedint tmp;

```

```

    unsignedint i, total_digits = 0;

```

```

    char buff[5];

```

```

    for(i=0;i<5;i++) {

```

```

        tmp = (int)( value % base10[i+1] );

```

```

        value -= tmp;

```

```

        buff[i] = (char)( tmp / base10[i] );

```

```

        buff[i] += '0';

```

```

        if(buff[i] != '0')

```

```

            total_digits = i+1;

```

```

    }

```

```

    if( total_digits < min_digits)

```

```

        total_digits = min_digits;

```

```
i = total_digits;
```

```
while(i) {
```

```
    *dest_string++ = buff[i-1];
```

```
    i--;
```

```
}
```

```
*dest_string = 0;
```

```
return dest_string;
```

```
}
```

APPENDIX C-2: CLOCK INITIALIZATION

```

/*-----
FILE NAME: mcu_init.c
-----
DESCRIPTION: System clock and processor mode initialization
-----
DETAILS: Adapted for M16C/62P
-----*/

#include "skp_bsp.h"
#include "sfr62p.h"           // M16C/62P special function register definitions

/*****

Name      : mcu_init()
Returns   : nothing

Description: The starter kit startup file initializes the clock circuit to the main crystal with a divide by 1.
This function also sets the main clock to divide by 1 in case the SKP startup file is not used.

*****/

void mcu_init(void)
{
    unsigned int i, j;

    /* Change XCin and Xcout to inputs and start the 32Khz crystal sub clock */
    pd8_7 = 0;           // setting GPIO to inputs (XCin/XCout)

    pd8_6 = 0;

    prc0 = 1;           // Unlock CM0 and CM1

    cm04 = 1;           // Start the 32KHz crystal

    /* add some time delay for 32kHz to stabilize */

    for (i=0; i<0x7ff; i++){

```

```
    _asm("NOP");  
    for (j=0; j<0x7ff; j++)  
        _asm("NOP");  
    }  
    cm03 = 0;           // Set Xc clock to low drive  
    prc0 = 0;          // Lock the System Clock Control Register  
}
```

APPENDIX C-3: LCD INITIALIZATION

```

/*****
*FILE NAME:          QSK_LCD.c
* DESCRIPTION:      Driver for ACM0802C LCD Module on Renesas' QSK boards.
* (8 characters by 2 lines)
*****/

#include"qsk_bsp.h"

/* Used for Renesas Logo bit mapping */
char logo_map[8*8] =
{
    0x03,0x00,0x00,0x00,0x07,0x07,0x07,0x00,
    0x1E,0x03,0x03,0x1E,0x18,0x0C,0x03,0x00,      // R
    0x0F,0x10,0x10,0x1F,0x10,0x10,0x0F,0x00,      // E
    0x11,0x19,0x1D,0x15,0x17,0x13,0x11,0x00,      // N
    0x0F,0x10,0x10,0x1F,0x10,0x10,0x0F,0x00,      // E
    0x0F,0x10,0x10,0x0E,0x01,0x01,0x1E,0x00,      // S
    0x04,0x0A,0x0A,0x11,0x11,0x11,0x17,0x00,      // A
    0x0F,0x10,0x10,0x0E,0x01,0x01,0x1E,0x00,      // S
};

```

```

/*****
Name:      InitDisplay
Returns:   none
Description:  Intializes the LCD display.
*****/

void InitDisplay( void )
{
    int i;

    // initial port directions
    prc2=1; // unprotect as Port 9 is used
    PORT_DDR = PORT_DDR_VALUE;

    EN_PIN = HIGH;
    EN_PIN_DDR = HIGH; // set port that controls EN as output
    RS_PIN = HIGH;
    RS_PIN_DDR = HIGH; // set port that controls RS as output

    EN_PIN = LOW;

    LCD_write(CTRL_WR,0x33);
    DisplayDelay(20);
    LCD_write(CTRL_WR,0x32);
    DisplayDelay(20);
    LCD_write(CTRL_WR,FUNCTION_SET); /* reset sequence */
    LCD_write(CTRL_WR,FUNCTION_SET);
    LCD_write(CTRL_WR,LCD_CURSOR_OFF);
    LCD_write(CTRL_WR,LCD_CLEAR);

```

```
LCD_write(CTRL_WR,LCD_HOME_L1);
```

```
// Map the Renesas logo characters into CG RAM
```

```
LCD_write(CTRL_WR,0x40);
```

```
for( i=0;i<64;i++)
```

```
    LCD_write(DATA_WR,logo_map[i]);
```

```
}
```

```

/*****

```

Name: DisplayString

Returns: none

Description: This function controls LCD writes to line 1 or 2 of the LCD.

```

*****/

```

```

void DisplayString(unsignedchar position, _far constchar * string)

```

```

{

```

```

    staticunsignedchar next_pos = 0xFF;

```

```

    /* Set line position if needed. We don't want to if we don't need
       to because LCD control operations take longer than LCD data
       operations. */

```

```

    if( next_pos != position)

```

```

    {

```

```

        if(position < LCD_LINE2)

```

```

        {

```

```

            /* Display on Line 1 */

```

```

            LCD_write(CTRL_WR, (unsignedchar)(LCD_HOME_L1 + position) );

```

```

        }

```

```

        else

```

```

        {

```

```

            /* Display on Line 2 */

```

```

            LCD_write(CTRL_WR, (unsignedchar)(LCD_HOME_L2 + position - LCD_LINE2) );

```

```

        }

```

```

        next_pos = position;                    // set position index to known value

```

```

    }

```

```

do

```

```
{  
    LCD_write(DATA_WR, *string++);  
    next_pos++;           // increment position index  
}  
while(*string);  
}
```

```

/*****

```

```

Name:          LCD_write

```

```

Returns:       none

```

```

Description:   Writes data to display. Sends command to display.

```

```

*****/

```

```

void LCD_write(unsignedchar data_or_ctrl, unsignedchar value)

```

```

{

```

```

    RS_PIN = data_or_ctrl;                // RS SELECT (HIGH=DATA, LOW=CTRL)

```

```

    /* Write upper nibble first */

```

```

    DATA_PORT &= 0xF0;                   // Clear lower part of port

```

```

    DATA_PORT |= (value & 0xF0)>>4;     // OR in upper nibble

```

```

    EN_PIN = HIGH;                        // EN enable chip (HIGH)

```

```

    DisplayDelay(0);                      // We only need a very little delay

```

```

    EN_PIN = LOW;                         // Latch data by dropping EN

```

```

    DisplayDelay(0);                      // We only need a very little delay

```

```

    if(data_or_ctrl == CTRL_WR)

```

```

        DisplayDelay(1);                 // extra delay needed for control writes

```

```

    /* Write lower nibble second */

```

```

    DATA_PORT &= 0xF0;                   // Clear lower part of port

```

```

    DATA_PORT |= (value & 0x0F) ;       // write to port

```

```

    EN_PIN = HIGH;

```

```

    DisplayDelay(0);                      // We only need a very little delay

```

```

    EN_PIN = LOW;                         // Latch data by dropping EN

```

```

    DisplayDelay(1);                      // needed to put delay in between writes.

```

```
if(data_or_ctrl == CTRL_WR)
    DisplayDelay(40);           // extra delay needed for control writes
}
```

```
/******
```

Name: DisplayDelay

Returns: none

Description: Delay routine for LCD display.

```
*****
```

```
void DisplayDelay(unsignedlongint units){
```

```
    unsignedlongint counter = units * 0x100;
```

```
    while(counter--){
```

```
        _asm ("NOP");
```

```
        _asm ("NOP");
```

```
        _asm ("NOP");
```

```
    }
```

```
}
```

APPENDIX D: RECOGNIZED WORKS

Peer Reviewed Publications

Cilip, C.M., Pierorazio, P.M., Ross, A.E., Allaf, M.E., and Fried, N.M. High-Frequency Ultrasound Imaging During Noninvasive Laser Coagulation of the Canine Vas Deferens. Lasers in Surgery and Medicine 43:838-842, 2011.

Cilip, C.M., Ross, A.E., Jarow, J.P., and Fried N.M. Application of an optical clearing agent during noninvasive laser coagulation of the canine vas deferens. Journal of Biomedical Optics 15(4), 048001, 2010.

Cilip, C.M., Jarow, J.P., and Fried, N.M. Noninvasive laser vasectomy: Preliminary ex vivo tissue studies. Lasers in Surgery and Medicine 41(3):203-207, 2009.

Schweinsberger, G.R., Cilip, C.M., Trammel, S.R., Cherukuri, H., and Fried, N.M. Noninvasive Laser Coagulation of the Human Vas Deferens: Optical and Thermal Simulations. Lasers in Surgery and Medicine 43(5); 443-449, 2011.

Tozburun, S., Cilip, C.M., Lagoda, G.A, Burnett, A.L., and Fried, N.M. Continuous-wave infrared optical nerve stimulation for potential diagnostic applications. Journal of Biomedical Optics 15, 055012, 2010.

Scott, N.J., Cilip, C.M., and Fried, N.M. Thulium fiber laser ablation of urinary stones through small-core optical fibers. IEEE Journal of Selected Topics in Quantum Electronics 15(2):435-440, 2009.

Conference Proceedings

Cilip, C.M., Allaf, M.A., and Fried, N.M. Optical coherence tomography vs. high-frequency ultrasound during noninvasive laser coagulation of the canine vas deferens. Proc. SPIE 8207: 820715, 2012.

Cilip, C.M., and Fried, N.M. Comparison of three near-infrared laser wavelengths for non-invasive thermal coagulation of the canine vas deferens, ex vivo. Proc. SPIE 78831B, 2011.

Schweinsberger, G.R., Cilip, C.M., Trammel, S.R., Cherukuri, H., and Fried, N.M. Optical and thermal simulations of noninvasive laser coagulation of the human vas deferens. Proc. SPIE 78831C, 2011.

Tozburun, S., Cilip, C.M., Lagoda, G.A., Burnett, A.L, and Fried, N.M. Continuous-wave vs. pulsed infrared laser stimulation of the rat prostate cavernous nerves. Proc. SPIE 78831A, 1-6, 2011.

Cilip, C.M., Ross, A.E., Jarow, J.P., and Fried, N.M. Noninvasive laser coagulation of the canine vas deferens, in vivo. Proc. SPIE 7548: 75481D:1-5, 2010.

Cilip, C.M., Ross, A.E., Jarow, J.P., and Fried, N.M. Use of an optical clearing agent during noninvasive laser coagulation of the canine vas deferens, ex vivo and in vivo. Proc. SPIE 7548: 75481C:1-6, 2010.

Cilip, C.M., Jarow, J.P., and Fried, N.M. Noninvasive laser coagulation of the canine vas deferens, ex vivo. Proc. SPIE 10:1-6, 2009.

Scott, N.J., Cilip, C.M., and Fried, N.M. Thulium fiber laser lithotripsy. 2009. Proc. SPIE 1E:1-7, 2009.

Cilip C.M., Scott N.J., Trammell S., and Fried N.M. Noninvasive thermal coagulation of deep subsurface tissue structures using a laser probe with integrated contact cooling. Conf Proc IEEE Eng Med Biol Soc 1:3657-3660, 2008.

Shein, P., Cilip, C.M., Quinto, G., Behrens, A., and Fried, N.M. Selective laser suture lysis with a compact, low-cost, red diode laser. Conf Proc IEEE Eng Med Biol Soc 1:4358-4360, 2008.

Abstracts

Cilip, C.M., Pierorazio, P.M., Ross, A.E., Allaf, M.E., and Fried, N.M. High Frequency Ultrasound Imaging During Noninvasive Laser Coagulation of the Canine Vas Deferens, In Vivo. Abstract 25. 26th EUS Annual Meeting. (40) 2011.

Schweinsberger, G.R., Cilip, C.M., and Fried, N.M. Computer Simulations of Thermal Damage to the Human Vas Deferens During Noninvasive Laser Vasectomy. Abstract 47. 26th EUS Annual Meeting. (62) 2011.

Stokes, E.B., Oliver, J., Giles, A., Monroe, G.C., Cilip, C.M., McEntyre, H., Pagan, J., and Batoni, P. Ultraviolet Optical Flow Cell for Point-of-Use Water Disinfection, Meet. Abstract - Electrochem. Soc. 1001, 1048. 2010,